TECHNISCHE UNIVERSITÄT WIEN

Institut für Computertechnik
Institute of Computer Technology

Master's Thesis

submitted by

Edwin Willegger

Implementation of a multi-band RTK receiver system with Arduino

In partial fulfillment of the requirements for the degree of

Diplom Ingenieur

Vienna, Austria, 2020

Study code:	1326324
Field of study:	Microelectronics and photonics.
Supervisor:	Univ. Prof. Dipl.-Ing. Dr. techn. Axel Jantsch
Co-Supervisor:	Univ. Ass. Dipl.-Ing. Stefan Wilker

If you find this work useful, please cite it using the following BibTeX entry:

```
@Thesis{Willegger2020,
 type        = {Master's Thesis},
 author      = {Edwin Willegger},
 title       = {Implementation of a multi-band RTK receiver system with Arduino},
 school      = {Vienna University of Technology (TU Wien)},
 year        = {2020},
 address     = {Gusshausstrasse 27--29 / 384, 1040 Wien},
 month       = {September},
}
```

Contact me:

willeggeredwin@gmx.at

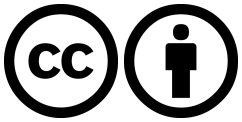

Acronyms

A | B | C | D | E | F | G | H | I | K | L | M | N | O | P | Q | R | S | T | U | V | W

A

American standard code for information interchange (ASCII)

Antenna reference point (ARP)

Anti-spoofing (AS)

Application specific qualification facility (ASQF)

B

Binary phase shift keying (BPSK)

Bits per second (BPS)

C

Carrier-to-noise ratio (CNR)

Circular Error probability (CEP)

Code division multiple access (CDMA)

D

Decibel-milliwatts (DBM)

Differential global positioning system (DGPS)

Dilution of precision (DOP)

Distance root mean square (DRMS)

E

Earth gravitational model 1996 (EGM96)

Earth-centered inertial (ECI)

Earth-centered, earth fixed (ECEF)

Electrically erasable programmable read-only memory (EEPROM)

Electronic design automation (EDA)

European geostationary navigation overlay service (EGNOS)

European global navigation satellite system agency (EGNSSA)

European Union (EU)

F

Frequency division multiple access (FDMA)

Full operational capability (FOC)

G

Galileo terrestrial reference frame (GTRF)

Geostationary orbit (GEO)

Global navigation satellite system (GNSS)

Global positioning system (GPS)

Global positioning system fix data (GGA)

Globalnaja nawigazionnaja sputnikowaja sistema (GLONASS)

GPS, dilution of precision (DOP) and active satellites (GSA)

Group repetition interval (GRI)

H

Handover words (HOW)

Height above ellipsoid (HAE)

Horizontal dilution of precision (HDOP)

I

I-Squared-C (I2C)

Inertial measurement unit (IMU)

International terrestrial reference frame (ITRF)

K

Kilobits per second (KBPS)

L

Line-of-sight (LOS)

Liquid crystal display (LCD)

Long range navigation (LORAN)

Low earth orbit (LEO)

M

Master control center (MCC)

Mean sea level (MSL)

Medium earth orbit (MEO)

Micro controller unit (MCU)

Multiple single message (MSM)

Multiple single messages 4 (MSM4)

N

National defense research committe (NDRC)

National marine electronics association (NMEA)

Navigation land earth station (NLES)

Navigation message (NAV)

Navy navigation satellite system (NNSS)

Network transport of RTCM via internet protocol (NTRIP)

Non-directional beacon (NDB)

O

On the fly (OTF)

P

Parametry zemli 1990 (PZ-90)

Performance assessment and checkout facility (PACF)

Position dilution of precision (PDOP)

Power spectrum density (PSD)

Power supply unit (PSU)

Precise point positioning (PPP)

Printed circuit board (PCB)

Pseudo random noise (PRN)

Pseudo-range correction (PRC)

Q

Quadrature phase shift keying (QPSK)

R

Radio technical commission for maritime services (RTCM)

Ranging and integrity monitoring station (RIMS)

Rate range correction (RRC)

Real time kinematics (RTK)

Receiver independent exchange format (RINEX)

Recommended minimum specific (RMC)

Reference station (RS)

Root mean square (RMS)

S

Satellite based augmentation system (SBAS)

Selective availability (SA)

Serial peripheral interface (SPI)

Standard positioning service (SPS)

Static random-access memory (SRAM)

T

Telemetry (TLM)

Time dilution of precision (TDOP)

Time of arrival (TOA)

U

Universal asynchronous receiver transmitter (UART)

Universal serial bus (USB)

Universal time coordinated (UTC)

Universal transverse mercator (UTM)

V

Vertical dilution of precision (VDOP)

Very high frequency omni-directional range (VOR)

W

Wide area augmentation system (WAAS)

Wide-area master station (WMS)

Wide-area reference station (WRS)

Wireless local area network (WLAN)

World geodetic system 1984 (WGS84)

Contents

List of Tables

List of Figures

Abstract

This thesis investigates the behaviour of a global navigation satellite system receiver system based on real time kinematics, without any additional differential global positioning system technologies such as the satellite-based augmentation system. The system consists of two receivers, one which was used as reference station and the second as a rover. The scientific difficulty lied in combining new hardware components and software algorithms in an innovative way to design a system with an accuracy in the centimetre range, with a baseline in the kilometre range and with a price tag of less than 1,000 €. The behaviour of the system was verified through static and dynamic measurements in various environments with six different antennas. The measurements also provide improvements in the knowledge set on the important relationship between global navigation satellite system antenna selection and the global navigation satellite system module applied. The dynamic measurements were conducted on cultivated fields and under conditions in the cm accuracy range. The static measurements were conducted in an urban area, which yields difficulties in achieving cm-range accuracy. The results nevertheless show that the system is able to conduct position estimations under 2 cm up to a baseline of 2 kilometres. The accuracy involved is up to 180 times better, and the range up to 10 times higher than in comparable work. The conclusion is that it could be used as a basis for other technologies like auto-steering of tractors or other agricultural vehicles. The receivers need a line of sight connection between them to transmit the Radio Technical Commission for Maritime Services correction signals. In addition, the satellite constellation must have a position dilution of precision below 1.5, and no multipath errors should be present.

Keywords: differential global positioning system, real time kinematics, global navigation satellite system

Kurzfassung

Diese Arbeit untersucht das Verhalten von einem globalen Satellitennavigationsemfängersystem basierend auf Echtzeitkinematik, ohne zusätzlicher differenzieller globaler Positionssystemtechnologien wie dem Satelliten basierten Verbesserungssystem. Das System besteht aus zwei Empfängern, einer wurde als Referenzstation und der zweite als mobile Station verwendet. Die wissenschaftliche Herausforderung war es neue Hardwarekomponenten und Softwarealgorithmen in einer innovativen Art und Weise zu kombinieren, um damit ein System mit einer Genauigkeit im Zentimeter Bereich, mit einer Basislinie im km Bereich und mit Kosten von unter 1.000 Euro zu entwickeln. Das Systemverhalten wurde mittels dem Durchführen von statischen und dynamischen Messungen in verschiedenen Umgebungen mit sechs unterschiedlichen Antennen verifiziert. Die Messungen verbesserten auch das Wissen über den wichtigen Zusammenhang zwischen der Antenne zum Empfang von globalen Satellitennavigationssignalen und dem verwendeten globalen Satellitennavigationsmodul. Die dynamischen Messungen wurden auf Felder durchgeführt und unter diesen Bedingungen ist das System im Stande eine Genauigkeit im cm Bereich zu erreichen. Die statischen Messungen wurden im urbanen Gebiet durchgeführt und dabei hatte es Schwierigkeiten eine Genauigkeit im cm Bereich zu erreichen. Die Ergebnisse zeigen, dass es in der Lage ist Positionsabschätzungen unter 2 cm bis zu einer Basislinie von 2 Kilometern zu erzeugen. Die Genauigkeit ist bis zu 180 Mal besser, und die Reichweite bis zu 10 Mal höher als eine andere vergleichbare Arbeit. Die Folgerung daraus ist, dass es als Basis für andere Technologien wie autonomes Fahren von Traktoren oder anderen landwirtschaftlichen Fahrzeugen verwendet werden kann. Die Empfänger benötigen Sichtverbindung zwischen ihnen, um die Korrektursignale senden zu können, die Satellitenkonstellation muss eine Positionsabschwächung der Präzision unter 1.5 haben, und es dürfen keine Mehrwegfehler vorherrschen.

Acknowledgements

This thesis was written at the Institute of Computer Technology at the Technical University of Vienna. I would like to thanks my supervisors Univ. Prof. Dipl.-Ing. Dr. techn. Axel Jantsch and Univ. Ass. Dipl.-Ing. Stefan Wilker for their support during the thesis and for the opportunity to write my thesis on this topic.

Chapter 1

Introduction

This chapter provides a short overview of this work. It consists of three sections. The section "Motivation" answers the question of why this work is important and in what area the results can be used. The next section " Aim and Scope of this thesis" gives the reader an introduction into the thesis and answers the question of the scientific challenge involved and is followed by the section "Related work". This part gives the reader an impression of other similar studies or work which provide the foundation for my study. This chapter is concluded by the section "Thesis Outline" which introduces the other chapters of this study, and gives a brief review so that the reader may reference interesting topics.

1.1 Motivation

The Global Positioning System, or GPS, is widely used for different navigation applications ranging from autosteer technology used in agriculture [30], very specific geodesy tasks [15], to the tracking and tracing of trains [19]. GPS is also featured in autonomous devices like autonomous cars or drones, yet GPS alone would only provide a very limited accuracy resolution. Different augmentation methods are available for improving the accuracy in such a way that it suffices for the broad range of applications. Such augmentation methods like the differential global positioning system (DGPS) or real time kinematics (RTK) were used in high-cost industry solutions. The intensive research on this topic also made it possible to use the augmentation methods in low-cost devices for high-accuracy tasks. Other low-cost solutions are implemented, such as a single-frequency system which, however, leads to unacceptable accuracy of the position estimation for applications in the cm range. Additionally, the communication between the systems on the ground is hardly enough. This thesis tackles these questions from an electrical engineering perspective of the receiving devices in the satellite-to-ground and device-to-device communication.

1.2 Aim and Scope of this thesis

The aim of this thesis is to create a global navigation satellite system (GNSS) receiver system. Different commercial systems are available on the market and such companies as CaseIH or Trimble offer high-precision systems. Table 1.1 gives an overview of the situation as of the first quarter of 2020. To that extent, it is important to mention that the prices are from already used units since it is impossible to get any price information for new systems from the companies.

Table 1.1: High precision GNSSs on the market (First quarter 2020).

Company	Product	Price
CaseIH	FM 750 RTK	8.330 € [93]
Trimble	XCN-2050	5.998 € [17]
Trimble	Vario Guide RTK	10.115 € [92]
Trimble	FM 750 + EZ-Pilot	11.999 € [94]

This thesis compares the results with a Master's thesis already conducted in this field, namely, the work of Svatoň [87]. In terms of static measurements, the Svatoň system achieved the values in Table 1.2 and for dynamic measurements, as seen in Table 1.3 [87]. The baseline between both receivers was about 200 m and the costs of the electric components used, around 125 €.

Table 1.2: Results of static measurements by Svatoň.

Horizontal	Original [m]	Corrected [m]	Filtered [m]
DRMS	1.18-2.47	1.65-1.72	1.57
CEP (50%)	0.97-1.93	1.34-1.43	1.31
Vertical			
σ_{up}	1.22-1.76	1.65-2.83	2.78

Table 1.3: Results of dynamic measurements by Svatoň.

Horizontal	Original [m]	Corrected [m]	Filtered [m]
Arithmetic average	0.45-1.51	0.34-1.049	2.54
Vertical			
σ_{up}	1.01-1.49	0.96-2.37	2.14

This work should achieve an accuracy in the cm-range with a maximum baseline in the km-range and cost less than 1,000 €. New hardware components and software algorithms are combined in an innovative way to achieve these aims. If the system could accomplish an accuracy in cm-range, it would be suitable for high-precision navigation tasks like the automatic steering of agricultural systems.

The accuracy of the system is verified by means of conducting measurements with six different GNSS antennas and this approach should also increase knowledge of the relationship between the antenna selected, the accuracy and the robustness of the position estimation. It would be possible that, given a poor combination of GNSS antenna and GNSS module, the position estimation is nevertheless more inaccurate.

The proposed system therein consists of μ-blox f9p [102], an Arduino Nano [5] / Mega [4] as a micro controller unit (MCU) a power supply unit (PSU), a liquid crystal display (LCD) and antennas for receiving the GNSS-signals and for communicating wirelessly between both receivers. The rover could be connected or integrated to other embedded systems for a broad range of applications running on them, but this further integration does not fall within the scope of this thesis. The accuracy of the Arduino GNSS developed is tested by static and dynamic measurements in real application situations. The development of the different test set-ups is then integrated into this study. A theory chapter is included in this thesis which serves as the basis for the development of the entire system and only explains the functionality of global positioning system (GPS) and not other systems, like GALILEO [59], GLONASS [18] or Beidou [65], since the other systems are based on the same principles.

1.3 Related work

Related studies are the thesis of Svatoň [87] and Park [68]. Both studies implement different correction solutions. Park's work uses a satellite based augmentation system (SBAS) and online services, whilst Svatoň's work uses an implementation based on pseudo-range residuals and SBAS running on an Arduino Due [3]. The reference for this study is the thesis by Svatoň and the aim is to gain higher precision with a completely new design and circumvent the issue of a single frequency solution. The work of [33] was investigating the accuracy of industrial multi-GNSS receivers with precise point positioning (PPP). This study also involved static and dynamic experiments. Three different systems were used, including the Leica Viva GS10, Leica Viva GS15 and Trimble NetR9. In that study, the receivers were mounted on a truck. The static measurements reached a 2D accuracy of 19.6 mm and the dynamic ones, an average of 20.2 mm.
The novelty of this work lies in the usage of a multi-frequency GNSS with a complete new design and selection of new hardware and software algorithms working together. The system of Svatoň consisted of a μ-blox 6m [99], WiFi module ESP8266 [22] and an Arduino Nano. The reference station (RS) is based on an Arduino Due [3].
While Svatoň's work serves as the basis for this thesis, my study only uses the same principle design for the GNSS receiver system consisting of RS and the rover, but all hardware components and the algorithm for computing the GPS position are nevertheless completely different.

1.4 Thesis Outline

This thesis consists of seven chapters and this section gives a brief introduction into the following chapters. The next chapter "State of the Art" gives the reader a short overview on the development of GPS and how the system works. This chapter concludes with two sections which have a focus on a very brief introduction into two important and well-established correction techniques, which are SBAS and DGPS. It is followed by the chapter "RTK System proposal and design". In this chapter, the requirements of the low-cost Arduino GNSS are formulated. The entire hardware design and the software algorithms implemented are also introduced and characterized. The chapter "Test result demonstration and discussion" is then followed by a summary of the different test set-ups, as well as the most statically and dynamically significant test results based on them. It shows differences in the accuracy of the system used with and without correction measurements. Measurement results of the power consumption of the system are likewise included. The main part of this chapter is the discussion of the different test results. The Summary summarizes the most important findings of this thesis, while the chapter "Outlook" gives further ideas on future work. The chapter "Conclusion" summarizes the most important results gathered through the architecture implemented and provides insights on the system behaviour.

Chapter 2

State of the Art

This chapter contains two thematic sections - the first section focuses on the description of GNSS and GPS in a more in-depth discussion and the second section describes the most important position augmentation techniques.
GNSS is a feature which could be used for a broad range of applications and all these applications have different requirements. The first sections of this chapter additionally provide a brief introduction into the history and development process of GNSS, beginning with the first ancestor systems based on radio technology at the start of the 20^{th} century up to the latest improvements in GPS in the 21^{st} century. The following sections review the technique of positioning, errors to the system accuracy and different ways to improve the position quality. The emphasis of the discussion is on GPS. The last two remaining sections discuss the most important position augmentation techniques, which are SBAS and DGPS.

2.1 GNSS History

This section consists of six subsections and briefly gives the reader an introduction to the development process of GNSS technology. Ground-based navigation systems like long range navigation (LORAN) [25] or Decca were the predecessors of modern GNSS. In the very beginning of satellite-based navigation systems in the 1960s, the systems were only used by the military and in the following years, increasingly opened up for civil applications.

2.1.1 Radio based navigation systems

Radio-based navigation systems are mostly used today to enhance the overall performance of other navigation systems and had their peak in the 20^{th} century, but are still used in complementary ways or in different small areas. The German company, Schaller, invented the so-called dash-dot guiding path in 1907 [10]. Other applications like the very high frequency omni-directional range (VOR) or non-directional beacon (NDB) are based on this principle and still in use. The next two sections will cover two important radio-based navigation systems, which are the dash-dot system and LORAN.

2.1.2 DASH-DOT

The basic idea of the DASH-DOT system was to create a particular radiation pattern. Two identically crossed antenna loops were used to generate it. The improvement of this system was that both antenna loops were fed by the same signal source and each loop was fed with complementary currents. The result of this invention was that both antennas were transmitting the same pattern in a different rhythm, as illustrated in Figure 2.1. One was transmitting dot dash (. -) and the other was sending dash dot (- .). The dot dash pattern is equivalent to the Morse character A and the other pattern to the Morse character N [10].

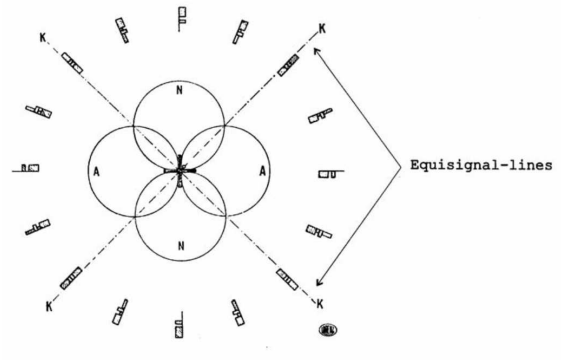

Figure 2.1: Principle of the dash-dot technique. With permission from [10].

In case of an aircraft, it is possible to hear the different letters while it is flying over an area which is covered by one of the antennas. The signal strength will increase if you are nearer to the antenna, and decrease if you are further away. This system is more or less just a simple audio-guided path for pilots.

2.1.3 LORAN

The development on the LORAN system started in 1940 by the US national defense research committe (NDRC) and its development continued after the second World War. The system is based on radio navigation and its aim was to be a long-range, precise aircraft navigation system. The requirements of the first system were to have at least a range of 322 km and an accuracy of 30.5 m. The system was improved several times and the requirements regarding range and accuracy increased with every system release. The successor of LORAN was LORAN-B and the last version is called LORAN-C. The requirements to LORAN-C were a range of 4023 km, which is 12.5 times more than the range of the first system, and features an accuracy of hundreds of feet. The successful path which semiconductors took in the 1970s made it possible to build up the system more cheaply and with less complexity. Marine and aircraft navigation used mainly LORAN-C but there are no further developments in the system at the moment. The system is still used to enhance the overall quality and robustness of a navigation system, seeing as GPS also has some weaknesses which could be overcome with LORAN-C. LORAN-C can, furthermore, be used where GPS-connection is difficult to establish, for example, in hidden areas. The LORAN system was designed based on one master and several slave stations. The master station transmitted the triggering impulses and the slave stations sent their impulses accordingly. The communication followed the pattern. That is, at first, the master had to transmit a defined set of patterns and after a fixed delay, the corresponding slave units sent their patterns. The system is based on a hyperbolic navigation principle and to achieve a surface fix, the receiver has to get signals from at least two different stations [61]. The position of the receiver can be

fully fixed if it is receiving signals from three different stations. First, the receiver decodes the signals from the master station and then waits for the corresponding signals to one of the slave stations. The position is defined on a hyperbolic curve where the time difference is constant, and this position is defined through the time delay between the signals from the master and slave station [25]. The receiver has to know the position of the base unit, and the distance between the master and slave units. This means that all receivers have to know all station positions and their corresponding information, which are stored in a database. The transmission of a full set of the navigation signals are repeated after the group repetition interval (GRI), and each chain of transmitting stations is characterized by one specific GRI.

2.1.4 Doppler-based navigation systems

The relative position is calculated by the frequency shift for Doppler-based navigation systems. If a transmitter moves and constantly sends a signal at a fixed frequency, the receiver obtains the signal with a higher frequency. Moreover, if the distance between transmitter and receiver gets smaller, but with a lower frequency, it gets larger [19]. These systems were especially used for atomic submarines, and were developed by the USA and USSR independently. The system was used in remote areas like the geographical poles, where radio-based systems were not applicable, but likewise used for sea rescue. It is possible to calculate the position of a disabled vessel with [19]

$$r = \frac{const\ c}{f_1 - f_2} \tag{2.1}$$

where

r is the distance of the disabled vessel to the transmitter,

c is the speed of light,

f_1 is the frequency, if the distance between transmitter and disabled vessel gets smaller

f_2 is the frequency, if the distance between transmitter and disabled vessel gets larger [19].

2.1.5 Transit / NAVSAT or navy navigation satellite system (NNSS)

The US NAVY was the first organization which had a working positioning system based on satellites. The system Transit or NAVSAT was operational in 1964, and in the first years, it was only used by military, but just three years after launch, it was also opened for civil ships [39]. Later on, the system was applied to other areas than ship navigation, such as hydro and geodetic research and very accurate time services. The system consisted of only six satellites, and they flew in the low earth orbit (LEO), which has an altitude of around two thousand kilometres. The satellites were placed in this altitude, since less energy was required to place them there and the communication latency is lower than in higher altitudes [78]. For example, the satellites for GPS are placed at an altitude of 20 thousand kilometres. The LEO-placed satellites had a wide radiation pattern due to the small number of them and their placement in low altitude. The respective user, however, could always use only one satellite at a time. The orbital period was 107 minutes, and as a result of the low number, and the time needed for one orbital period, the system was not time-continuous for the user. There were some improvements made during the operational phase and in the end, one satellite made it up to an availability of up to 30 minutes, and after this time, the next satellite was available for the user for a whopping 4 to 8 hours. Two carriers were transmitted by every satellite with a frequency of 150 and 400 MHz. The 150 MHz carrier was used to eliminate errors from the ionosphere [39]. The satellite movement caused a Doppler shift in the satellite frequency, and this shift was measured by one receiver. The calculation of the position on the surface depended strongly

on the Doppler shift measurement and the satellite parameters (ephemeris - which is the trajectory of a satellite) [105]. The position calculation and display were not done by a computer but a specialised receiver unit called AN/UYK-1 [95]. The entire decoding process took 16 minutes, and was based on the principles of bit overflow and sum. This was making the position location more difficult, seeing as the movement of the object (for example, a ship) has to be taken into consideration during the decoding process.

The accuracy of the entire position calculation was influenced by various factors, and in the following sections, the two main contributors are discussed. At the beginning of the usage, only single channel receiver units were used. These units, however, unfortunately yielded high inaccuracy due to ionospheric and tropospheric effects. These effects could even lead to a deviation of about 100 metres. It was possible to reduce the impact of these effects by using dual channel receivers. The deviation of the dual channel receivers dropped to values of between 18 and 35 metres, meaning the error was more or less only a quarter compared to the single channel receivers. The next important possible error in the calculation of the position was the result due the uncertainties of the satellite orbit. Long-term evaluation or translocation are methods for reducing the impact of this error. Compared to LORAN, TRANSIT offered different advantages, and the most important two were higher coverage and improved accuracy. The major drawback was the limited availability, since it was not possible to have a time-continuous navigation service. The system was working for 32 years and only finally came to a close in 1996. The successor of TRANSIT is GPS, which improved the quality and availability of a navigation system in many different ways.

2.1.6 Current GNSS situation

The US was leading in the development of a superior navigation system when they started the development of the US military project NAVSTAR – GPS in 1973. For the military, it was and remains important for delivering weapons precisely on target [40]. The new system features different advantages compared to TRANSIT, but the two most important were again improved accuracy and a higher availability, which made it possible to calculate the current position without any interruptions. GPS is described in more detail in the next section. Other countries also developed or are currently developing their GNSS. The next country with its own GNSS was Russia and their system is called globalnaja nawigazionnaja sputnikowaja sistema (GLONASS), and is developed and operated by the Russian Ministry of Defence [31]. The European Union (EU) started to develop their system called Galileo, and it has been operational since the 15^{th} of December 2016, consisting of 30 satellites. Galileo is led by the european global navigation satellite system agency (EGNSSA), which is a civilian organization, and one of the main goals of this system is to have a GNSS which is not controlled by a military [31]. China has also developed its own system called BEIDOU, which will consist of 35 satellites in 2020, and this system will be more accurate than all other systems. Currently, 21 satellites are already operational [72].

2.2 Principle of satellite navigation

The principles of navigation have been the same since sailors used sextants, and are illustrated in Figure 2.2. Prior to satellite navigation, seamen used the coordinates of three stars to locate their own position. The measuring of three stars thus involves three circles and their common point of intersection is the current position, but not the current longitude, as, the current time is also needed for determining longitude [18].

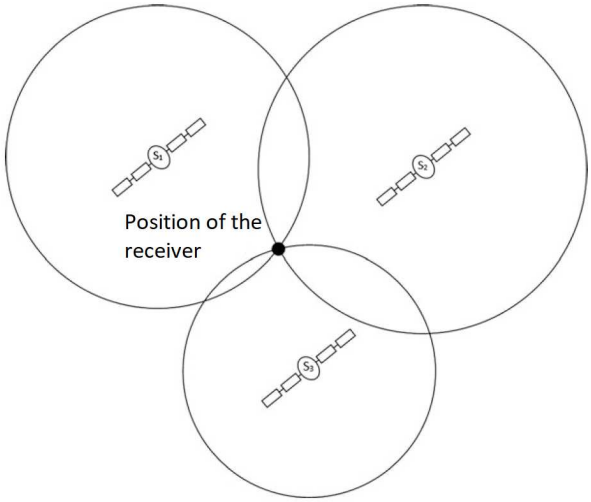

Figure 2.2: Principle of satellite navigation. With permission of [78].

GNSS replaces the stars, since the info about their exact position and the time when the signals are transmitted, are broadcast to the receivers, and it is possible to obtain the current position with the following four equations [18]:

$$\begin{aligned} d_1 &= \sqrt{(x_1 - x)^2 + (y_1 - y)^2 + (z_1 - z)^2} = c \cdot (t_1 - t), \\ d_2 &= \sqrt{(x_2 - x)^2 + (y_2 - y)^2 + (z_2 - z)^2} = c \cdot (t_2 - t), \\ d_3 &= \sqrt{(x_3 - x)^2 + (y_3 - y)^2 + (z_3 - z)^2} = c \cdot (t_3 - t), \\ d_4 &= \sqrt{(x_4 - x)^2 + (y_4 - y)^2 + (z_4 - z)^2} = c \cdot (t_4 - t) \end{aligned} \tag{2.2}$$

where

x, y, z and t are the four unknown,

x_i, y_i and z_i, is the position of a satellite,

d_i is the distance between the current position and a satellite,

t_i is the time at the receiver,

t is the time at the satellite and

c is velocity of light.

The accuracy of the position estimation is better if the satellites are in a more orthogonal position to each other [18].

2.3 GPS

NAVSTAR or GPS is currently the satellite system most widely used, but it is not possible to say which system will be the most used in the next years. It is used in a wide range of applications and they range from very precise navigations - systems used by civil and military aviation - to lightweight mobile devices. The development of NAVSTAR was divided into the following three phases [70], [87]:

- First Phase - 1973 - 1979 (Block-I): During this phase, a total of eleven space crafts were launched and the goal was to explore the basic principles of satellite positioning. Every spacecraft was equipped with three atomic clocks.
- Second Phase - 1979 - 1985 (Block-II): In this phase, 28 satellites were launched and every satellite featured four atomic clocks. The satellites were able to operate for 14 days without any corrections by the control centre. The development of the control segment began during this phase.
- Third Phase - 1985 - 1994: GPS reached in 1995 the full operational capability (FOC) status. The satellites of Block-I were replaced by all satellites launched during the second phase. The system consists now of 24 operational satellites. The satellites are orbiting in such a way so that all over the world, at any time, at least four satellites are visible. This means that it is possible to have correct localisation, which is also called the 3D navigational fix [19].

2.3.1 System composition

GPS consists of three segments like its ancestor TRANSIT and these are the cosmic, control and user segment [16]. The cosmic segment consists of the space crafts, while the different control stations on earth form the control segment. All the different receivers and users constitute the user segment [86]. The next sections introduce the different segments in more detail.

2.3.2 Cosmic Segment

This segment currently consists of 31 operational satellites, with at least 24 of them are always in operation at any given point in time [51]. The satellites orbit in six different equally-spaced planes and have an inclination of 55°. They fly in the medium earth orbit (MEO) at an altitude of around 20.200 km, which is an altitude ten times higher than the spacecraft of the TRANSIT system. One satellite needs 11 hours and 58 minutes for one orbit, which is the half of a sidereal day. The satellites currently operational are assigned to the following blocks of the time phases [78]:

- Block IIA (1990-1997) 1 satellite
- Block IIR (1997-2004) 11 satellites
- Block IIR-M (2005-2009) 7 satellites
- Block IIF (2010-2016) 12 satellites
- Block III/IIIF (2018 - today) 1 satellite in checkout

The satellites of the Block IIF currently have the most modern equipment, with improved atomic clocks and a 12-year lifespan for one spacecraft. The third generation of civil signals called L5 is also supported by them. It is transmitted at a frequency of 1176.45 MHz and has a greater bandwidth than the generations before, which leads to an improved resistance against jamming. The satellites also have an improved shielding against cosmic rays [50].
All satellites beginning from the Block IIR are able to communicate with each other. This communication feature makes debugging easier in the case of a malfunction. Currently, the last satellite was launched in 2018 which is a part of Block III/IIIF, but this satellite is inoperable at the moment. It is expected that, due to the limited lifespan, the older satellites will be replaced by satellites of this Block in upcoming years [50].

2.3.3 Control Segment

The control segment has to track the satellites, monitor their transmission, and do performance analysis [49]. In addition, commands and data are sent to the satellites. It consists of different kinds of facilities. It has a master control station, an alternate master control station, different monitor, control and tracking stations and some ground antennas. The different facilities have different tasks to fulfil.

The master control station has the following tasks [49]:

- It sends commands and controls to the GPS constellation.
- It uses the monitor stations' data to calculate the location of the satellites.
- Navigation messages are generated for the satellites and uploaded to them.
- Satellite maintenance and anomaly resolution are performed.

The monitor stations are responsible for the following tasks [49]:

- Satellites are tracked if they pass overhead.
- Navigation signals, range/carrier measurements and atmospheric data are collected.
- The master control station receives all observations from them.

The ground antennas have the following three tasks [49]:

- They transmit commands, perform navigation data uploads and processor program loads to the satellites.
- Telemetry data is collected.
- Communication is done via S-band (2 - 4 GHz) and additionally perform S-band ranging to provide anomaly resolution and early orbit support.

2.3.4 User Segment

The user segment consists of different receivers which can have very diverse purposes and requirements. The antenna of the different devices can receive the signal on different carrier frequencies, for example L1 (1575.42 MHz) and L2 (1227.6 MHz) [86]. It is possible to receive only one frequency or in the case of a dual band receiver, two. If an advanced receiver is desgined to meet the saftey-for-life transportation requirements, then it has to receive the signal on the L5 channel (1176.45Mhz) [86].

2.4 GPS signals

The satellites from the IIF generation are able to transmit information on three carrier frequency bands, called L1, L2 and L5. The bands used in this thesis are the L1 and L2 band and they are right-hand circularly polarized and derived from a fundamental frequency $f_0 = 10.23$ [86]. Meanwhile, binary phase shift keying (BPSK) is the code sequence used to modulate some carrier frequencies. Only two signal states are used by BPSK to transmit the signal and the different signals are detected due to the different phases of both states. The principle is illustrated in Figure 2.3 and the digital data

signal has only the states "0" and "1". To that extent, the transmitted signal only changes the phase, while the amplitude and the frequency remain unchanged.

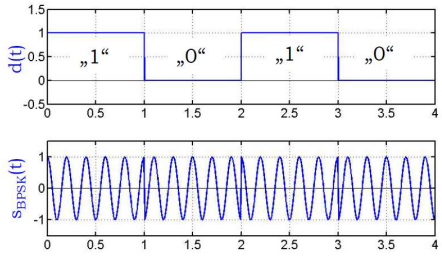

Figure 2.3: BPSK of a binary data source, with the permission of [28]

The receiver gets a clock reading and orbital parameters (navigation message) from the satellite [21] while the satellites transmit messages on the frequency bands L1, L2 and L5, and on all bands, different codes are transmitted. The *Coarse/Acquisition (C/A) code* is used for the standard positioning service (SPS). One sequence consists of 1023 bits and is repeated every millisecond and only transmitted on the L1 band [27]. The GPS L1 band is the most important band used for navigation applications [76]. All low-cost single band receivers work with L1 band and only C/A code ranging. The pseudo random noise (PRN) *C/A code* is a gold code of one millisecond in length, with a chipping rate of 1.023 Mbps.

The *precision code P(Y)* is used by the military and other authorised users. One sequence takes 266 days and every satellite transmits a part of it on a weekly basis; this part is called a PRN sequence. Every code uses a PRN sequence, which makes it possible to transmit different information at the same frequency, also known as code division multiple access (CDMA). The precision code is used to code the precision signal of the *P code*. It is available on L1 and L2.

A modernised civil signal is transmitted in the L2 band called L2C, together with the *P(Y)* and *M-Code*. Two additional PRN codes, called L2 CM (civil moderate) and L2 CL (civil long), are also transmitted in a time-multiplexed fashion. L2C makes it possible to remove ionospheric and tropospheric refraction in the code-ranging domain. On the other hand, however, special hardware is needed to be able to receive this signal properly. The L2C code could be used to develop low-cost dual-frequency civil GPS receivers. The L2C code has a higher effective power level than the L1 code and this makes it easier to receive the signal underneath trees or inside buildings [86]. Another signal used by the military is the *M-code*, which provides a better jamming resistance compared to the *P(Y) code*. The L5 band consists of two channels, called the data and pilot channel and is only broadcasted from IIF Block satellites. It has higher power and features an improved signal design compared to the L2 band, which makes it more robust against interference [86]. The different bands and the most important information about them are summarised in Table 2.1 [103].

Table 2.1: Transmitted codes of Block IIF satellites

Band	Code	Availability	Code frequency
L1	C/A (Coarse, Acquisition)	Civil	1.023 MHz
L1/L2	P(Y) (Precise)	Authorised	10.23 MHz
L2	L2CM	Civil	511.5 kHz
L2	L2CL	Civil	511.5 kHz
L1/L2	M (Military)	Authorised	5.115 MHz
L5	I/Q	Civil	10.23 MHz

The signal spectrum for the L1 band is illustrated in Figure 2.4 for the L2 band in Figure 2.5 and for the L5 band in Figure 2.6. The figures illustrate the already quadrature phase shift keying (QPSK) split components of the signals. The signal consists of one component in-phase (I) and the quadrature-component (Q). The quadrature component also has a phase shift of 90°. For example, in Figure 2.4, the *GPS C/A code* has only significant parts in the *in-phase component* and none in the *quadra-phase*. All figures illustrate the power spectrum density (PSD), which is the power distribution of the signal over the entire frequency spectrum [44].

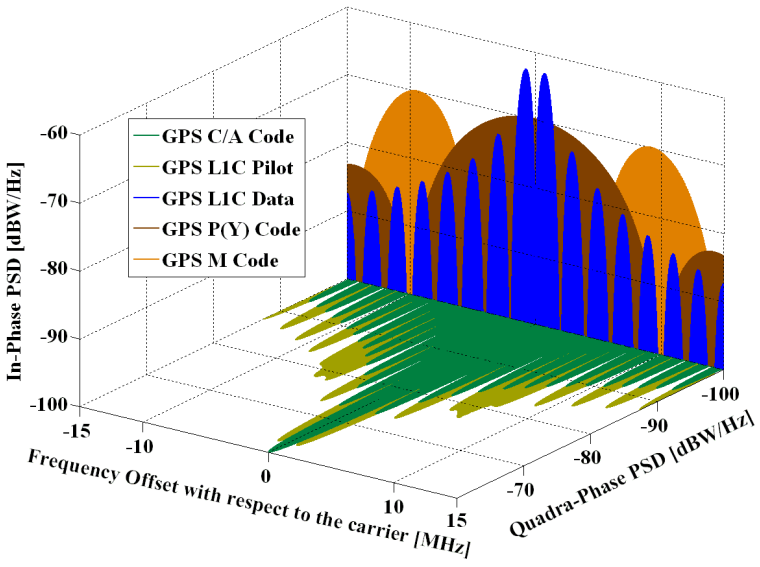

Figure 2.4: Signal Spectrum of L1 band, source: [76].

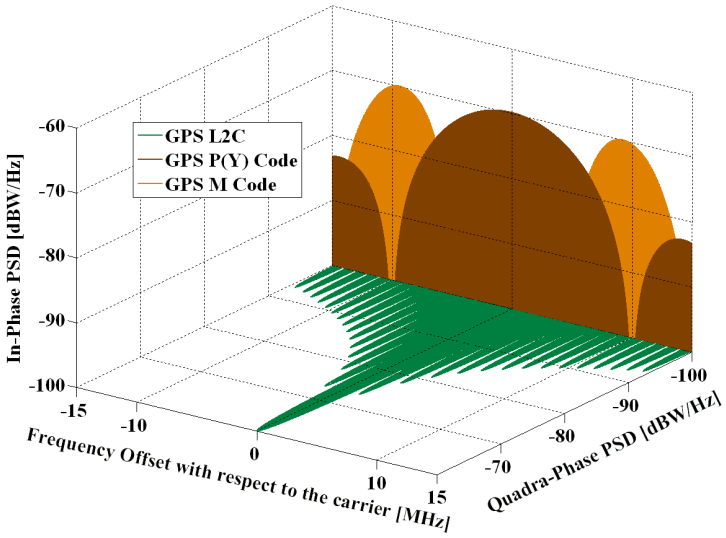

Figure 2.5: Signal Spectrum of L2 band, source: [76].

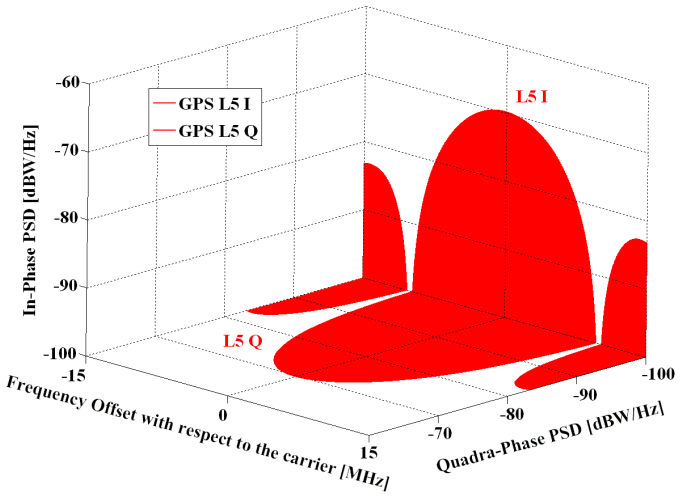

Figure 2.6: Signal Spectrum of L5 band, source: [76].

2.4.1 Code measurement determination

The *L1 band* is modulated by a *C/A PRN* which every satellite transmits. One of the tasks of the receiver is to demodulate the *L1 signal* and after demodulation, only useful signals are further processed. The PRN sequence for all satellites is known by the receiver. Through this knowledge, it is possible for the receiver to generate the same signal pattern for any dedicated satellite. There is no synchronisation to the GPS time for every signal generated by the receiver. There are three reasons for not synchronising this signal [44]. First, it is generated by a cheap crystal clock which is far more inaccurate than the atomic clocks on every satellite. The atomic clocks on the satellites are corrected and drift only about 1 ns per day [69], for which, however, without correction of the control segment, the error would always increase. What's more, the quartz crystal clocks in the receiver drift at about 0.1 ns per second, which amounts to 8640 ns per day [71]. The next reason is a time shift of the signal already received through the transmission delay required and the last is the clock bias that every satellite has. All PRNs received and all PRN generated are continuously split by the receiver. A correlation coefficient calculated by it indicates whether both signals have been synchronised. The receiver shifts it for a defined time span in order to determine which PRN has been received. Synchronisation is established when the

correlation coefficient is one and then both signals (generated and received *C/A PRN*) are subtracted. After subtraction, the receiver will have only the *C/A PRN* modulated by the navigation message. Now the signal is demodulated and the raw navigation message is ready for further processing. It is possible to find out the transmission time of the *C/A PRN* sequence by using the raw navigation message and the *C/A PRN* [44]. If you calculate the delay between the time of transmission and the arrival time of the *C/A* sequence at the receiver, you get the so-called, time of arrival (ToA). Moreover, the so-called pseudo range is calculated by multiplying the ToA by the propagation speed of the signal which approximately equal to the speed of light. The period of the *C/A* carrier (1.023 MHz), which is about 1 μs, is the minimal resolution for ToA calculations.

2.4.2 GPS access regulation

It is possible to limit the access to GPS in different ways. These limitations were implemented because GPS was developed for military purposes and these restrictions only apply for civil cases. The two ways to limit access are selective availability (SA) and anti-spoofing (AS) [32]. The purpose of SA is to reduce the position accuracy. This is achieved by deliberately introducing errors into the GPS signal. The errors are generated randomly, so it is very difficult to predict and mitigate them [19]. The error was up to 50 meters horizontally and 100 meters vertically. Two methods are used to degrade the signal.

- Introduce an error into the satellite clock frequency transmitted.
- Introduce an error into the ephemeris transmitted, which causes an error into the estimation of the position of the satellite and for that reason, it is difficult to correct the satellite clock bias. Until May 2000, only authorized users with special codes were able to mitigate the error caused by the first method. It was always possible to reduce this error by DGPS.

In May 2000, SA was turned off as a result of a decision by US President Bill Clinton and as of 2020, the US has no intentions of turning it on again [52]. AS remains a possible option which could be used by the US government, for example, in case of war or other exceptional events. The P-code of the GPS signal is transmitted without any encryption and this makes the system vulnerable to spoofing [47]. In case of spoofing, an unauthorised system transmits its own GPS messages and it is not possible for the receiver to detect this malicious behaviour. This attack can be suppressed by encryption of the P-Code and the encrypted code is then called Y-Code. If the encrypted signal is transmitted, it is not easy to just transmit a fake GPS message from an unauthorised system to the receiver. This also means that a receiver has to be able to decrypt the encrypted messages correctly [19].

2.5 GPS data

This section describes the different data protocols used by GPS and DGPS. It gives an introduction into the structure of the raw navigation message, the national marine electronics association (NMEA) 0183, radio technical commission for maritime services (RTCM), UBX and receiver independent exchange format (RINEX) messages.

2.5.1 Raw navigation message

The raw navigation message is broadcast between satellite and various receivers. On a defined carrier (L1, L2 or L5), there is a modulated message which is transmitted by a satellite. The so-called navigation message (NAV) is the useful

data at hand. The NAV is divided over 25 frames and one frame consists of five subframes. It takes 12.5 minutes to transmit an entire L1 NAV at a rate of 50 bits per second (BPS). The structure of an NAV L1 message is shown in Figure 2.7. Each subframe carries telemetry (TLM), handover words (HOW) and other data. TLM and HOW information are used to identify the subframe correctly. The first subframe carries clock correction data, the second and third, ephemeris data, the fourth almanac and refraction model data, and the last, only almanac data [19].

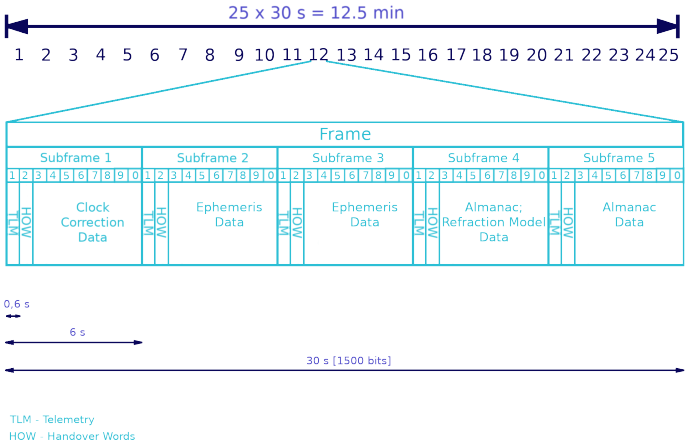

Figure 2.7: Composition of a NAV L1 frame, inspired by [78].

The most important part of the subframes is the ephemeris data. This data is used to estimate the satellite position by using orbital parameters. It consists of six Keplerian and different perturbation parameters, with all parameters as shown in Table 2.2. With these parameters, it is possible to estimate the line-of-sight (LOS) vector and the terrestrial position.

Table 2.2: Ephemeris parameters [54]

M_0	Mean Anomaly at Reference Time
$\triangle$n	Mean Motion Difference from Computed Value
e	Eccentricity
$(A)^{1/2}$	Square root of the semi-major axis
$(OMEGA)_0$	Longitude of ascending node of orbit pane at weekly epoch
i_0	Inclination angle at reference time
ω	Argument of perigee
OMEGADOT	Rate of right ascension
IDOT	Rate of inclination angle
C_{uc}	Amplitude of the cosine harmonic correction term to the argument of latitude
C_{us}	Amplitude of the sine harmonic correction term to the argument of latitude
C_{rc}	Amplitude of the cosine harmonic correction term to the orbit radius
C_{rs}	Amplitude of the sine harmonic correction term to the orbit radius
C_{ic}	Amplitude of the cosine harmonic correction term to the angle of inclination
C_{is}	Amplitude of the sine harmonic correction term to the angle of inclination
t_{oe}	Reference time ephemeris
IODE	Issue of data (ephemeris)

2.5.2 NMEA 0183

NMEA 0183 is the unified protocol used to provide GPS data in american standard code for information interchange (ASCII) format. This protocol is used by the different GPS receivers [85] and supports 19 different sentence types. Every

NMEA sentence starts with a $ symbol and is followed by a code word, which is used to identify the navigational system and sentence type. The code word has a length of five characters and the first two describe which system is used "GP" is used for GPS and "GL" for GLONASS. The other three characters are used to identify the sentence type and the three most important sentences are the recommended minimum specific (RMC), global positioning system fix data (GGA) and GPS, dilution of precision (DOP) and active satellites (GSA) [96].

- RMC contains minimum information needed like basic position coordinates, speed and course.
- GGA is used to synchronize time and for basic navigation applications.
- GSA carries the information which satellites were used to calculate the navigation solution [96].

2.5.3 RTCM

RTCM has been used by DGPS since 1985 as a standard for correction data transmission. Most receivers employed for maritime applications use this standard, but some companies have also developed their own data formats. For maritime and terrestrial differential satellite navigations systems, there is the RTCM 10402.3 Version 3.3, the current standard used [75]. In this standard, several message types are defined which provide correction data, and every message begins with a header and terminates with some parity bits. The message format of [75] version 3.3 is illustrated in Table 2.3.

Table 2.3: RTCM message format version 3.3 [43]

Preamble	Reserved	Message Length	Variable length Data message	Cyclic redundancy check
0xD3	6 bits	10 bits	0 - 1023 bytes	24 bits

In this thesis, the GPS information from RS to rover is transmitted with different RTCM messages of version 3.3 and these are the messages 1005, 1074, 1084, 1094, 1124 and 1230 [74]. In the RTCM-standard, different kinds of message groups are defined and the message 1005 belongs to the station coordinates group, while the messages 1074, 1084 and 1094 to the observations group, and message 1230 belongs to the auxiliary operation information group. There are also different sub-groups defined and message 1074 belongs to the GPS multiple single messages (MSMs), 1084 to the GLONASS MSMs, 1094 to the Galileo MSMs and 1230 to the GLONASS bias information sub-group. With the selected messages, it is possible to use the system for GNSS RTK standard precision operation, but not for high precision operation [74]. In message 1005, there are the earth-centered, earth fixed (ECEF)-coordinates of the antenna reference point (ARP) transmitted, whose format is illustrated in Table 2.4.

Messages 1074, 1084 and 1094 are all multiple single messages 4 (MSM4) and contain the full GNSS pseudo-ranges, phase-ranges and the carrier-to-noise ratio (CNR). The maximal length of these messages is 169 + Nsat*(18+49*Nsig), which is 3593 for Nsat = 16 and Nsig = 4, where Nsat is the number of satellites and Nsig the number of signals included in the message. During normal operation, however, the normal message length is anticipated to be shorter since not all satellites will transmit all signals constantly [74]. The pseudo-range [m] and the phase-range [m] of each signal of a satellite could be calculated with:

$$\begin{aligned} PseudoRange(i) &= \frac{c}{1000} * (Nms + \frac{RoughRange}{1024} + 2^{-24} * FinePseudoRange) \\ PhaseRange(i) &= \frac{c}{1000} * (Nms + \frac{RoughRange}{1024} + 2^{-29} * FinePseudoRange) \end{aligned} \tag{2.3}$$

Data Field	No. of Bits
Message Number	12
Reference Station ID	12
Reserved for international terrestrial reference frame (ITRF) Realization Year	6
GPS Indicator	1
GLONASS Indicator	1
Reserved for Galileo Indicator	1
Reference-Station Indicator	1
Antenna Reference Point ECEF-X	38
Single Receiver Oscillator Indicator	1
Reserved	1
Antenna Reference Point ECEF-Y	38
Quarter Cycle Indicator	2
Antenna Reference Point ECEF-Z	38

Table 2.4: RTCM Message 1005 - Coordinates of the stationary ARP.

Every MSM message is divided into three blocks, which are the message header, satellite data and signal data. The message header contains information about the satellites and the signals transmitted in the message. The satellite data contains information that are common for all signals of a given satellite (e. g. rough range) and the signal data information which are specific to every signal (e. g. fine range). The content of the message header for MSM-messages is illustrated in Table 2.5.

Data Field	No. of Bits
Message Number	12
Reference Station ID	12
GNSS epoch time	30
Multiple Message Bit	1
Issue of data station	1
Reserved	7
Clock Steering Indicator	2
External Clock Indicator	2
GNSS Divergence-free Smoothing Indicator	1
GNSS Smoothing Interval	3
GNSS Satellite Mask	64
GNSS Signal Mask	32
GNSS Cell Mask	X(X<=64)

Table 2.5: Content of an MSM message header.

The size of the cell mask depends on the number of satellites and signals in the message and is calculated with

$$X = Nsat * Nsig \tag{2.4}$$

where

$Nsat$ is the number of satellites, and

$Nsig$ is the number of signals.

The satellite data is only transmitted when in the header, the corresponding bit is set to 1 in the field satellite mask, as illustrated in Table 2.6

Data Field	No. of Bits
The number of integer milliseconds in GNSS satellite rough ranges	8*Nsat
GNSS satellite rough ranges modulo 1 millisecond	10*Nsat

Table 2.6: Satellite data for MSM 4 and 6.

The signal data contains only information to signals for which the bit was set to 1 in the cell mask and the structure for a MSM 4 is illustrated in Table 2.7.

Data Field	No. of Bits
GNSS signal fine pseudo ranges	15*Ncell
GNSS signal fine phase range data	22*Ncell
GNSS phase range lock Time Indicator	4*Ncell
Half-cycle ambiguity indicator	1*Ncell
GNSS signal CNRs	6*Ncell

Table 2.7: Signal data for MSM 4.

The message 1230 contains the information necessary for compensating the first-order inter-frequency phase range bias due to the base station code-phase bias, the structure of which is illustrated in Table 2.8.

2.5.4 UBX

Meanwhile, μ-blox developed their own binary protocol, which could be used to communicate between an μ-blox receiver and a host computer [100] and an overview of the protocol is shown in Figure 2.8. A message starts with the characters 0xB5 and 0x62 and the third byte carries the information if the message is a navigational configuration or monitoring message. The next byte is the message identifier and the fifth and sixth bytes contains the length of the message without synchronization characters, class, ID, length or checksum bytes. The payload could be of variable size up to maximal 65535 bytes and the two checksum bytes terminate this proprietary format [100].

Data Field	No. of Bits
Message Number	12
Reference Station ID	12
GLONASS code-phase bias indicator	1
Reserved	3
GLONASS frequency division multiple access (FDMA) signals mask	4
GLONASS L1 C/A code-phase bias	16
GLONASS L1 P code phase bias	16
GLONASS L2 C/A code phase bias	16
GLONASS L2 P code phase bias	16

Table 2.8: Content of RTCM message 1230.

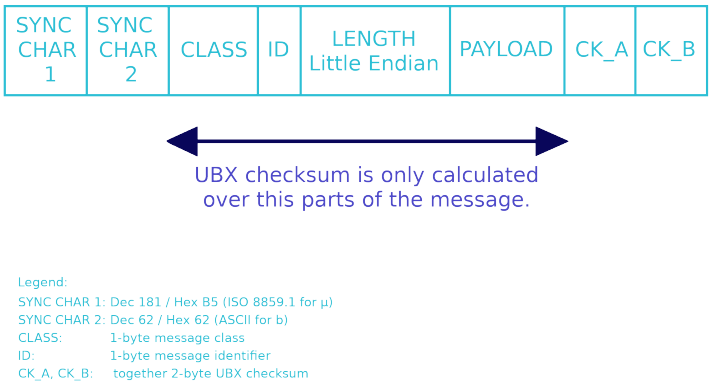

Figure 2.8: Proprietary μ-blox protocol, inspired by: [100].

2.5.5 RINEX

Another message format is the so-called RINEX format. The aim of this protocol is to preserve compatibility between different software applications due to the several data formats like NMEA or UBX [48]. It is in ASCII format and the current version is 3.04, consisting of three different files, with each file having a header. The header contains information about the RINEX version and global definitions of the data contained. The main content follows the header. The three different files are the observation, navigation file and the meteorological archive [41].

- The observation file contains information about pseudo-range, Doppler shift and raw observables.
- The navigation file features data about ephemeris, satellite time correction coefficients and other parts of the GPS NAV.
- The meteorological archive provides information about weather-like temperature and wind for atmospheric error modelling and is connected to a specific observed website.

RINEX is used by many professional software applications and is favourable for GPS data processing.

2.6 Reference System

A reference system is needed to be able to calculate the position of the receiver on earth. The parameters needed for the next computation step are defined within this system. All GNSSs use the space and earth reference system together to calculate the position correctly. The space system, also called inertial system, contains the information about the satellite movement (ephemeris).
The earth system, also called terrestrial system, contains the observer position.
The position in the earth system could be expressed in any kind of coordinate system, but by convention, the Cartesian (X, Y, Z) system is used. Another convention defines the position of the axes of the Cartesian coordinate system to have unity between all terrestrial ECEF and space earth-centered inertial (ECI) reference frames. The most important features of the systems are the following [86]:

ECEF

- The earth's geocenter is the origin of the coordinate system.
- The x-axis is connected to the mean Greenwich meridian and the equator.
- The z-axis is assigned to the axis of the earth rotation.
- The y-axis is orthogonal to the x- and z-axis [44].

ECI

- The x-axis points to the vernal equinox.
- The z-axis is the same as in the ECEF system.
- The y-axis is again orthogonal to the x- and z-axis [73].

The difference between both systems is that the space system does not move with the earth rotation but the terrestrial does, since it is fixed to the meridian of the earth and this means that the system changes its position with the rotation. Different GNSSs use different reference frames. For example, GPS uses world geodetic system 1984 (WGS84), GLONASS parametry zemli 1990 (PZ-90), and GALILEO uses galileo terrestrial reference frame (GTRF).

2.6.1 WGS84

GPS uses the WGS84 which is a 3-dimensional, terrestrial, global reference frame. In this system, the shape of the earth is defined by a set of constant variables and the origin is defined by the centre of the mass of the earth and the Greenwich meridian is used for defining the [78].
An ellipsoid is the model for the shape of the earth and is defined by the parameters of Table 2.9 [44].

Table 2.9: WGS84 Ellipsoid Parameter Set [44]

Parameter	Description
a = 6378137.0 m	Semi major axis of the ellipsoid
μ = 3986004.418 10^8 m^3/s^2	Gravitational constant of the earth
ω_e = 7292115 10^{-11} rad/s	Angular velocity of the earth
f=1/298.257223563	Flattening of the ellipsoid

The earth gravitational model 1996 (EGM96) is used by WGS84 to model gravity and in this model, a nominal sea level (geoid) is defined. Cartesian coordinates are used to compute a position, while the geodetic set of coordinates is used for navigation tasks. The geodetical set features the advantage that it is easier to use and a position on the earth is defined by three parameters, which are latitude, longitude and height [77]. The height perpendicular to the surface of the ellipsoid is used by GPS and this height is called height above ellipsoid (HAE), but this height is not used by navigation applications. The altitude used by them is the so-called mean sea level (MSL), which is the height above the geoid.

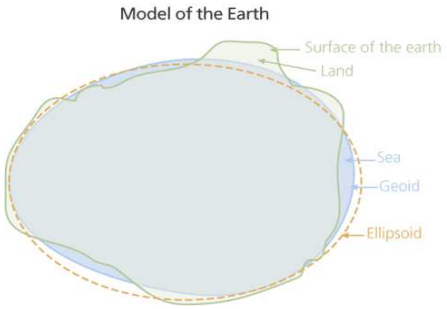

Figure 2.9: Difference between surface, geoid and ellipsoid. With permission of [23]

The difference between HAE and MSL is the so-called geoid separation N and the range of it is -105 $\leq$ N $\leq$ 85 m and it is calculated by [23]

$$N = HAE - MSL \tag{2.5}$$

There will be always a deviation between the real position on earth and the calculated position due the fact that the mathematical models used are a simplification of the real shape of the earth. The earth's shape is permanently changing. Sea level, for example, could change up to 0.7mm per year [60]. In such cases, the reference frames are updated from time to time [23]. Two parameters were used to take the changes of the earth into account. The first parameter is called *stability* and expresses the ability to predict the frame parameters. The other one is called*drift* and this parameter expresses the relative diversion between different frames.

2.6.2 Position quality

Specific systematic or random errors are generated by calculating the estimated position in the reference plane and the terms *precision* and *accuracy* are used to estimate them. *Precision* expresses the difference between one particular measurement to others. The standard deviation σ is used to define it and is calculated for every horizontal and vertical direction. It is expressed with [67]

$$\sigma_{1D} = \sqrt{\frac{\sum_{i=1}^{n}(x_i - x_t)^2}{n-1}} \tag{2.6}$$

where

x_i is the value of the measurement

x_t is the mean value overall measurements and *1D* represents one dimension.

The difference between the reference position and the position measured is expressed by the term *accuracy*. It is also calculated by using the standard deviation but instead of the mean value, the parameter x_t is used for the true position. The different standards use various respective definitions for the mapping of the position. Most times, it is connected to *confidence* and the *confidence* is expressed as a percentage value of $0 \leq$ *confidence* ≤ 1. Different percentage points involve various confidence levels defined in such a way that a certain number of measured points were inside

a circle or sphere where the maximum deviation defines the radius. The root mean square (RMS) is used to compress the deviations of all directions in one number and the result is called distance root mean square (DRMS). The DRMS is an indicator of the *accuracy* in two or three-dimensional space and for the two-dimensional space, it is calculated with [56]

$$DRMS = \sqrt{\sigma_x^2 + \sigma_y^2} \tag{2.7}$$

The circular Error probability (CEP) could also be used to calculate the *accuracy* in two-dimensional space, with a confidence level of 50 %. The CEP is one of several accuracy standards which are summarized in Table 2.10. It is often used by developers of GPS receivers due to the low confidence level which also produces small error values [56].

Table 2.10: Confidence levels and accuracy standards [56].

Confidence Level	Accuracy standard
CEP	50 %
$DRMS_{2D}$	65 %
2 $DRMS_{2D}$	95 %
3 $DRMS_{2D}$	97.5 %
1 σ_{1D}	68.27 %
2 σ_{1D}	95.45 %
3 σ_{1D}	99.73 %

2.7 Positioning Method

This section describes the methodologies of range measurement together with the core range positioning method.

2.7.1 Pseudo-code measurement

The range between satellite and receiver is measured based on the code-word frequency and is performed by the code measurement. The receiver calculates the ToA between the current time at the receiver (t_R) and the time of the satellite carried by an C/A word (t_S). There is a big difference between the quality of the time measurement between receiver and satellite due to the fact that the satellite is equipped with a very precise atomic clock, but the receiver only has an inaccurate crystal clock at its disposal. The GPS navigation system uses its own time system to achieve synchronisation between its different parts, but both the satellite and the receiver clock could deviate slightly from the system time. The difference between a satellite and the system time is called satellite clock bias (δ_S) and between receiver and system time, it is called receiver clock bias (δ_R). The time difference between satellite and receiver is calculated with [37] [43]

$$\triangle t = t_r - t_s = \triangle t(GPS) + \triangle \delta \tag{2.8}$$

and

$$\triangle \delta = \delta_R - \delta_S \tag{2.9}$$

and at the same time, the navigation message carries the satellite clock correction and is automatically applied to

the range measurement, which leads to

$$\triangle\delta = \delta_R \tag{2.10}$$

The GPS signal propagates with the speed of light c. It is also possible to calculate the range between satellite and receiver. The time difference between the satellite and the receiver is then multiplied by the speed of light to arrive at what is called pseudo-range R.

The pseudo-range R is calculated with

$$R = c \triangle t = c \triangle t(GPS) + c \triangle \delta \tag{2.11}$$

The frequency of the ranging code defines the precision of the pseudo-range measurement. The C/A code frequency is about 1 MHz and this leads to a wavelength of about 300 m, with a resulting error of about 1-2 % of the wavelength. This means that due the wavelength of the C/A code, the error is about 3 m [43] [37]. The resulting error can be minimized if the wavelength of the code is reduced and for example, the P-code has a code frequency of 10.23 MHz, which results in a corresponding wavelength of about 30 m and an error of 0.3 m. It is worth mentioning that in the error estimations above, no environmental errors like ionospheric and tropospheric influences were considered.

2.7.2 Pseudo-range phase measurement

The pseudo-range assessment is done by measuring the carrier phase of the GPS signal. The number of wavelengths between receiver and satellite are counted for the carrier phase measurement. It is difficult to evaluate the number of wave cycles between the receiver and the satellite and the result is called a wavelength cycle (N) , also referred to as *ambiguity* [43]. The final cycle used is only a fraction of the total number of wavelengths, but the receiver could easily estimate this partial length more precisely. The principal of the measurement is illustrated in Figure 2.10.

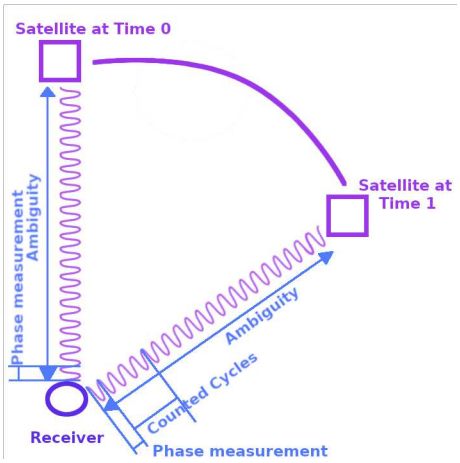

Figure 2.10: Principle of the measurement of the carrier phase. Inspired by: [53]

Different methods like Teunissen's LAMBDA or on the fly (OTF) could be used to calculate the *ambiguity*. After determination of the principal value of it, the receiver could detect the phase shift of the signal. The *ambiguity* is a part

of the formula for calculating the number of cycles of the measured carrier phase between receiver (r) and satellite j and the equation is [43], [37]

$$\Phi_r^j(t) = \frac{1}{\lambda}\rho_r^j(t) + N_r^j + f^j \triangle \rho_{RS}^j(t_0) \tag{2.12}$$

where

$\Phi_r^j(t)$ is the number of measured cycles of the carrier phase between receiver and satellite,

λ is the wavelength,

$\rho_r^j(t)$ is the geometric distance between receiver and satellite,

N_r^j is the *ambiguity* which is an integer.

f^j is the frequency of the carrier and

$\triangle\rho_{RS}^j(t_0)$ is the resulting clock bias between receiver and satellite.

The GPS L1 has a wavelength of about 19 cm which is the equivalent to a carrier frequency of 1575.42 MHz. The code based measurement uses a wavelength of around 300 m which is about 1500 times greater than the wavelength of this method. The maximum precision is equal to 1-2 % of the wavelength which would lead - by this kind of measurement - to an accuracy of around 38 mm. This implies that this method has a better accuracy and is used often in geodetic applications where such accuracy is necessary. This kind of measurement, however, also has a major drawback if the signal is interrupted. In the case of an interruption, the measurement has to start again from the beginning because the former *ambiguity* is lost due to the phase jump, which is also called cycle slip.
The pseudo-ranges and the satellite position are the basis of the position calculation while the position error depends on the precision of the pseudo-range measurement. All the prior statements about positioning error only take precision calculation into account but the positioning error is also influenced by other effects and these effects are clock, ionospheric, tropospheric, ephemeris and multipath errors and dilution of precision (DOP). The resolution of the different pseudo-range measurements techniques is summed up in Table 2.11.

Table 2.11: Phase and code pseudo.range techniques and their resolution

Technique	Frequency [MHz]	Wavelength λ	Resolution (1% λ)
Phase pseudo-range	L1 1575,42	$\approx$ 19 cm	$\approx$ 1.9 mm
Code pseudo-range	P 10.23	$\approx$ 29 m	$\approx$ 0.29 m
Code pseudo-range	C/A 1.023	$\approx$ 293 m	$\approx$ 2.93 m

2.7.3 Lateration

The position calculation could also be performed by using the range of observables and this method is called circular *lateration*. The calculation is based on solving the j non-linear equations of [43]

$$R^j(x,y,z) = c \triangle t^j(GPS) + c \triangle \delta = \rho^j + \triangle\rho_r^j + \triangle\rho^j + \triangle\rho_r \tag{2.13}$$

where

j is the number of the satellite to which the distance is calculated [43],

$$\rho_r = \sqrt{(X^j - x)^2 + (Y^j - y)^2 + (Z^j - z)^2} \tag{2.14}$$

$X^j Y^j Z^j$ are the ECEF coordinates of the j-th satellite,

x, y, z are the ECEF position coordinates which are of interest,

ρ^j is the geometrical range between the j-th satellite and the receiver

$\triangle\rho_r^j$ is the range bias, and this bias depends on the position of the satellite (it takes ephemeris, ionospheric and tropospheric effects into account),

$\triangle\rho^j$ is the clock error of the j-th satellite,

$\triangle\rho_r$ is the clock bias of the receiver r and takes the multipath error into account.

Three ranges to three different satellites have to be observed so that it is possible to accomplish a full 3-D fix (X, Y and Z) and this technique is called *trilateration*. The range calculated is called pseudo-range due to the difficulties and errors which influence the measurement. The least square method is used to solve the position problem iteratively but for this approach, the non-linear terms of equation 2.13 have to be linearised. The linearisation is done through the following equations [43]:

$$\begin{aligned} x_{tr+1} &= x_{tr} + \triangle x_{tr} \\ y_{tr+1} &= y_{tr} + \triangle y_{tr} \\ z_{tr+1} &= z_{tr} + \triangle z_{tr} \end{aligned} \tag{2.15}$$

where

tr is the number of iterations, x_{tr}, y_{tr} and z_{tr} are random position approximations and

$\triangle x_{tr}$, $\triangle y_{tr}$ and $\triangle z_{tr}$ are correction vectors.

The receiver position is calculated by adopting the values until no change occurs between two iterations. Three iterations are needed in most cases to get the receiver position. A Taylor expansion could be used to express the range equation after linearisation and for the position fix, only first order terms are needed whilst all higher terms are neglected and this leads to [43]

$$R^j(x_{tr+1}, y_{tr+1}, z_{tr+1}) = R^j(x_{tr}, y_{tr}, z_{tr}) + \frac{\partial R^j(x_{tr}, y_{tr}, z_{tr})}{\partial x_{tr}} \triangle x_{tr} + \frac{\partial R^j(x_{tr}, y_{tr}, z_{tr})}{\partial y_{tr}} \triangle y_{tr} + \frac{\partial R^j(x_{tr}, y_{tr}, z_{tr})}{\partial z_{tr}} \triangle z_{tr} \tag{2.16}$$

and the partial derivatives could also be expressed with [43]

$$\begin{aligned}\frac{\partial R^j(x_{tr},y_{tr},z_{tr})}{\partial x_{tr}} &= -\frac{X^j - x_{tr}}{\rho^j_{tr}} = a_j \\ \frac{\partial R^j(x_{tr},y_{tr},z_{tr})}{\partial y_{tr}} &= -\frac{Y^j - y_{tr}}{\rho^j_{tr}} = b_j \\ \frac{\partial R^j(x_{tr},y_{tr},z_{tr})}{\partial z_{tr}} &= -\frac{Z^j - z_{tr}}{\rho^j_{tr}} = c_j\end{aligned} \tag{2.17}$$

where ρ^j_{tr} is

$$\rho^j_{tr} = \sqrt{(X^j - x_{tr})^2 + (Y^j - y_{tr})^2 + (Z^j - z_{tr})^2} \tag{2.18}$$

after linearisation the pseudo-range equation has the form of [43]

$$R^j_{tr} = \rho^j_{r,tr} + \triangle\rho^j_{r,tr} - c \triangle \delta_{s,tr} + c \triangle \delta_{r,tr} + M_{tr} + a_j \triangle x_{tr} + b_j \triangle y_{tr} + c_j \triangle z_{tr} \tag{2.19}$$

and in matrix form it is [43]

$$\begin{bmatrix} -\frac{X^j - x_{tr}}{\rho^j_{tr}} & -\frac{Y^j - y_{tr}}{\rho^j_{tr}} & -\frac{Z^j - z_{tr}}{\rho^j_{tr}} & 1 \end{bmatrix} \begin{bmatrix} \triangle x_{tr} \\ \triangle y_{tr} \\ \triangle z_{tr} \\ c \triangle \delta_{r,tr} \end{bmatrix} = \\ R^j_{tr} - \rho^j_{t,tr} - \triangle\rho^j_{r,tr} + c \triangle \delta_{s,tr} - M_{tr} \tag{2.20}$$

consisting of the observation matrix H [43]

$$\begin{bmatrix} -\frac{X^j - x_{tr}}{\rho^j_{tr}} & -\frac{Y^j - y_{tr}}{\rho^j_{tr}} & -\frac{Z^j - z_{tr}}{\rho^j_{tr}} & 1 \end{bmatrix} \tag{2.21}$$

and the correction vector [43] $\overrightarrow{\triangle \mathbf{E_{tr}}}$

$$\begin{bmatrix} \triangle x_{tr} \\ \triangle y_{tr} \\ \triangle z_{tr} \\ c \triangle \delta_{r,tr} \end{bmatrix} \tag{2.22}$$

and the pseudo-range difference **b** between two iterations is [43]

$$R_{tr}^{j} - \rho_{t,tr}^{j} - \triangle\rho_{r,tr}^{j} + c \triangle \delta_{s,tr} - M_{tr} \tag{2.23}$$

The position shift is expressed by the pseudo-range difference **b**.
The finite correction vector $\overrightarrow{\triangle \mathbf{E_{tr}}}$ could be derived with

$$\overrightarrow{\triangle \mathbf{E_{tr}}} = (H^T H)^{-1} H^T \overrightarrow{b} \tag{2.24}$$

After a few iterations, the correct position is gained by the sum of the correction vector with the previous position estimation.

2.7.4 Doppler shift positioning

It is also possible to use the Doppler shift to calculate the position. The satellite transmits a signal with the frequency of L1 and due to the Doppler shift, the receiver will receive the signal with a different frequency f_r. A difference between the frequency received, f_r and a local frequency, f_0, is used to calculate the shift. It is calculated with a defined time interval to the next measurement and this interval is generated by the satellite (time mark [s]). The frequency difference is calculated by [87]

$$\triangle f = f_0 - f_r \tag{2.25}$$

At every time mark, the $\triangle$f period counting is started, and this counting could be calculated by solving an integral over time between two successive incoming signals and this could be done by [87]

$$N_i = \int_{t_i+\triangle_i}^{t_{i+1}+\triangle_{i+1}} \triangle f dt \tag{2.26}$$

where

$t_i + \triangle_i$ is the time when the time mark was received by the receiver,

$\triangle_i$ is the travelling time of the signal and

N_i is the result of one measurement.

It could be assumed that the period T between the received time marks is the same as the period between the time marks transmitted by the satellite and the resulting equation for calculating the position is [87], with

$$N_i = TF + \frac{f_0}{c}\left[\sqrt{(X_{i+1}-x)^2 + (Y_{i+1}-y)^2 + (Z_{i+1}-z)^2} - \sqrt{(X_i-x)^2 + (Y_i-y)^2 + (Z_i-z)^2}\right] \tag{2.27}$$

where

F is the frequency difference between transmitted and received frequency and

(X, Y, Z) are the derived coordinates from the ephemeris of the satellite.

Three successive measurements ,(N_i, N_{i+1}, N_{i+2}) have to be evaluated to solve the 3D position fix (x, y, z).

2.8 GPS errors

The pseudo-range measurement is influenced by different errors. The SA is the main limiting factor for the precision of the position calculation. The time when the message was sent is a very crucial parameter for estimating the pseudo-range correctly and this is a part of the navigation message of the C/A code. The errors influencing the GPS measurement are the

- Clock error
- Ionospheric error
- Tropospheric error
- Ephemeris error
- Errors due to multipath
- Dilution of precision

2.8.1 Clock errors

The atomic clock and the GPS time could slightly deviate from one other. This deviation between the two clocks is calculated and transmitted from the GPS ground segment to the satellites. The clock error is a part of the navigation message and used in the user segment. It is present in the message in the form of three coefficients. The satellite clock state is described by a polynomial model and these coefficients are a part of it. The state of it is calculated with [43]

$$\triangle t_{sv} = a_{f0} + a_{f1}(t - t_{0c}) + a_{f2}(t - t_{0c})^2 + \triangle t_r \tag{2.28}$$

$$t = t_{sv} - \triangle t_{sv} \tag{2.29}$$

where a_{f0}, a_{f1} and a_{f2} are the coefficients of the polynomial model,

t is the time of the GPS,

t_{oc} is the reference time of the last approach, and

$\triangle t_r$ is a relativistic correction due to the location in lower gravitational space of the satellite.

The current GPS time is then calculated by subtraction of the satellite clock correction of the original transmission time. It is important to note that the sensitivity of t_{sv} and t is negligible because equations 2.28 and 2.29 are coupled. Due to the negligible sensitivity, the user could approximate t by substituting it with t_{sv} in equation 2.28. The difference between the clocks could lead to a deviation of some meters or up to 10 ns between them.

2.8.2 Ionospheric errors

In the ionosphere, the signal propagation is different than in a vacuum and this difference causes the ionospheric error. The size of the error is dependent on the time of day since some lower ionospheric layers disappear during the night. Compared to the clock error, the deviation could be 10 times larger which means that it could deviate up to 100 m, but there are different models in use to reduce this error. For example, the ionospheric model proposed by J. Klobucher is used for many single frequency band low-cost GPS receivers. The polynomial coefficients of the navigation message are used in this empirical model of J. Klobucher and in his model, they are called alpha and beta. The coefficients are updated every 10 days and computed from a global, empirical model due to the fact that the delay of the signal in the ionospheric layers is caused by the electron content. The fluctuation of the electron content could be estimated and this could lead to a reduction of the ionospheric error of up to 50% RMS, which would imply that the error is cut from 100 m to 50 m [43].

2.8.3 Tropospheric error

The tropospheric error depends on the elevation of the satellite. The elevation is the angle between the satellite direction vector, with its origin at the user location, and the horizon plane. The troposphere has a range from the surface of the earth to about 40 km above it. Its low altitude is the reason for the dependency on elevation [43]. The current weather situation (temperature, humidity, pressure and others) influences the error and it could be up to 30 m in range. There are two kinds of categories of delays to the signal which are called hydrostatic and wet. The dry gasses in the troposphere are the reason for the hydrostatic delay while water vapour and clouds, which are a form of condensed water, are the reason for the wet delay. Fortunately, however, both influences can be measured very easily and are easy to predict. Empirical models use the estimated refraction index due to the meteorological data for calculating the tropospheric propagation delay. There is one important remark about this kind of error; the tropospheric environment is non-dispersive which means that there is no frequency dependency in the propagation delay. Due to the non-dispersive characteristic of the troposphere, for example, the L1, L2, phase and code measurement have the same delay, which makes the calculation easier [43].

2.8.4 Ephemeris error

The difference between the current satellite position and the position information in the navigation message is the so-called ephemeris error. The position estimation is done by these orbital parameters and there are three different types of them, including almanac, broadcast ephemerides and precise ephemerides [37]. Almanac carries the orbital information about all satellites and this information is valid for some months. This also means that this information does not contain any precise position values. Almanac is used to plot the satellite's visibility chart and for the initial locating of the satellite after power-up. Every satellite transmits broadcast ephemerides and this information contains precise values of the satellite position. The receivers use it for real-time satellite position calculation. The satellite transmits this information every 30 seconds and it is valid for half an hour.

The Naval Surface Warfare Centers have the precise ephemerides information. This information is based on historical observation and also contains prediction algorithms for future position estimation. It is available for about two weeks with a short time delay for post-processing tasks. This information is available free of charge. Table 2.12

Table 2.12: Different ephemeris erros and their resulting uncertainty [37].

Ephemerides error	resulting uncertainty
Almanac	≈ 2 km
Broadcast	≈ 1 m
Precise	≈ 5 - 20 cm

summarises the different ephemeris errors and the resulting uncertainty.

2.8.5 Multipath

If a signal is received via different paths, it is called multipath and this phenomenon is due to reflection on buildings, water planes and all other objects [44]. The receiver could, for example, receive one signal via a direct path and then also get the same reflected signal with some delay and phase offset, which means one signal with the same data is received more than once. One major drawback of this setup is that it is very difficult to mitigate. Multipath phenomena happen very randomly and also involve very different geometries. It is possible only to accept the shortest path without any reflections, since the direct signal path should always be the shortest. This functionality is difficult to implement and most low-cost GPS receivers do not possess this feature. It is also possible to use multi-band receivers in combination with L1 and L2 code and phase measurement to mitigate the problem [14]. For static objects, it is easier to mitigate this effect because you could just place the object in an area where no reflecting objects are nearby. Another possible solution for mitigating this effect is to use a higher elevation mask which would discard all low elevated satellites and their signals. Figure 2.11 shows principally how multipath could happen.

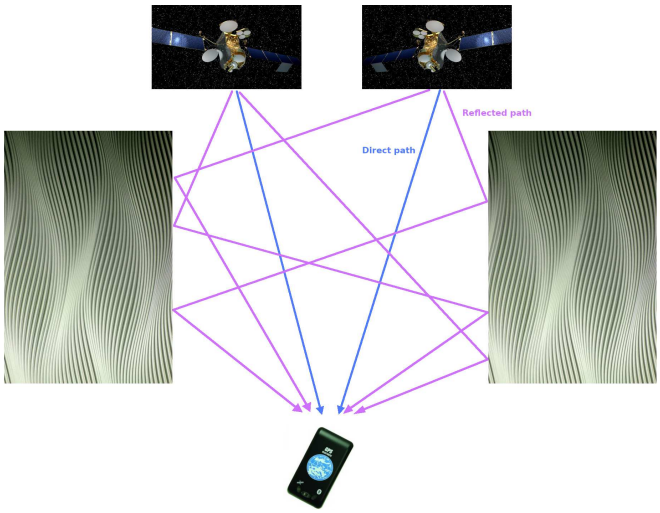

Figure 2.11: Multipath of signals, from sources [1], [55].

2.8.6 Dilution of precision

Satellite constellation is the main influence on DOP. The accuracy and precision of the position depends on the current satellite position, but it has an interesting behaviour [19].

If the distance between the satellites is bigger the precision is better and it is worse as many satellites are moved in together into a very small area. This unwanted behaviour is indicated with the DOP parameters. The relative position of the satellites to the other satellites are used to calculate the parameters and so it is possible to estimate the position precision, whereby a higher precision has smaller DOP values and a smaller precision has higher ones. There are four

kinds of DOP parameters and they are [19]

- horizontal dilution of precision (HDOP) - Horizontal deviation
- vertical dilution of precision (VDOP) - Vertical deviation
- position dilution of precision (PDOP) - All directions are taken into account to calculate this kind of deviation
- time dilution of precision (TDOP) - Time deviation

For example the values of PDOP has three categories of values which are the following [19]

- < 4 - The satellite geometry is good.
- 5 - 7 - The geometry is acceptable.
- > 7 - The geometry is poor.

Worse geometries can be discarded by the definition of a limitation mask.

2.9 Position augmentation techniques

This part describes two well-known *position augmentation techniques*, which are SBAS and DGPS. This section only focuses on them because both methods are used for GPS receivers.

2.9.1 SBAS

In civil aviation, SBAS is used to improve the GPS accuracy and it is used for GPS, GALILEO and GLONASS. Satellites are located in the geostationary orbit, which cover a defined region and these satellites transmit augmentation data to the receivers on GPS L1 frequency, so there is no additional hardware necessary for receiving these signals [19].
The information sent out contains correction data for satellite position and time bias and tropospheric and ionospheric errors. For all satellites which are in view at the moment of the ground segment correction, data is provided. A big advantage of SBAS is that it is available without any charges but it also has two major drawbacks. The major problems involved are the weak signal strength and the limited number of satellites which leads to limited coverage. Five SBAS types were developed to cover different regions of the world and their principal coverage is illustrated in Figure 2.12 [19].

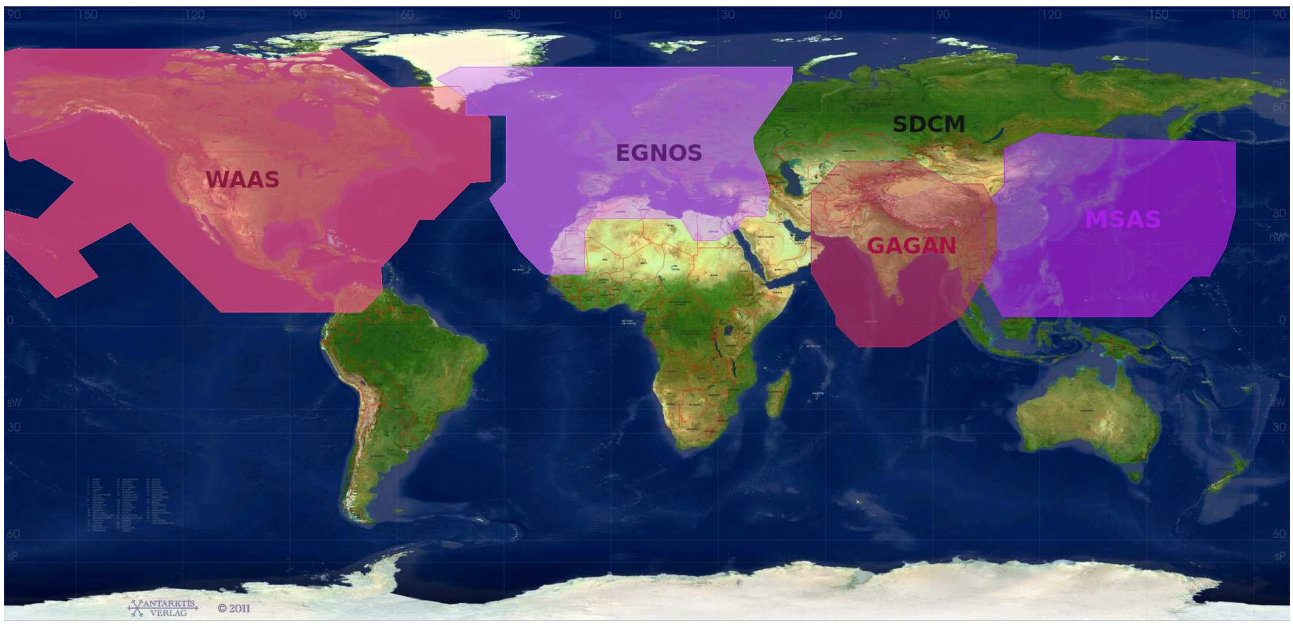

Figure 2.12: Overview of the coverage of the different SBAS systems, with the permission of [2], [13]

From the five different systems the european geostationary navigation overlay service (EGNOS) and the wide area augmentation system (WAAS) are discussed in more detail in the following sections.

EGNOS

EGNOS has been in operation since 2006 and was developed before GALILEO, with its main purpose being to improve the accuracy of GPS and GLONASS [19]. It consists of four segments which are the ground, support, space and user segment. A description of the different segments is summarised in Table 2.13 [24].

Table 2.13: Summary of the different segments of EGNOS [24]

Segment	Description
User	All receivers which could receive and parse a EGNOS signal, it does not require any additional hardware but additional software fo parsing the information correctly.
Space	Three satellites which transmit on GPS L1 PRN 120, 126 and 136 are the components of it. All satellites are placed on geostationary orbits (GEOs).
Support	The stations in this segment assist in operation planing and performance assessment and the facilities in this segment are the performance assessment and checkout facility (PACF) and the application specific qualification facility (ASQF).
Ground	It consists of 40 reference stations called ranging and integrity monitoring station (RIMS) which are spread out all over the world and navigation land earth stations (NLESs). The task of the RIMSs is to measure current errors of the GPS satellites with the information then transmitted to the master control centers (MCCs). The task of the NLESs is to upload correction data to the EGNOS satellites.

The accuracy gained has a confidence of up to 95 Information like satellite clock errors could change very fast and are transmitted as fast correction data and on the other hand, signals like ionospheric signal delay, ephemeris error or long-term satellite clock drift are transmitted as slow correction data. The major drawback of this system is that the signal is generally very weak. The satellites orbit above the equator and this is the reason for the poor signal strength. Especially in higher altitudes, the signal is lost very easily. It is worth mentioning, moreover, that it is possible to lose

the entire signal due to solar rays. Generally, it is not recommended to use SBAS for surface roving devices due to the problems of the signal strength. Another problem is the switching between normal mode and SBAS mode, which can lead to additional errors if the receiver is not well designed.

WAAS

The aim of WAAS is to improve the accuracy and integrity of air traffic in the USA. Any arbitrary receiver which receives GPS L1 and supports SBAS can access this data. The system also consists of three segments and the most important information about them is summarised in Table 2.14 [43]. It processes the information like EGNOS and also has two kinds of correction messages which are again fast and slow ones.

Table 2.14: Summary of the different segments of WAAS [44].

Segment	Description
User	Only high-end receivers which are a part of an aircraft avionic system.
Space	Three satellites which transmit on GPS L1 PRN 133, 135 and 138 are the components of it [29].
Ground	It consists of 38 reference stations called wide-area reference station (WRS) which are spread out all over the world. The task of the WRSs is to measure current errors of the GPS satellites and these information is transmitted to the wide-area master stations (WMSs).

2.9.2 DGPS

The aim of this section is to give a short introduction into the basic principles of DGPS, which should serve to mitigate the systematic error of SA. The position error without any augmentation techniques is in the size of hundreds of meters and through DGPS, it can be reduced to an accuracy of about 10 m. The basic idea of it is illustrated in Figure 2.13.

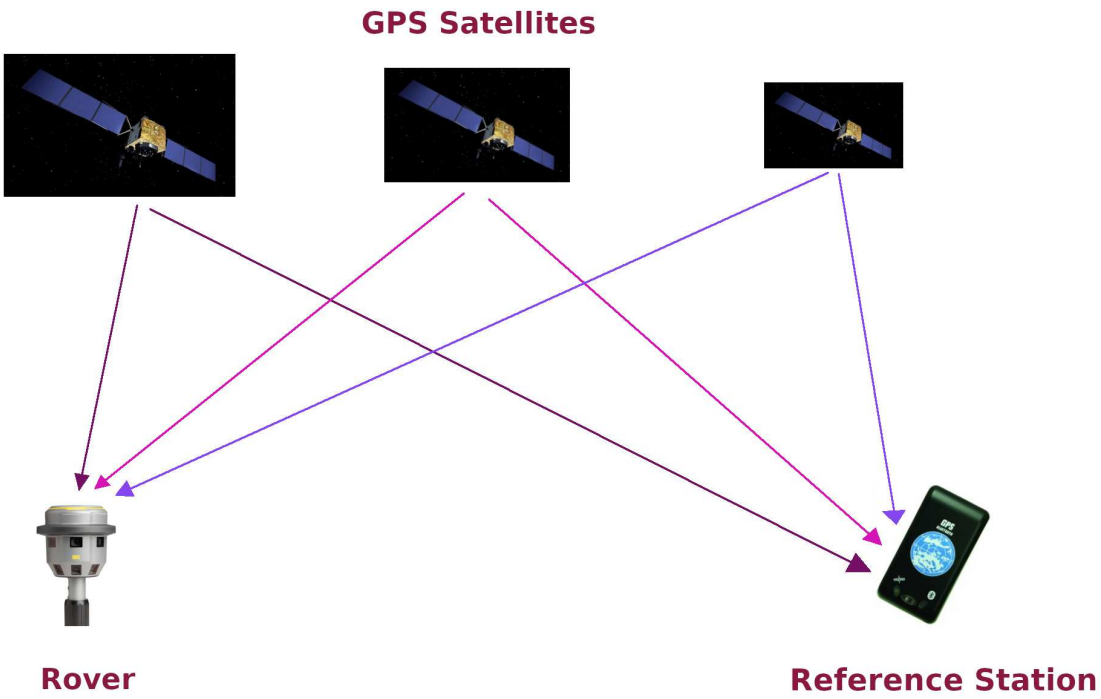

Figure 2.13: Basic idea of DGPS, with permission of [81]

.

The system consists of two parts, a so-called RS, and a so-called rover station. The RS is first placed in a stationary position with a known GPS location. It then calculates the difference between the GPS signal position received and the known position and this information is used by the rover. The rover station uses this correction information to improve its own position quality and therein mitigates the position error and accuracy [38]. This kind of correction is applied to position and range domain. DGPS is only possible if both receivers have at least a signal of four satellites which is equivalent to the permanent 3D fix [19]. During the time when SA was turned on for GPS, the precision can jump very quickly from 10 to 200 meters within a minute, but since it is turned off, the stability of the precision is much better. This leads to a higher robustness of DGPS because the rate of sending correction data still remains the same as during the time when SA is turned on.

Position domain DGPS

Position domain DGPS subtracts the known from the measured position and this difference is used to improve the measurement of the rover. The difference is added to the position of the rover which improves the quality of the estimated position. *Lateration* (Section 2.7.3 is used to iteratively measure the position of the RS. The correction of the position error δ_x is calculated with [68]

$$\overrightarrow{\delta}_x = \overrightarrow{X}_{RS,known} - \overrightarrow{X}_{RS} \tag{2.30}$$

The rover gets the correction from the RS transmitted and uses the data to mitigate the position error and to

improve the accuracy of the position, which is calculated with [68]

$$\overrightarrow{X}_{Rover,\text{DGPS}} = \overrightarrow{X}_{Rover,measured} + \overrightarrow{\delta}_x \tag{2.31}$$

The solution of equation 2.31 is, however, only valid if both stations calculate the position of the data of the same satellites. This assumption is, however, hardly always valid. If the station uses different satellites, then a different *observation matrix (H)* is calculated and this will increase the position error and not mitigate it. In the worst case, the position error is worse than without any augmentation technique. There are two possible solutions to this problem. One way to solve it would be to have both stations negotiate which satellites are used or the other way would be to have the RS calculate all possible solutions for all possible combinations of satellites in view. It is very difficult to get access to the satellite selection process of receivers and even high-end GPS receivers do not provide this feature.

Range domain DGPS

It is also possible to use the pseudo-range correction (PRC) of the individual satellites to mitigate the position error. The satellite constellation and the pseudo-ranges are used to measure the position. It is very important to know the current position of the satellite to compute the PRC. Most low-cost GPS receivers use ephemeris information to calculate the satellite position. The raw navigation message carries the information about the satellite position, whose true position can be calculated. The pseudo-range measured and the time bias are subtracted from the true satellite range to derive the PRC. The PRC can be derived by two means. The first way is via the code range and the second is via the phase range, both of which are discussed here.

Code range based DGPS

The method for doing the code based pseudo-range measurement was described in section 2.7.1.
The range measured is observable between the transmitted and the received code word, referred to as *code range R* and is calculated with [38]

$$R^j_{RS}(t_0) = \rho^j_{RS}(t_0) + \triangle\rho^j_{RS}(t_0) + \triangle\rho^j(t_0) + \triangle\rho_{RS}(t_0) \tag{2.32}$$

where
$R^j_{RS}(t_0)$ is the code range between the RS and satellite at each time t_0. The bias description is explained in equation 2.14.
A better approximation for the true range between the RS and the satellites can be derived by adding the PRC to the measured pseudo-range.
At the RS the pseudo range correction $PRC^j_{RS}(t_0)$ and the time derivative of the range rate correction $RRC^j_{RS}(t0)$ are calculated with [38]

$$PRC^j_{RS}(t_0) = \rho^j_{RS}(t_0) - R^j_{RS}(t_0) \tag{2.33}$$

$$PRC^j_{RS}(t) = PRC^j_{RS}(t_0) + RRC^j_{RS}(t_0)(t - t_0) \tag{2.34}$$

The PRC at time t is calculated by using the rate range correction (RRC). The pseudo-range variation depends on different interferences and the most important one was the SA. Currently, the RRC is very low (below 100 meters) because the SA was turned off and now the major interferences are due to variations of the ionosphere and troposphere. These variations are very difficult to predict and it is easier and better to set the RRC to zero. The rover station gets the PRC in real-time of the RS and estimates it in the same way as the RS does with the following equation [38]

$$R^j_r(t) = \rho^j_r(t) + \triangle\rho^j_r(t) + \triangle\rho^j(t) + \triangle\rho_r(t) \tag{2.35}$$

At the rover, the PRC is always added. The sign is selected in Equation 2.33 and the corrected pseudo-range is calculated with [38]

$$R^j_r(t)_{corrected} = R^j_r(t) + PRC_{RS}j(t) \tag{2.36}$$

while the corrected pseudo-range for the j-th satellite could be rewritten with [38]

$$\begin{aligned} R^j_r(t)_{corrected} &= \rho^j_r(t) + \triangle\rho^j_r(t) + \cancel{\triangle\rho^j(t)} + \triangle\rho_r(t) + \left(-\triangle\rho^j_{RS}(t) - \cancel{\triangle\rho^j(t)} - \triangle\rho_{RS}(t)\right) \\ R^j_r(t)_{corrected} &= \rho^j_r(t) + \left(\triangle\rho^j_r(t) - \triangle\rho^j_{RS}(t)\right) + (\triangle\rho_r(t) - \triangle\rho_{RS}(t)) \end{aligned} \tag{2.37}$$

It is possible to suppress the satellite clock error by subtracting the clock bias as in Equation 2.37. Furthermore, with another valid assumption, it is possible to simplify this equation further. There is a high correlation between the biases of the pseudo-range measurements of adjacent satellites and this fact allows for a cancelling out of atmospheric refraction and orbital errors. The second part of equation 2.37 is equal to the combined receiver clock bias without any multipath effects and the simplified equation is [38]

$$R^j_r(t)_{corrected} = \rho^j_r(t) + \left(\triangle\rho^j_r(t) - \triangle\rho^j_{RS}(t)\right) = \rho^j_r(t) + \triangle\rho_{r,RS}(t) \tag{2.38}$$

Phase range based DGPS

The second method for calculating the PRC is based on the measurement of the phase and this also relates to RTK. This method is used for applications which need a higher precision like geodesy or land survey and in principle, both methods' code range based-DGPS and phase range based-DGPS work very similarly. In this case, the pseudo-range could be expressed with [38]

$$\lambda\Phi^j_{RS}(t_0) = \rho^j_{RS}(t_0) + \triangle\rho^j_{RS}(t_0) + \triangle\rho^j(t_0) + \triangle\rho_{RS}(t_0) + \lambda N^j_{RS} \tag{2.39}$$

where all parameters are equal to the parameters of the code range measurement and

$\lambda\Phi^j_{RS}(t)$ $[m]$ is the calculated pseudo-range

λ is the wavelength and

$\Phi^j_{RS}(t)$ is the number of wavelength cycles, and

λN^j_{RS} is the ambiguity.

The PRC is then expressed with [38]

$$\begin{aligned} PRC^j_{RS}(t) &= \rho^j_{RS}(t_0) - \lambda\Phi^j_{RS}(t_0) \\ PRC^j_{RS}(t) &= -\triangle\rho^j_{RS}(t_0) - \triangle\rho^j(t_0) - \triangle\rho_{RS}(t_0) - \lambda N^j_{RS} \end{aligned} \tag{2.40}$$

The rover (r) receives the pseudo-range correction and the PRC is used in the pseudo-range calculation with [38]

$$\lambda\Phi^j_r(t) = \rho^j_r(t) + \triangle\rho_{r,RS}(t_0) + \lambda N^j_{r,RS} \tag{2.41}$$

where

$\triangle\rho_{r,RS}(t_0)$ is the calculated difference of the satellite positions based on range bias,

$N^j_{r,RS}$ is the calculated difference of the ambiguity between rover and RS.

It is important to mention that the relationship between phase based D DGPS and RTK is limited by the update frequency of the PRC and this latency, however, limits the relationship. If the update frequency of the PRC is close to zero, then the glsrtk specifications are equal to the precise phase DGPS.

2.9.3 Low-cost receivers and DGPS

Low-cost GPS receivers normally only use one channel and use only one basic navigation service like NMEA messages. This setting is normally sufficient for non-DGPS, but for DGPS, the pseudo-ranges and satellite positions also have to be known to calculate the DGPS position estimation correctly. A special algorithm was developed to enable DGPS with this kind of receivers, but this work does not use this algorithm due to improved hardware solutions and dual frequency solutions.

2.9.4 DGPS errors

DGPS could increase the precision of a receiver dramatically and the difference of the most important errors between a normal GPS and a DGPS receiver are summarized in Table 2.15.

Only the multipath error is not reduced but all other errors are mitigated through DGPS. The multipath error could not be mitigated because of the general situation. The RS station could be statically at a position without any multipath errors like an open area but the rover could nevertheless move around in the vicinity of buildings or other obstacles where this kind of error may randomly occur. The RS is not in the position to predict the multipath error of the

Table 2.15: Difference of errors between GPS and DGPS receivers [87].

Kind of error	DGPS C/A code range (m RMS)	GPS C/A code range (m RMS)
Satellite clock	0	1 - 3
Ephemeris	0 - 0.1	2.5 - 7
Ionospheric	0.1 - 1.5	2 - 15
Tropospheric	0.1 - 1.5	0.4 - 2
Multipath	2 - 5	2 - 4
Resulting range	2 - 6	4 - 18
Resulting position H	3 - 9	6 - 27
Resulting position V	5 - 15	10 - 45

rover and could not mitigate it. Satellite clock errors could be totally eliminated, however, since this error is done in the pseudo-range measurement and for different receivers, the error can be observed as equally large. Since the error can, in case of the different receivers, be equal, it can be subtracted accordingly. Ephemeris and ionospheric or tropospheric errors depend also on the distance between the receivers because at different locations, different errors are generated and the variance of these errors depends on the distance between both devices. If the distance increases, the variance also increases and this is the reason why this kind of error is only reduced but not totally eliminated. Generally, the position error of the rover should not be more than 10 m in a circumference of 100 km around the RS [87].

Chapter 3

RTK System proposal and design

This chapter describes the proposal for the RTK system and at the end of this chapter, the different components used for both stations are discussed and the software algorithms also implemented. An overview of the system is illustrated in Figure 3.1.

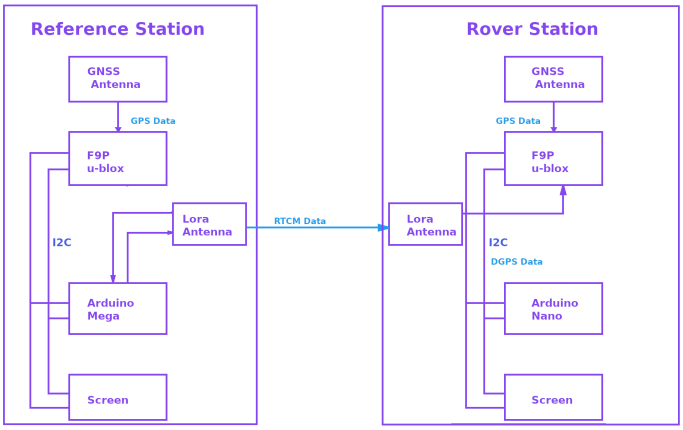

Figure 3.1: Overview of the RTK system

The system consists of two parts - one RS and a rover station. Both devices consist of five main elements which are the GNSS antenna, a μ-blox F9P, an Arduino Nano/Mega, a screen and a LoRa antenna. The computation of the RTCM data is done at the RS station in the μ-blox F9P. It is not necessary to compute it in the Arduino Mega. This improves the precision in the calculation of the PRC. The μ-blox F9P, moreover, features multi-band GNSS capabilities and this important feature is fully utilised in this thesis. The μ-blox F9P supports two frequencies from GNSS which are L1C/A (1572,42 MHz) and L2C (1227,60 MHz) [102]. This multi-band feature makes the entire design more reliable in areas where the GNSS-signal can be easily lost. The correction data is transmitted via the LoRa antenna from the RS to the rover in RTCM format. At the rover, the μ-blox F9P calculates the RTK solution and uses the GNSS data and the RTCM data of the RS which are received. In this thesis, one RS is connected to one rover. The advantage of this system is the compactness, because it consists only of elements which are necessary for engineering a RTK-system. One disadvantage is that the system only transmits corrected data from the RS to the rover via radio. This limits the

possible applications of the system, where line of sight exists or where no major obstacles stand between both receivers. This disadvantage could be avoided by using mobile communication modules in both stations and by using additional servers for temporarily storing the data and transmitting it from the RS via a mobile telecom provider via a server and then again via a mobile telecom provider to the rover. Another possible way to prevent these problems would be to use the network transport of RTCM via internet protocol (NTRIP) correction data for the rover. Both possible solutions would however increase the costs of the system and this is the reason why it was decided only to use radio connection between both receivers.

3.1 Functional proposal

This GNSS receiver system operates only in one mode. In this mode, GNSS data is processed by the μ-blox F9P chip and the resulting RTCM data is sent to the rover. The rover also receives GNSS data and uses the correction data of the RS to improve the quality of the GNSS solution and tries to get a RTK fix. In this mode, no additional computation is needed and the task of the Arduino Nano is only to set up the LoRa antenna and to initialize the μ-blox F9P along with the screen. It is possible to work only with this mode because of the design of the μ-blox F9P, which is illustrated in Figure 3.2. In the reference work, the μ-blox NEO 6 chip employed has a design as illustrated in Figure 3.3.

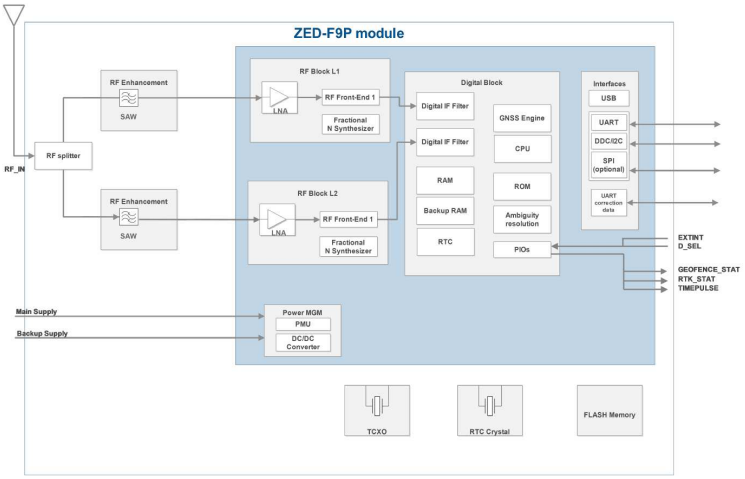

Figure 3.2: Block diagram of the μ-blox F9P, with permission of [102].

The μ-blox F9P has two single frequencies path and they are both synchronised.
This makes it possible to use only one F9P for calculating a RTK solution due to the dual frequency capability.

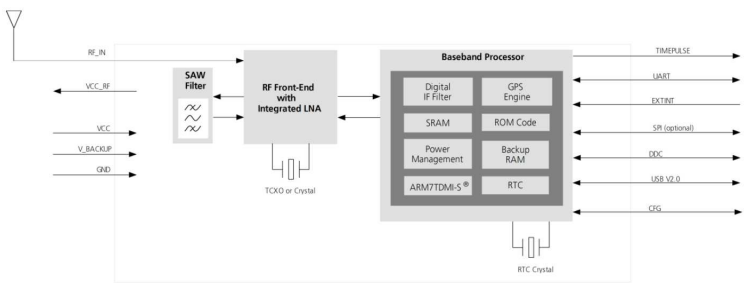

Figure 3.3: Block diagram of the μ-blox M6, with permission of [98].

3.2 GPS receiver settings

For the purposes of this thesis, a μ-blox F9P chip is used as a GNSS receiver module at the RS and rover and the general structure of it is illustrated in Figure 3.2. The settings used for both receivers are discussed in this section.

3.2.1 RS settings

Figure 3.1 illustrates the design of the RS. The Arduino Mega is the main component for controlling the entire behaviour of the RS and it sets the parameters of the μ-blox F9P and the LoRa antenna, which is an active antenna. The Arduino Mega first sets the settings for the F9P via I-Squared-C (I2C) and the most important are illustrated in Listing 3.1. The F9P is set to exchange data only in μ-blox format and then all RTCM message types, which are used as defined.

In this case the enabled RTCM messages are [100]

- 1005 - Stationary RTK reference station ARP.
- 1074 - GPS MSM4, MSM4 contains code, phase and CNR measurements [57].
- 1084 - GLONASS MSM4.
- 1094 - GALILEO MSM4.
- 1124 - BeiDou MSM4.
- 1230 - GLONASS code-phase biases.

The settings of the F9P and the LoRa antenna are both initialised together in the function *setup* and Listing 3.4 illustrates how the LoRa antenna is configured.

Listing 3.1: Settings for the μ-blox F9P at the RS.

```
//only u-UBX messages were exchanged between F9P and Arduino Nano
myGPS.setI2COutput(COM_TYPE_UBX);
//Save the current settings to flash and BBR
myGPS.saveConfiguration();

// very important settings.
// different RTCM formats
response &= myGPS.enableRTCMmessage(UBX_RTCM_1005, COM_PORT_I2C, 1);
response &= myGPS.enableRTCMmessage(UBX_RTCM_1074, COM_PORT_I2C, 1);
response &= myGPS.enableRTCMmessage(UBX_RTCM_1084, COM_PORT_I2C, 1);
response &= myGPS.enableRTCMmessage(UBX_RTCM_1094, COM_PORT_I2C, 1);
response &= myGPS.enableRTCMmessage(UBX_RTCM_1124, COM_PORT_I2C, 1);
//Enable message every 10 seconds
response &= myGPS.enableRTCMmessage(UBX_RTCM_1230, COM_PORT_I2C, 1);
```

After the initialisation of the F9P, it starts to receive GPS data and with the condition of Listing 3.2, it starts to transmit the RTCM data via I-Squared-C (I2C) to the Arduino Mega and proceeds to send that data - without any changes - over to the antenna. The *accuracy* of the signal has to be below 10 meters and it waits 60 seconds to start the transmission. The accuracy of the position estimation is calculated by a *weighted mean* method.

Listing 3.2: Start condition to transmit data at the RS.

```
    //60 seconds or 10 meters
    //both conditions have to be met.
    response = myGPS.enableSurveyMode(obs_time, mean_prec);
```

The source code of Listing 3.3 shows when the RTCM data is transmitted to the Arduino Mega. First the Arduino Mega waits until the conditions of Listing 3.2 are met and then it configures the F9P to transmit RTCM messages via the I2C bus.

Listing 3.3: Data transmission between F9P and Arduino Mega at the RS.

```
  //Begin waiting for survey to complete
  while (myGPS.svin.valid == false)
  {
    //get the accuracy every 2 seconds
    response = myGPS.getSurveyStatus(2000);
    delay(1000);
    ...
  }

  if (myGPS.svin.valid == true)
  {
    myGPS.setI2COutput(COM_TYPE_RTCM3);
  }
```

Listing 3.4 illustrates one part of the initialisation of the LoRa antenna. First, the Arduino Mega waits until the serial interface is ready and then it calls the function *lora_read_conf* where the current configuration is read out. The source code of function *lora_read_conf* is illustrated in Listing 3.5.

Listing 3.4: Set-up of the LoRa antenna at the RS.

```
void setup()
{
  pinMode(P1_ch, OUTPUT);
  pinMode(P2_ch, OUTPUT);



  Serial.begin(115200);
  Serialuno.begin(57600);

  //wait until serial interface is ready
  while (!Serial);

  lora_read_conf(InData, numbytes_in);
  show_lora_sett(freq, txRate, pwr);
  ...
```

Listing 3.5: Reading and writing the settings of the LoRa antenna at the RS.

```
void lora_read_conf(act_paramstruct_t *InData, int numbytes_in)
{
```

```
  boolean get_new_conf = false;

  byte *ptr = &(InData->preamble);
  byte *ptr_out = &(InData->preamble);

  lora_conf_mod(true);

  while (Serialuno.available())
  {
    Serialuno.read();
  }

  Serialuno.write(read_message, sizeof(read_message));
  delay(1000);

  if (Serialuno.available() > 0)
  {
    Serialuno.readBytes(inBuf, sizeof(inBuf));
    get_new_conf = true;
  }
  lora_conf_mod(false);

  if (get_new_conf = true)
  {
    for (int i = 0; i < numbytes_in; i++)
    {
      *ptr = inBuf[i];
      ptr++;
    }
    parse_read_conf(InData);
  }
}
```

The function call *lora_conf_mod(false)* configures the LoRa antenna so that it can receive data and *lora_conf_mod(true)* to receive settings. After *lora_conf_mod(false)* takes place, the serial buffer is emptied to be sure that no false data is transmitted to the antenna and then the data is sent to it [8]. A delay of 1 second is inserted [7] to leave in the necessary waiting time for the LoRa antenna to transmit data to the Arduino and the message is then read from the LoRa antenna until the buffer is full and the antenna is ready to receive data after the call of *lora_conf_mod(false)*. The source code of the function *lora_conf_mod()* is illustrated in Listing 3.6.

Listing 3.6: Switch between data and configuration mode of LoRa antenna at the RS.

```
void lora_conf_mod(boolean val)
{
        if (val == true)
        {
                change_baud(9600);
                //settings to the LoRa antenna
                digitalWrite(P1_ch, HIGH);
                digitalWrite(P2_ch, HIGH);
```

```
                delay(3000);
        }
        else
        {
                delay(1000);
                change_baud(57600);
                //data to the LoRa antenna
                digitalWrite(P1_ch, LOW);
                digitalWrite(P2_ch, LOW);
        }
}
```

Listing 3.6 illustrates that the antenna can only receive configuration information with a baud rate of 9600, but it could process data with different baud rates and in this case, 57600 is selected [45]. Through the LoRa interface, only RTCM messages are transmitted and on average, not more than 8213 bps are sent from RS to rover [74]. It is not allowed to have an update rate of RTCM messages at the RS higher than at the rover, or, otherwise, cyclic slip correction stops working properly. Nevertheless, the design at the F9P recommend higher rates than 38400 baud due to the capacity on the universal asynchronous receiver transmitter (UART) interface [101]. Baud rates below 19200 baud would be only possible to use if the rover also updates its own RTCM calculation with lesser frequency than selected. Both configuration pins are set to the documentation of the antenna accordingly. If both configuration pins are set to high, the antenna goes into *setup mode* and can then be configured, while if both pins are set to low, it then goes into *normal mode* [45]. It also provides two additional modes, which are the *wake-up mode* and the *power-saving mode* and these modes are not used, however, because the antenna has to always be transmitting data between both stations. The data received is processed in the function *parse_read_conf* and in this function, only valid data is parsed and the frame of a valid response is illustrated in Table 3.1.

Table 3.1: Valid response of LoRa antenna to a settings request [45].

Content	Preamble	Model Name	FW Version	LoRa MAC Address	Group ID	RF Frequency
Value	0x24	any value	any value	any value	any value	any value
Number of bytes	1	4	7	8	1	3
Start byte number	0	1	4	11	19	20
Content	RF TRx Rate	RF Power	UART Baud Rate	UART Parity	Wakeup Time	End Word
Value	any value	any value	any value	any value	any value	0x21
Number of bytes	1	1	1	1	1	1
Start byte number	21	22	23	24	25	26

Listing 3.7: Parsing of data received from the LoRa antenna at at RS.

```
void parse_read_conf(act_paramstruct_t *InData)
{
    if (InData->preamble == 0x24 &&
        InData->endw_29 == 0x21)
    {
        //txrate = baudrate of the LoRa antenna
```

```
    //for free space signal transmission

            // set the tx rate
            switch(InData->trxrate_24){
              case 0x00: txRate = 0.81;
                break;
              case 0x01: txRate = 1.46;
                break;
              case 0x02: txRate = 2.6;
                break;
              case 0x03: txRate = 4.56;
                break;
              case 0x04: txRate = 9.11;
                break;
              case 0x05: txRate = 18.23;
                break;
            }
            // set the power
            switch(InData->rfpwr_25){
              case 0x00: pwr = 6;
                break;
              case 0x01: pwr = 8;
                break;
              case 0x02: pwr = 10;
                break;
              case 0x03: pwr = 12;
                break;
              case 0x04: pwr = 14;
                break;
              case 0x05: pwr = 16;
                break;
              case 0x06: pwr = 18;
                break
              case 0x07: pwr = 20;
                break
            }
...
    unsigned long freq_value = (unsigned long)str[0] << 16
                             | (unsigned long)str[1] << 8
                             | (unsigned long)str[2];
    // set the frequency to the
    // calculated one
    freq = freq_value;
...
```

The values received from the LoRa antenna are displayed in another function for allowing feedback on the current settings. After the initialisation of all parts, the GNSS data which comes in is updated every 0.5 seconds and transmitted to the antenna, as illustrated in Listing 3.8.

Listing 3.8: Sending data from μ-blox F9P to the LoRa antenna at RS.

```
void loop()
{
        //calls processRTCM
        myGPS.checkUblox();
        delay(500);
}


void SFE_UBLOX_GPS::processRTCM(uint8_t incoming)
{
        Serialuno.write(incoming);
        delay(1);
}

}
```

For every data byte the function *processRTCM* is called and every byte is sent via the serial interface of the Arduino to the antenna [83].

3.2.2 Rover settings

Meanwhile, at the rover, the Arduino Nano also sets the configuration for the LoRa antenna and the F9P. The initialisation is done in the function *setup*, as illustrated in Listing 3.9.

Listing 3.9: Initialisation of the LoRa antenna and F9P at the rover.

```
void setup()
{
    Serial.begin(9600);
    portOne.begin(9600);

    pinMode(p1_ch, OUTPUT);
    pinMode(p2_ch, OUTPUT);

    digitalWrite(p1_ch, LOW);
    digitalWrite(p2_ch, LOW);
    Wire.begin();
    delay(1000);

    //Connect to the u-blox module using Wire port
    if (myGPS.begin() == false)
    {
        Serial.println(F("Ublox GPS not detected"));
        while (1);
    }
    delay(1000);
    lora_read_conf(InData, numbytes_in);

    show_lora_sett(freq, txRate, pwr);
}
```

First, it is checked to see if there is a connection to a F9P and then the settings of the LoRa antenna are checked and set the RS in analogue. The default settings of the F9P and the LoRa antenna are used to process the data from the RS. The default settings of the F9P already has the ubx, NMEA and RTCM 3.3 protocols enabled and in this thesis, the rover uses as additional input, namely, the RTCM correction data of the RS [101]. The rover enters the RTK float mode as soon as the first RTCM correction messages have been processed. The RTK float mode implies that the ambiguity resolution is not an integer but a floating point number, and this takes place at the initialisation phase or in case of a low number of satellites or a poor satellite constellation being currently available [20]. If the satellite constellation is good, the rover enters into RTK fix mode with an *accuracy* at cm-level, whereupon, the rover transmits NMEA messages to the Arduino Nano and the Arduino Nano redirects the information directly to the screen.

3.3 Data Transmission

The RTCM correction is transmitted from the RS to the rover via the LoRa antenna [101]. The antenna transmits the data at 57600 BPS and at a frequency of 862 to 1020 MHz. The F9P only supports RTCM messages from version 3.3 and the RTCM messages 1074, 1084, 1094, 1124 and 1230 are transmitted from the RS to the rover in this thesis. The F9P implemented the RTCM message formats according to RTCM STANDARD 10403.3 DIFFERENTIAL GNSS but unfortunately, this standard is not free of charge [100].

3.4 GNSS module

The μ-blox ZED-F9P is used as a GNSS module and it is illustrated in Figure 3.4.

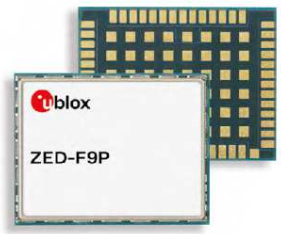

Figure 3.4: μ-blox ZED-F9P, with the permission of[102].

It is a multi-band receiver and provides multi-band RTK. Furthermore, the F9P has an update rate for raw GNSS navigation messages of 25 Hz and of RTK messages of 20 Hz. It supports the L1C/A band (1575.42 MHz) and the L2C band (1227.60 MHz) and also two bands of every other GNSS. If the device is operating in RTK mode, then only RTCM messages of version 3 are supported. It supports the NMEA, RTCM 3.3 and ubx protocols. The operational voltage is 3.3 V. It provides different communication interfaces like UART, serial peripheral interface (SPI), I2C and universal serial bus (USB). In this thesis, the F9P communicates with the Arduino Mega/Nano via I2C and to the LoRa antenna via an SPI interface [102]. For both stations, the GPS-RTK2 Board of Sparkfun is used, as illustrated in Figure 3.5.

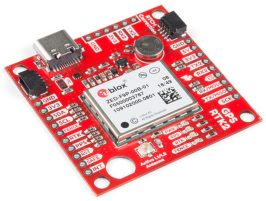

Figure 3.5: SparkFun ZED-F9P Board. Source: [82]

3.5 Antenna

For the communication between the RS and the rover, the LoRa antenna LM-210 is used, as illustrated in Figure 3.6.

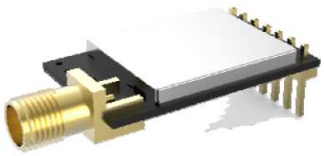

Figure 3.6: LoRa antenna, with the permission of[45]

The antenna is designed to transmit data over distances of between 1 and 10 km (10 km at a data rate of 0.81 kilobits per second (Kbps)) and the maximum power transmission is 100 mW, which is in the magnitude of a wireless local area network (WLAN) antenna. The antenna communicates in a frequency band of 862 to 1020 MHz and is of the type 210 H. It is possible to select between different baud rates from 1200 to 57600 BPS. The maximum receiving sensitivity is -132 decibel-milliwatts (dBm) at a rate of 0.81 Kbps [45].

3.6 Micro controllers

The main controller for the rover is the Arduino Nano and the micro controller on it is a ATmega168-20AU and the entire board is illustrated in Figure 3.7a [6]. For the RS, it is the Arduino Mega, as illustrated in Figure 3.7b [4]. At a frequency of 20 MHz, the controller process data, has a static random-access memory (SRAM) of 6 KB, a flash memory of 48 KB and an electrically erasable programmable read-only memory (EEPROM) of 256 bytes. The micro controller on the mega is a ATmega2560 and it has SRAM of 8 KB, a flash memory of 256 KB and an EEPROM of 4 KB, with a clock speed of 16 MHz.

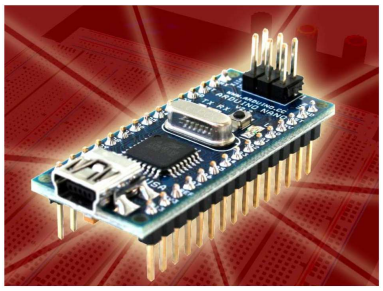

(a) Arduino Nano. Source: [6]

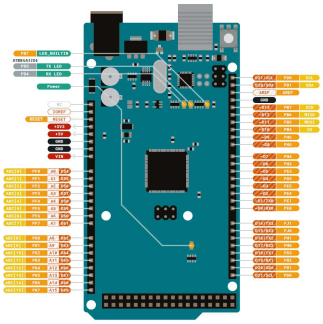

(b) Arduino Mega. Source: [4]

3.7 GNSS antenna

It is recommended to operate the F9P only together with an active antenna [101]. Different antennas are used in this thesis to explore the influence of the antenna on the accuracy of the position estimation. An overview of the different antennas used in this thesis is illustrated in Table 3.2.

Table 3.2: GNSS Antennas

Company	Antenna Name	Gain [dB]	Supported GNSS
Harxon	D-Helix HX-CHX600A	33	GPS, GLONASS, GALILEO, BEIDOU [36]
	UAV/Helix HX-CH6601A	33	GPS, GLONASS, BEIDOU [34]
	D-Helix HX-CH7603A	33	GPS, GLONASS, GALILEO, BEIDOU [35]
TAOGLAS	AQHA.50	18-27	GPS, GLONASS, BEIDOU [89]
	GPSF.36.7.A.30	no gain	GPS, GLONASS, GALILEO, BEIDOU [91]
	GPDF.47.8.A.02	no gain	GPS, GLONASS, GALILEO, BEIDOU [90]
	A.80.A.101111	no gain	GPS, GLONASS, GALILEO, BEIDOU [88]
μ-blox	ANN-MB	28	GPS, GLONASS, GALILEO, BEIDOU [97]

3.8 Screen

The status of the RS and rover is displayed on a LCD screen. It has a size of 98x20 mm and displays 4x20 characters [42]. It is illustrated in Figure 3.8.

Figure 3.8: LCD screen used. Source: [42]

It could be programmed via I2C. The screen could be operated at voltage levels of 3.3V up to 5V. An existing library for the communication with the Arduino platforms is used and code was written only at an application level.

3.9 Hardware design of the RS and the rover

The printed circuit board (PCB) design between RS and rover is different because the rover will also have additional components needed for other tasks on the board. Both prints were designed in Eagle, which is an electronic design automation (EDA)-tool for this purpose. The schematic of the RS is illustrated in Figure 3.9 and the layout in 3.10, and for the rover, in 3.11 and in 3.12.

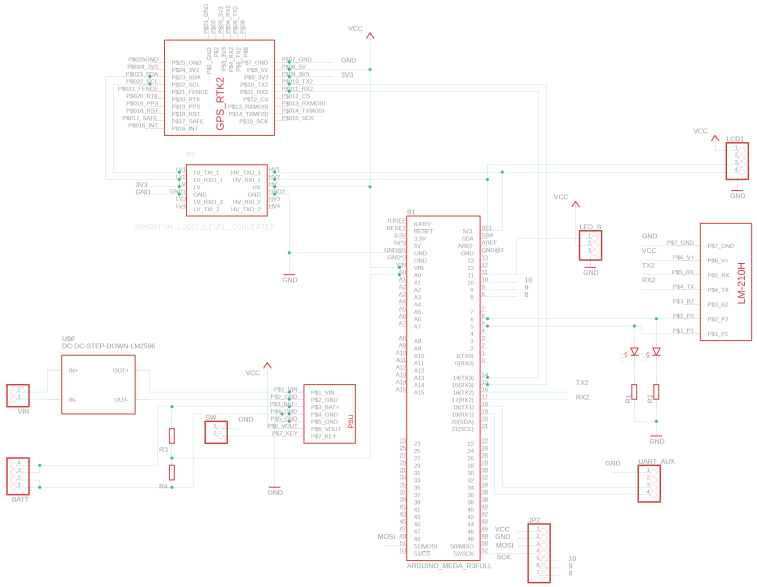

Figure 3.9: Schematic of RS.

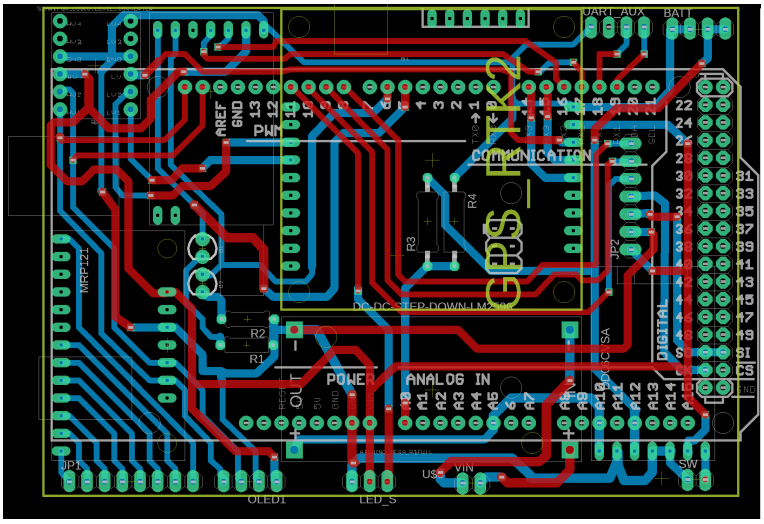

Figure 3.10: Layout of RS.

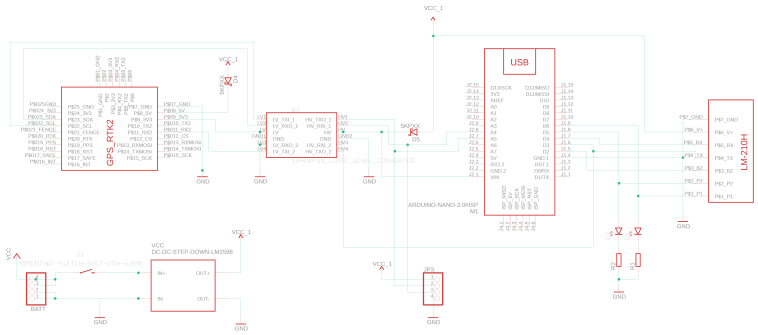

Figure 3.11: Schematic of the rover.

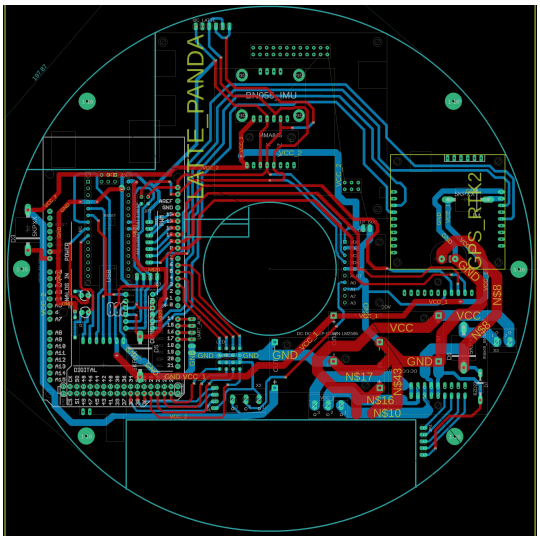

Figure 3.12: Layout of the rover.

3.10 Costs

Costs are an important factor, as already stated in Chapter 1. Based on the components used, the costs for one system are calculated in Table 3.3.

Table 3.3: Costs of one system (first quarter 2020).

Element	Price [€]
GPS RTK2 Board	200,80
Antenna	32,05
Display	13,41
Arduino Nano/Mega	12,53 / 35,08
LoRa-Module	15,89
All other small parts below 10 €	34,19
Costs of RS	331,42
Costs of rover	308,87
Costs of one system	**640,28**

The costs in Table 3.3 do not include any other extraneous costs for other embedded devices (like a RaspBerry Pi), which are however necessary for possibly having a product developed. The costs for housing the entire components are also not taken into consideration.

Chapter 4

Test result demonstration and discussion

This chapter discusses the different tests conducted for verification of the accuracy of the design. The test suits are analogous to the tests used of Svatoň [87] to have comparable results. Static and dynamic measurements were conducted. The first test set-up consisted of only one receiver and the second of a RS and rover. It was decided also to take measurements with one receiver in order to better illustrate how big the improvement is due to the RTK approach. All six different antennas were used during the tests to investigate their influence on the overall system performance. For the analysis, the NMEA-stream 0183 Version 4.10 was recorded and only GGA and RMC messages were used. Their structure is referenced in appendix A. The analysis was done in the universal transverse mercator (UTM)-coordinate system and all latitude and longitude values were converted accordingly. The messages were processed in a python program and for the conversion from the WGS84 to the UTM system, the library *utm* was used [11]. Meanwhile, for the data analysis and visualization, the *matplotlib*, *pandas*, *numpy* and *seaborn* libraries were used [46], [66], [58], [104]. The analysis was conducted offline after the measurements were taken. For all RTK-measurements, the so-called *SURVEY-IN-TIME* was also recorded in order to determine how long it takes on average, for a predefined position of accuracy for the RS to be achieved. This additional information is an indicator of whose accuracy could be used for practical applications since it can take 24 hours to get an RS position estimation of below 1 m. The F9P will not achieve position accuracy less than 0.5 m in good conditions and in case of multi-path conditions, it will be even worse [101]. The PDOP was below 1.5 for all measurements. The average power consumption of one receiver is 1.30 W during position estimation.

4.1 Static measurements

The static tests lasted 45 minutes like the measurement of Svatoň [87]. All static measurements with one receiver started with the same GPS satellite constellation, since the error in the position estimation depends also on it, as illustrated in Figure 4.1. The same positions were reached four minutes later every day and so the measurement started at the same amount of time later every day [12].

The position of the RS was always the same for all measurements, namely at a latitude of 48.180989 and a longitude of 7116.393559, which is 603587.9957 m UTM-easting and 5337355.6366 m UTM-northing, in zone 33U, as shown in Figure

4.2 [64] [9] and Table 4.1. In the table, the latitude and longitude are in the format degrees and fractional minutes and the UTM positions, in meters. The UTM-system is chosen in this thesis because it is easier for the reader to see the magnitude of the different deviations of the measurements in meters.

Latitude [dd.mmmmmm]	Longitude [dd.mmmmmm]	UTM-Northing [m]	UTM-Easting [m]	UTM-Zone
48.180989	16.393559	603587.9957	5337355.6366	33U

Table 4.1: Position of the RS for static measurements.

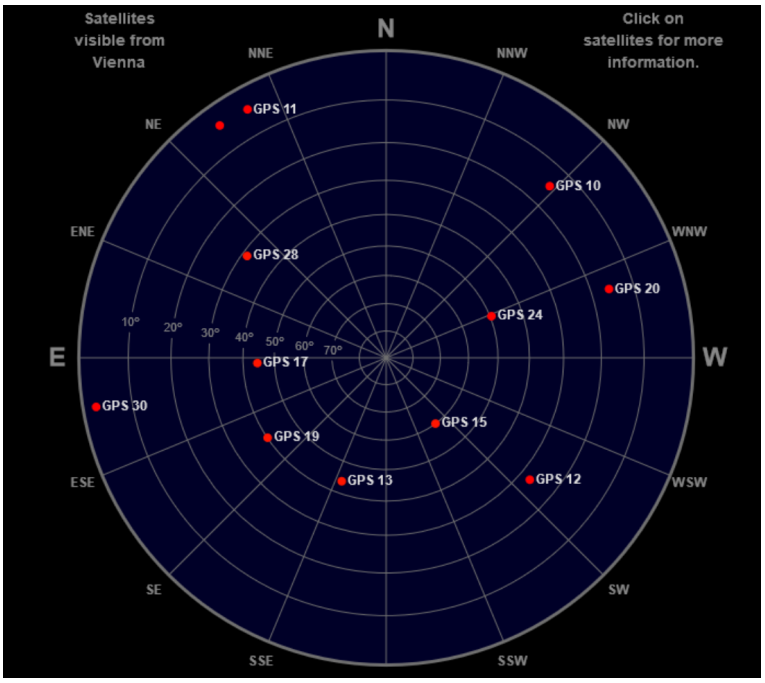

Figure 4.1: GPS satellite positions used for static measurement, with the permission of [26].

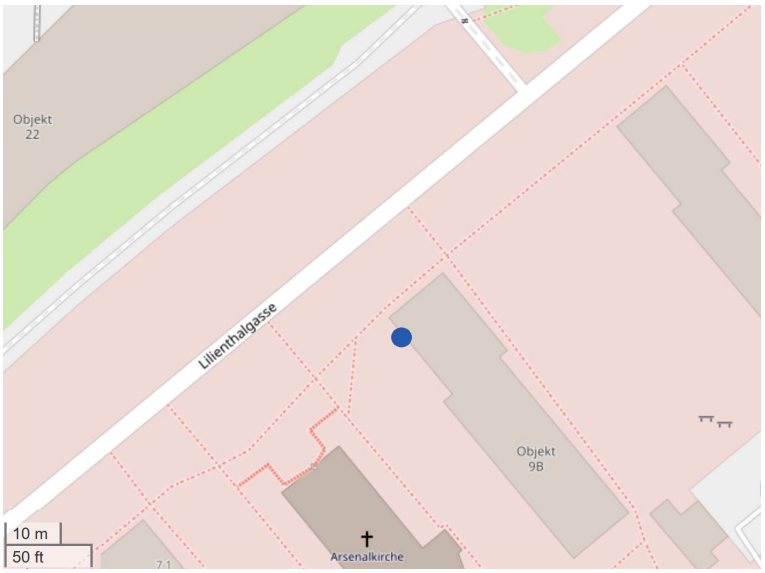

Figure 4.2: Point of static measurements, source: [64].

Figure 4.3 shows the side of the PCB with the F9P of the RS. Figure 4.4 shows the side of the PCB with the F9P and Figure 4.5 the PSU of the rover. Both GNSS-receivers are shown in Figure 4.6 where the basis transmits RTCM-data

to the rover and the rover has a fixed-position.

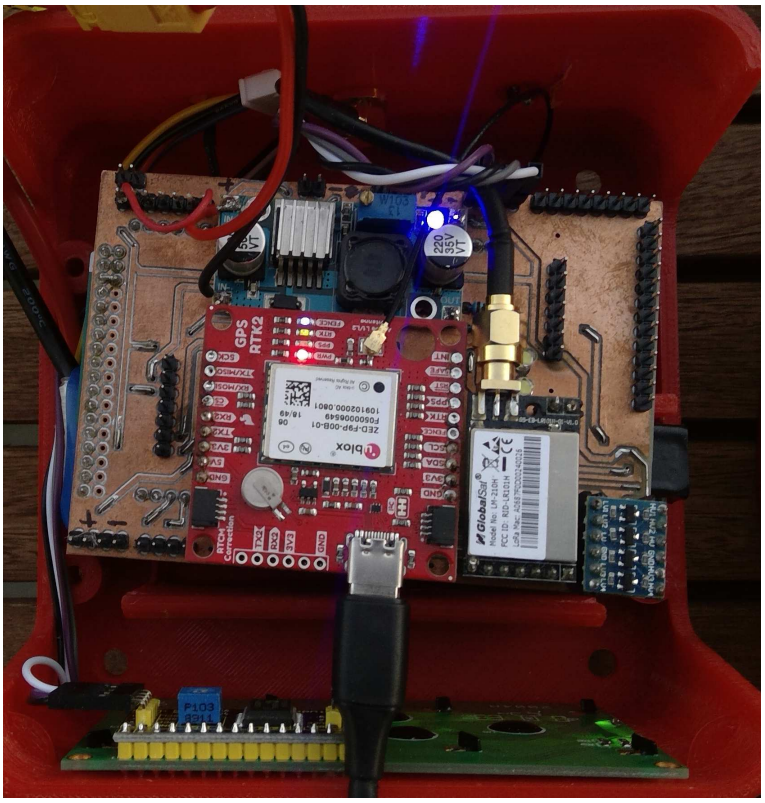

Figure 4.3: View to the side with the F9P module of the RS.

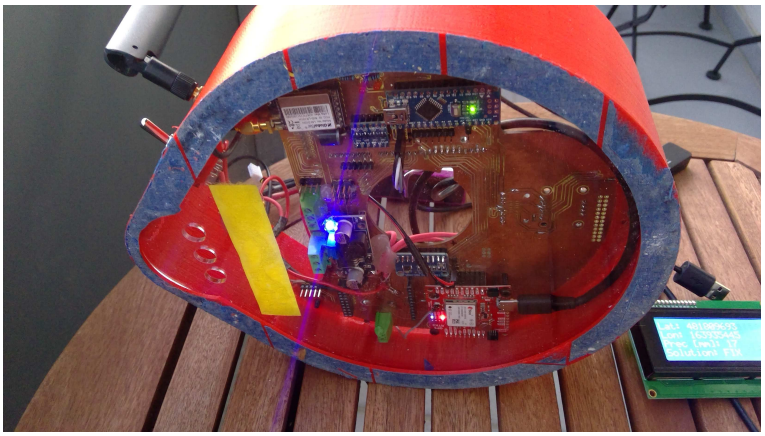

Figure 4.4: View to the side with the F9P module of the rover.

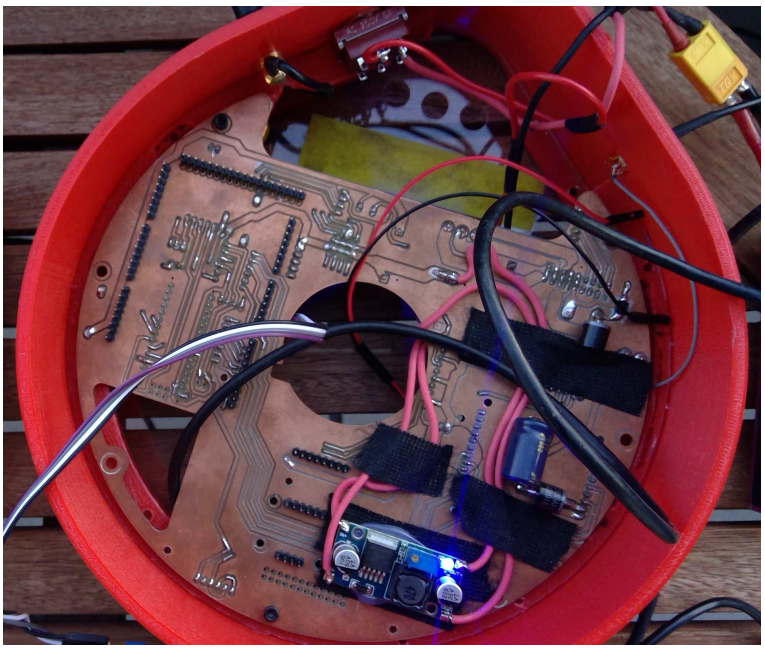

Figure 4.5: View to the side with the PSU of the rover.

Figure 4.6: RS (left) and rover (right) during static RTK-measurements.

4.1.1 Static measurements with one receiver

This section shows and discusses all static measurements with only one system used without any correction data.

Results with μ-blox ANN-MB antenna

The results of the data analysis are illustrated in Figures 4.7a, 4.7b and Table 4.2.

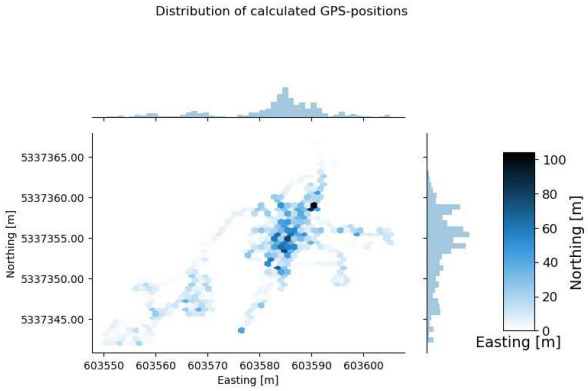

(a) Scatter plot and histogram of one receiver with ANN-MB antenna.

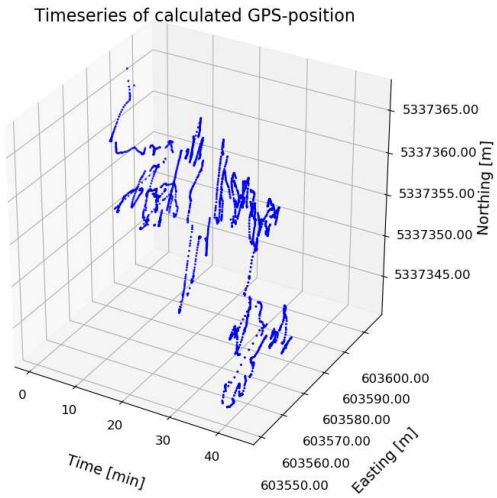

(b) Time series of one receiver with ANN-MB antenna.

Figure 4.7: Visualization of GPS position data of one receiver with ANN-MB antenna.

Table 4.2: Statistical values of one receiver with ANN-MB antenna.

Name	Maximum [m]	Mean [m]	Minimum [m]	σ [m]	Total number of elements	Unique number of elements
UTM-easting	603605.20	603582.52	603550.58	10.28	5344	2654
UTM-northing	5337366.74	5337353.81	5337342.00	4.59	5344	2654

The RMS value calculated stood at 11.26 m. Figure 4.7a shows that most estimated positions are around 603590 m easting and 5337365 m northing. More than 100 estimations fall into those coordinates. A second position estimation with about 80 estimations fall at the coordinates 603585, 5337355 m. A further analysis of the data shows that the maximum number of a position estimation is four times. 18 easting and northing positions are estimated four times and all other position estimations were calculated twice. Figure 4.7b shows that the position estimation changes constantly over time and that both coordinates do not follow a trend.

Results with HARXON HX CHX600A antenna

The results of the data analysis are illustrated in Figures 4.8a, 4.8b and Table 4.3.

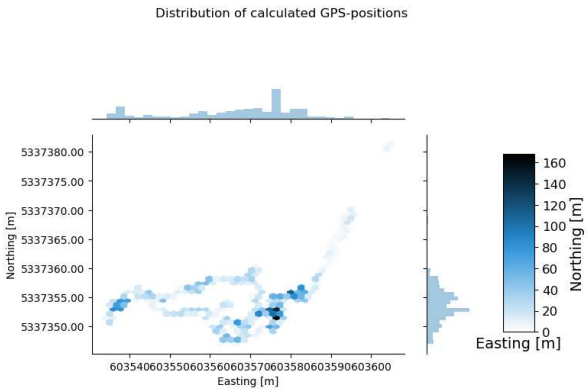

(a) Scatter plot and histogram of one receiver with an HX CHX600A antenna.

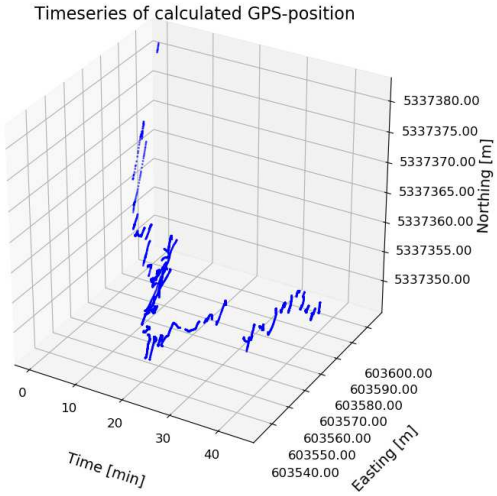

(b) Time series of one receiver with an HX CHX600A antenna.

Figure 4.8: Visualization of GPS position data of one receiver with HX CHX600A antenna.

Table 4.3: Statistical values of one receiver with an HX CHX600A antenna.

Name	Maximum [m]	Mean [m]	Minimum [m]	σ [m]	Total number of elements	Unique number of elements
UTM-easting	603604.74	603566.47	603534.28	15.30	4831	2394
UTM-northing	5337381.25	5337353.99	5337346.95	3.85	4831	2394

The RMS value calculated stood at 15.78 m. Figure 4.8a shows that most estimated positions are around 603576 m easting and 53337353 m northing. More than 160 estimations are at those coordinates with two peaks. Further analysis of the data shows that the maximum number of a position estimation is six times. 2 easting and northing positions are estimated six times and all other position estimations are calculated four times, twice and once. Figure 4.8b shows that the position estimation changes constantly over time and that both coordinates do not follow a trend. It also shows that the receiver was not able to get a valid position estimation between minute 22 and 30. The receiver has a drop in the northing coordinates from 5337380 m to estimations of below 5337350 m.

Results with HARXON HX CH6601A antenna

The results of the data analysis are illustrated in Figures 4.9a, 4.9b and Table 4.4.

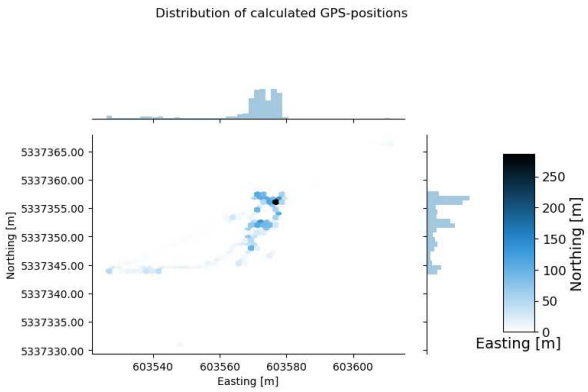

(a) Scatter plot and histogram of one receiver with an HX CH6601A antenna.

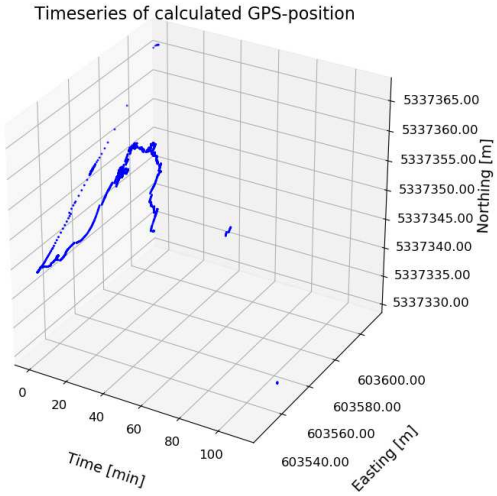

(b) Time series of one receiver with an HX CH6601A antenna.

Figure 4.9: Visualization of GPS position data of one receiver with an HX CH6601A antenna.

Table 4.4: Statistical values of one receiver with an HX CH6601A antenna.

Name	Maximum [m]	Mean [m]	Minimum [m]	σ [m]	Total number of elements	Unique number of elements
UTM-easting	603611.16	603569.26	603526.03	12.09	3787	1857
UTM-northing	5337366.22	5337352.51	5337331.08	4.33	3787	1857

The RMS value calculated was 12.84 m. Figure 4.9a shows that most position estimations are around 603576 m easting and 5337355 m northing. Two easting and northing positions are estimated six times and all other positions are calculated four times, twice and once. Figure 4.9b shows that the receiver underwent difficulties obtaining a valid GPS signal. It was able to calculate successive estimations until minute 38 and then again had trouble detecting a valid GPS signal.

Results with HARXON CH7603A antenna

This antenna was not able to get a valid GNSS signal during the 45-minute measurement time despite the fact that different settings were tested.

Results with Taoglas A.80.A.101111 antenna

The results of the data analysis are illustrated in Figures 4.10a, 4.10b and Table 4.5.

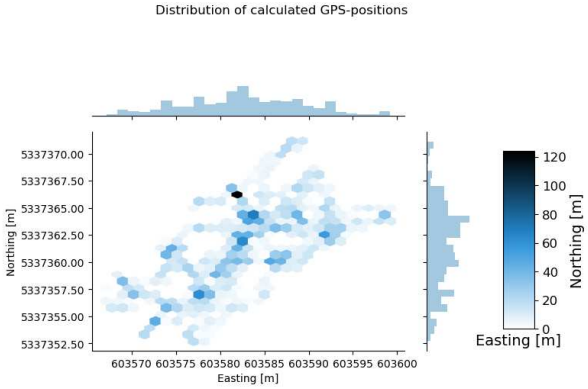

(a) Scatter plot and histogram of one receiver with an A.80.A.101111 antenna.

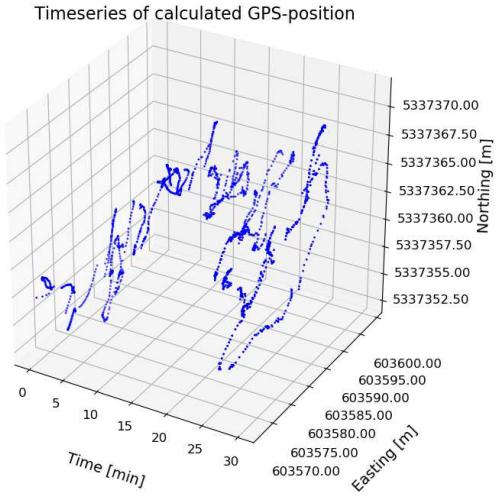

(b) Time series of one receiver with an A.80.A.101111 antenna.

Figure 4.10: Visualization of GPS position data of one receiver with an A.80.A.101111 antenna.

Table 4.5: Statistical values of one receiver with an A.80.A.101111 antenna.

Name	Maximum [m]	Mean [m]	Minimum [m]	σ [m]	Total number of elements	Unique number of elements
UTM-easting	603599.21	603582.72	603567.17	6.63	3676	1831
UTM-northing	5337371.13	5337361.47	5337352.72	3.80	3676	1831

The RMS value calculated was 7.64 m. Figure 4.10a shows that most position estimations are around 603582 m easting and 533766 m northing. 7 northing and easting positions are estimated four times and all other positions are calculated twice. Figure 4.10b shows that the receiver has no distinct trend in the position estimation. Northing and easting position estimations are constantly changing.

Results with Taoglas AQHA.50.A.301111 antenna

It was not possible to get a valid satellite signal during the 45-minute measurement, despite testing of different settings. One reason for this behaviour could be the design of the antenna itself, as, the antenna consists of four different antennas and this antenna design could be prone to difficulties with multipath errors in an urban area.

4.1.2 Static measurements with the RTK system

For these measurements, the basis was receiving a GNSS signal with the μ-blox ANN-MB antenna. The rover had a different antenna each time and the measurements lasted 45 minutes. The RS was equipped with the ANN-MB antenna, since it is the recommended antenna for the F9P receiver. The RS was configured with three different position accuracy estimations by setting the value in register *CFG-TMODE-SVIN_ACC_LIMIT* to 5, 1.5 and 0.5 meters. These three different accuracies were chosen because the receiver should be able to get a fixed position under 5 meters and it is, furthermore, questionable that a better accuracy than 1.0 m could be achieved [101]. First, a position fix of the RS is achieved and then RTCM correction messages are transmitted to the rover. For this purpose, the RS has to do the *survey-in process*. This process stops at the RS, when the given position accuracy is achieved. The different position accuracies were

used to show at which accuracy level the estimation is more precise than the results achieved in the work of Svatoň [87]. Higher accuracy is achieved if one measurement contains few different position estimations with a high level of counting involved.

Results with μ-blox ANN-MB antenna with an RS position estimation accuracy less than 5 m.

The results of the data analysis are illustrated in Figures 4.11a, 4.11b and Table 4.6. The average 3D standard deviation of the position estimation was 5 m and the *survey in process* took 5 hours, 7 minutes and 32 seconds to achieve.

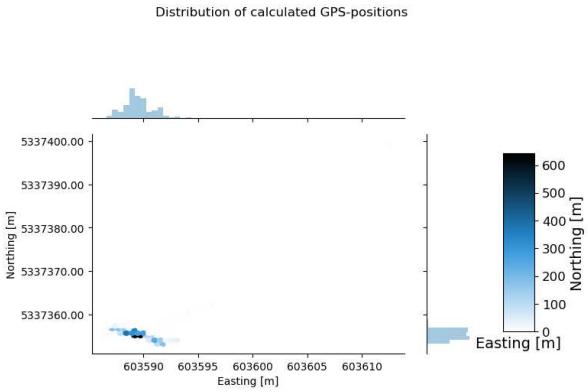

(a) Scatter plot and histogram of RTK system with ANN-MB antenna.

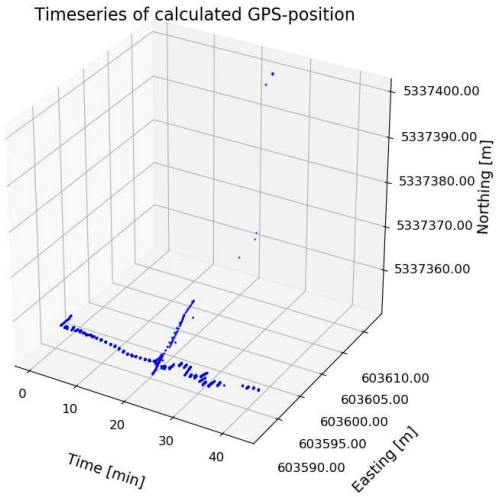

(b) Time series of RTK system with ANN-MB antenna.

Figure 4.11: Visualization of GPS position data with RS accuracy < 5 m with ANN-MB antenna.

Table 4.6: Statistical values of RTK system RS accuracy < 5 m with ANN-MB antenna.

Name	Maximum [m]	Mean [m]	Minimum [m]	σ [m]	Total number of elements	Unique number of elements
UTM-easting	603612.58	603589.61	603586.61	1.82	4792	1550
UTM-northing	5337399.41	5337355.38	5337353.16	2.29	4792	1550

The calculated RMS value was 2.93 m. Figure 4.11a shows that most position estimations were around 603589 m easting and 5337355 m northing. Two northing and easting positions were estimated 37 times and other positions were estimated at between 24 and 2 times. Figure 4.11b shows that the receiver was conducting estimates of its position very constantly most of the time. Only around minute 20 did several outliers surface.

Results with μ-blox ANN-MB antenna with an RS position estimation accuracy less than 1.5 m.

The results of the data analysis are illustrated in Figures 4.12a, 4.12b and Table 4.7. The mean 3D standard deviation of the RS was 1.499 m. The *survey in process* was initiated three times and all three processes lasted 33 minutes and 43 seconds altogether for achieving the desired accuracy.

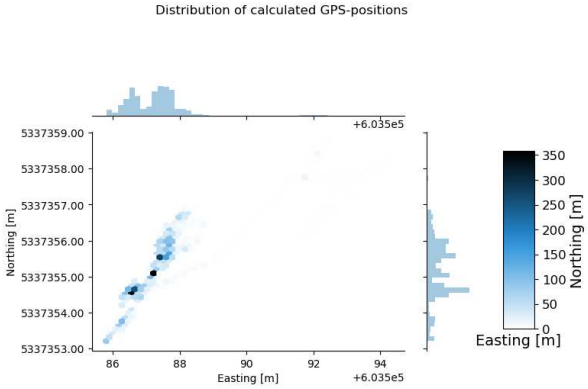

(a) Scatter plot and histogram of RTK system with an ANN-MB antenna.

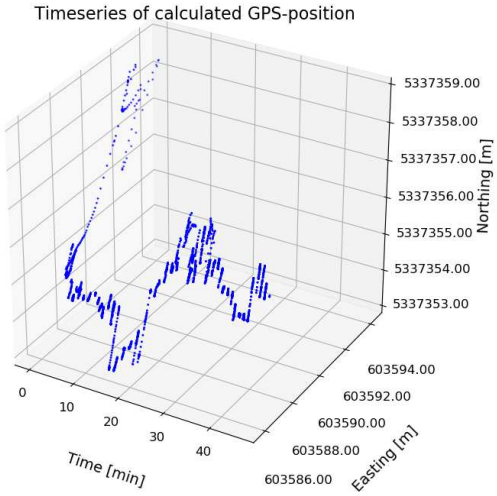

(b) Time series of RTK system with an ANN-MB antenna.

Figure 4.12: Visualization of GPS position data with RS accuracy < 1.5 m with an ANN-MB antenna.

Table 4.7: Statistical values of RTK system RS accuracy < 1.5 m with an ANN-MB antenna.

Name	Maximum [m]	Mean [m]	Minimum [m]	σ [m]	Total number of elements	Unique number of elements
UTM-easting	603594.30	603587.30	603585.81	1.03	5526	1465
UTM-northing	5337358.76	5337355.20	5337353.21	1.90	5526	1465

The RMS value calculated was 1.37 m. Figure 4.12a shows that most position estimations were around 603587 m easting and 5337355 m northing. 2 northing and easting positions were estimated 38 times and other positions were estimated between 34 and 2 times. Figure 4.12b shows that the receiver had outliers at the beginning of the measurement and that at around minute 20, the position estimation changed to 603594 m easting and 7337358 m northing.

Results with HARXON HX CHX600A antenna with an RS position estimation accuracy less than 5 m.

The results of the data analysis are illustrated in Figures 4.13a, 4.13b and Table 4.8. The mean 3D standard deviation from the position was 1.8118 m and the *survey in process* lasted 61 seconds to achieve this accuracy.

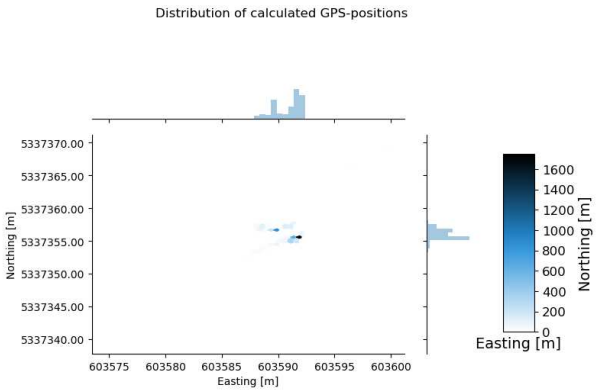

(a) Scatter plot and histogram of RTK system with an HX CHX600A antenna.

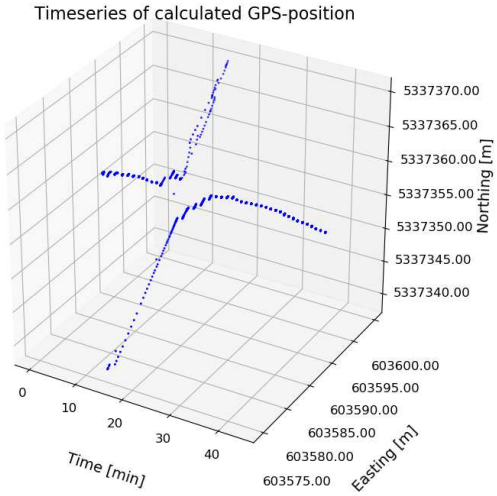

(b) Time series of RTK system with an HX CHX600A antenna.

Figure 4.13: Visualization of GPS position data with RS accuracy < 5 m with an HX CHX600A antenna.

Table 4.8: Statistical values of RTK system RS accuracy < 5 m with an HX CHX600A antenna.

Name	Maximum [m]	Mean [m]	Minimum [m]	σ [m]	Total number of elements	Unique number of elements
UTM-easting	603599.95	603590.83	603574.77	1.90	5365	1030
UTM-northing	5337369.73	5337355.98	5337339.29	2.07	5365	1030

The RMS value calculated was 2.81 m. Figure 4.13a shows that most position estimations were around 603592 m easting and 5337355 m northing. One northing and easting position was estimated 60 times and other positions were estimated between 54 and 4 times. Figure4.13b shows that the receiver estimated the position very constantly until minute 12. During minute 12 and 15, outliers appeared and afterwards, it again began estimating the position very constantly.

Results with HARXON HX CHX600A antenna with an RS position estimation accuracy less than 1.5 m.

The results of the data analysis are illustrated in Figures 4.14a, 4.14b and Table 4.9. The mean 3D standard deviation from the RS position was 1.3763 m and the *survey in process* lasted 60 seconds to achieve this accuracy.

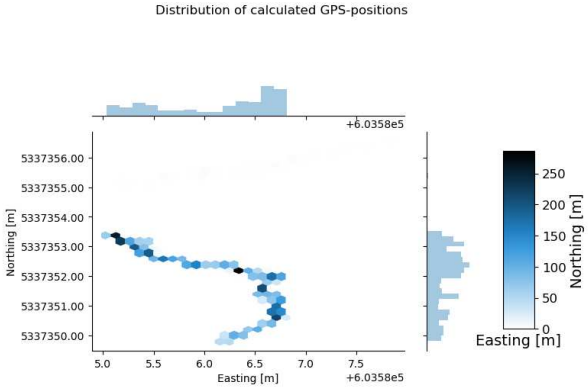

(a) Scatter plot and histogram of RTK system with an HX CHX600A antenna.

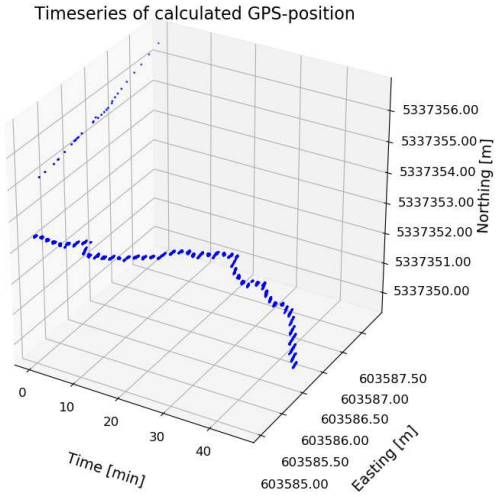

(b) Time series of RTK system with an HX CHX600A antenna.

Figure 4.14: Visualization of GPS position data with RS accuracy < 1.5 m with an HX CHX600A antenna.

Table 4.9: Statistical values of RTK system RS accuracy < 1.5 m with an HX CHX600A antenna.

Name	Maximum [m]	Mean [m]	Minimum [m]	σ [m]	Total number of elements	Unique number of elements
UTM-easting	603587.83	603586.12	603585.04	0.58	5588	779
UTM-northing	5337356.54	5337351.95	5337349.80	1.08	5588	779

The RMS value calculated was 1.22 m. Figure 4.14a shows that most position estimations were around 603586 m easting and 5337352 m northing. One northing and easting position was estimated 38 times and other positions were estimated between 32 and 2 times. Figure 4.14b shows that the receiver encountered outliers during the first minutes of the measurement, but then began estimating the position constantly.

Results with HARXON HX CH6601A antenna with an RS position estimation accuracy less than 5 m.

The results of the data analysis are illustrated in Figures 4.15a, 4.15b and Table 4.10. The mean 3D standard deviation of the RS position was 2.1371 m and the *survey in process* lasted 60 seconds.

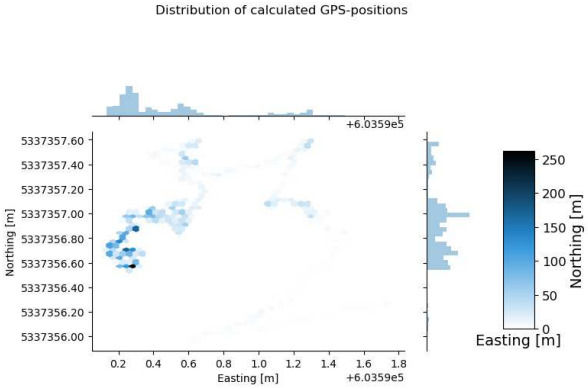

(a) Scatter plot and histogram of RTK system with an HX CH6601A antenna.

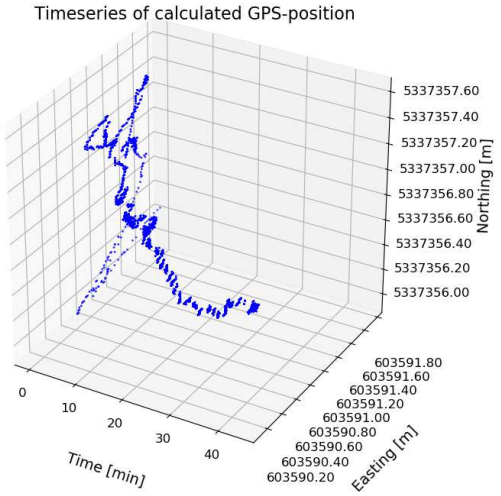

(b) Time series of RTK system with an HX CH6601A antenna.

Figure 4.15: Visualization of GPS position data with RS accuracy < 5 m with an HX CH6601A antenna.

Table 4.10: Statistical values of RTK system RS accuracy < 5 m with an HX CH6601A antenna.

Name	Maximum [m]	Mean [m]	Minimum [m]	σ [m]	Total number of elements	Unique number of elements
UTM-easting	603591.75	603590.48	603590.13	0.34	5172	636
UTM-northing	5337357.59	5337356.89	5337355.96	0.30	5172	636

The RMS value calculated was 0.45 m. Figure 4.15a shows that most position estimations were around 603590 m easting and 5337356 m northing. One northing and easting position was estimated 108 times and other positions were estimated between 90 and 2 times. Figure 4.15b shows that the receiver was estimating the position very constantly until minute 4. Between minute 4 and 5, outliers were measured and from minute 10 to 12, whereupon outliers arose once again. Afterwards, the receiver began estimating the position constantly.

Results with HARXON HX CH6601A antenna with an RS position estimation accuracy less than 1.5 m.

The results of the data analysis are illustrated in Figures 4.16a, 4.16b and Table 4.11. The mean 3D standard deviation of the RS position was 1.4998 m and the *survey in process* lasted 122 seconds.

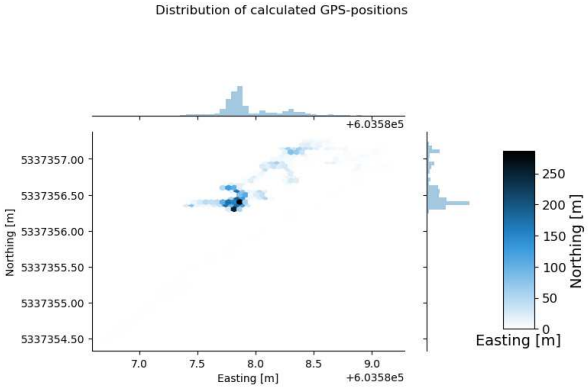

(a) Scatter plot and histogram of RTK system with an HX CH6601A antenna.

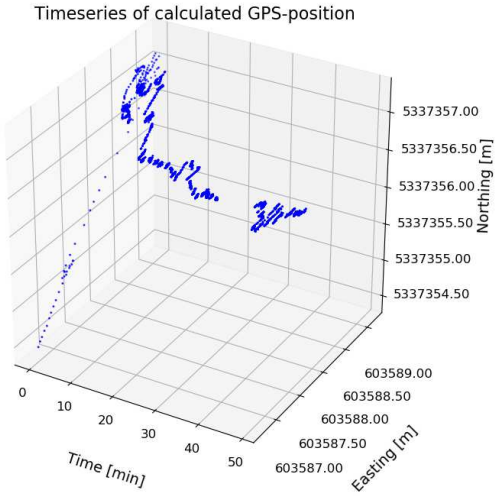

(b) Time series of RTK system with an HX CH6601A antenna.

Figure 4.16: Visualization of GPS position data with RS accuracy < 1.5 m with an HX CH6601A antenna.

Table 4.11: Statistical values of RTK system RS accuracy < 1.5 m with an HX CH6601A antenna.

Name	Maximum [m]	Mean [m]	Minimum [m]	σ [m]	Total number of elements	Unique number of elements
UTM-easting	603589.16	603587.96	603586.72	0.30	4966	669
UTM-northing	5337357.24	5337356.57	5337354.46	0.32	4966	669

The RMS value calculated was 0.44 m. Figure 4.16a shows that there were two different centres of position estimations. One centre was around 603591 m northing and 5337358 m easting, and the second was around 603572 m northing and 5337348 m easting. 4 northing and easting positions are estimated 26 times and other positions were estimated between 24 and 2 times. Figure 4.16b shows that the receiver estimated the position constantly until minute 40, whereupon the estimation changed and remained constant until minute 60. At minute 60, the position estimation switched back to the area of the first estimations.

Results with HARXON HX CH7603A antenna with an RS position estimation accuracy less than 5 m.

The results of the data analysis are illustrated in Figures 4.17a, 4.17b and Table 4.12. The mean 3D standard deviation of the RS position was 1.6123 m and the *survey in process* lasted 60 seconds.

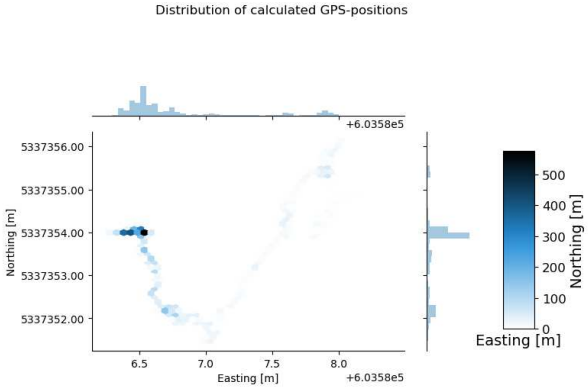

(a) Scatter plot and histogram of RTK system with an HX CH7603A antenna.

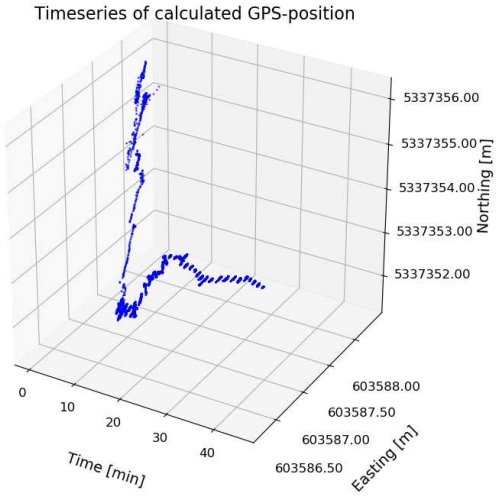

(b) Time series of RTK system with an HX CH7603A antenna.

Figure 4.17: Visualization of GPS position data with RS accuracy < 5 m with an HX CH7603A antenna.

Table 4.12: Statistical values of RTK system RS accuracy < 5 m with an HX CH7603A antenna.

Name	Maximum [m]	Mean [m]	Minimum [m]	σ [m]	Total number of elements	Unique number of elements
UTM-easting	603588.39	603586.78	603586.25	0.47	5448	870
UTM-northing	5337356.12	5337353.58	5337351.47	0.98	5448	870

The RMS value calculated was 1.09 m. Figure 4.17a shows that most position estimations were around 603586 m easting and 5337354 m northing. One northing and easting position was estimated 86 times and other positions were estimated between 84 and 2 times. Figure 4.17b shows that the receiver was having difficulties finding a constant position estimation until minute 25. From minute 25 to the end of the measurement, the position estimation remained rather constant.

Results with HARXON HX CH7603A antenna with an RS position estimation accuracy less than 1.5 m.

The results of the data analysis are illustrated in Figures 4.18a, 4.18b and Table 4.13. The mean 3D standard deviation of the RS position was 1.4998 m and the *survey in process* lasted 12 hours 34 minutes and 49 seconds (initiated twice).

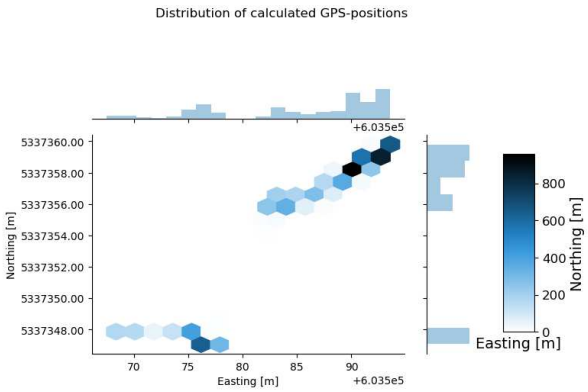

(a) Scatter plot and histogram of RTK system with an HX CH7603A antenna.

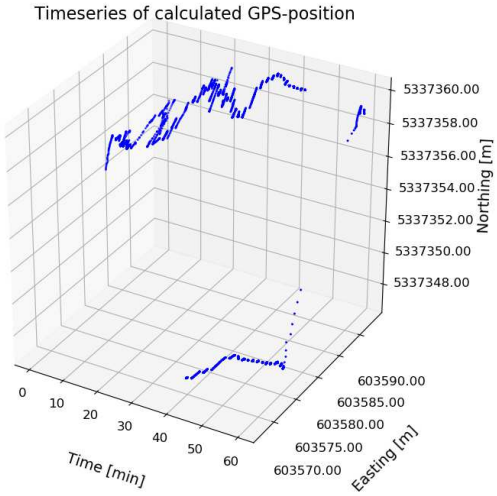

(b) Time series of RTK system with an HX CH7603A antenna.

Figure 4.18: Visualization of GPS position data with RS accuracy < 1.5 m with an HX CH7603A antenna.

Table 4.13: Statistical values of RTK system RS accuracy < 1.5 m with an HX CH7603A antenna.

Name	Maximum [m]	Mean [m]	Minimum [m]	σ [m]	Total number of elements	Unique number of elements
UTM-easting	603593.57	603585.61	603567.47	7.26	7228	2501
UTM-northing	5337359.80	5337355.30	5337347.08	4.74	7228	2501

The RMS value calculated was 8.67 m. Figure 4.18a shows that there were two centres of position estimations. The first centre was around 603572 m easting and 5337348 m northing and the second was around 603590 m easting and 5337358 m northing. 4 northing and easting positions were estimated 26 times and other positions were estimated between 24 and 2 times. Figure 4.18b shows that the receiver estimated a position constantly over most of the 40 minutes and it was estimating a second one between minute 40 to 60, whereupon it then returned to the first position estimations.

Results with Taoglas A.80.A.101111 antenna with an RS position estimation accuracy less than 5 m.

The results of the data analysis are illustrated in Figures 4.19a, 4.19b and Table 4.14. The mean 3D standard deviation of the RS position was 4.9942 m and the *survey in process* lasted 66 seconds.

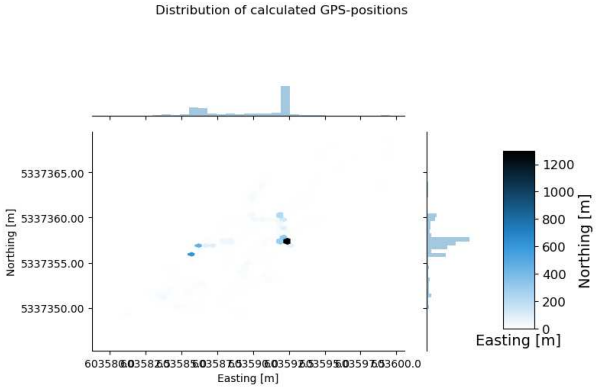

(a) Scatter plot and histogram of RTK system with an A.80.A.101111 antenna.

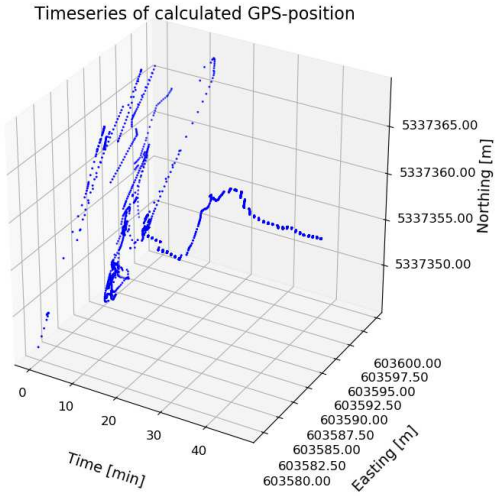

(b) Time series of RTK system with an A.80.A.101111 antenna.

Figure 4.19: Visualization of GPS position data with RS accuracy < 5 m with an A.80.A.101111 antenna.

Table 4.14: Statistical values of RTK system RS accuracy < 5 m with an A.80.A.101111 antenna.

Name	Maximum [m]	Mean [m]	Minimum [m]	σ [m]	Total number of elements	Unique number of elements
UTM-easting	603599.57	603589.91	603579.79	3.19	5740	1720
UTM-northing	5337368.44	5337357.23	5337346.30	2.97	5740	1720

The RMS value calculated was 4.36 m. Figure 4.19a shows that most position estimations stood at around 603592 m easting and 5337357 m northing. One northing and easting position was estimated 46 times and other positions were estimated between 42 and 2 times. Figure 4.19b shows that the receiver was estimating many different positions until minute 10. Between minute 10 and minute 20, it began estimating constantly around one position and around minute 20, it started to estimate another position constantly.

Results with Taoglas A.80.A.101111 antenna with an RS position estimation accuracy less than 1.5 m.

The results of the data analysis are illustrated in Figures 4.20a, 4.20b and Table 4.15. The mean 3D standard deviation of the RS position was 1.4992 m and the *survey in process* lasted 34 minutes and 25 seconds.

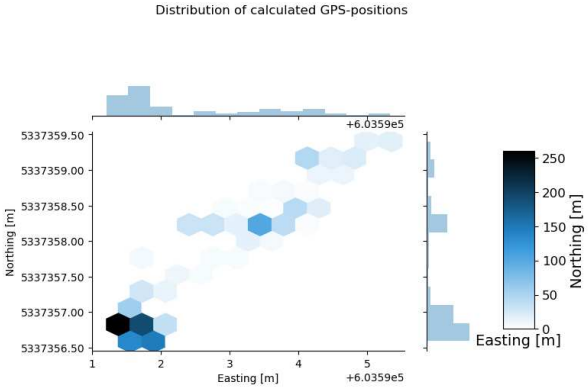

(a) Scatter plot and histogram of RTK system with an A.80.A.101111 antenna.

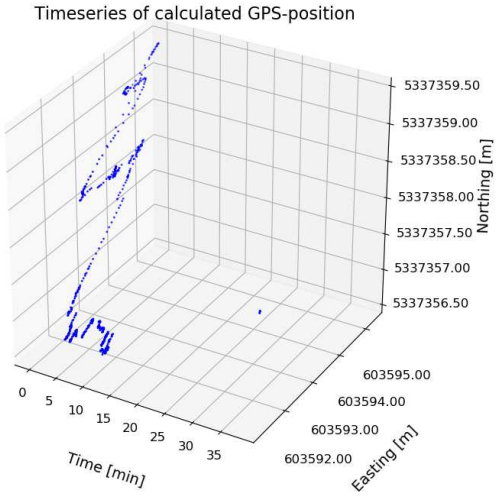

(b) Time series of RTK system with an A.80.A.101111 antenna.

Figure 4.20: Visualization of GPS position data with RS accuracy < 1.5 m with an A.80.A.101111 antenna.

Table 4.15: Statistical values of RTK system RS accuracy < 1.5 m with an A.80.A.101111 antenna.

Name	Maximum [m]	Mean [m]	Minimum [m]	σ [m]	Total number of elements	Unique number of elements
UTM-easting	603595.34	603592.40	603591.21	1.12	1391	460
UTM-northing	5337359.40	5337357.45	5337356.59	0.87	1391	460

The RMS value calculated was 1.41 m. Figure 4.20a shows that most position estimations were around 603591 m easting and 5337357 m northing. One northing and easting position was estimated 16 times and other positions were estimated between 14 and 2 times. Figure 4.20b shows that the receiver estimated many different positions up until minute 5. From minute 5 to minute 15, it was estimating positions very close to each other and after minute 15, it was not able to calculate a position estimation.

Results with Taoglas AQHA.50.A.301111 antenna with an RS position estimation accuracy less than 5 m.

The results of the data analysis are illustrated in Figures 4.21a, 4.21b and Table 4.16. The mean 3D standard deviation of the RS position was 2.5871 m and the *survey in process* lasted 60 seconds.

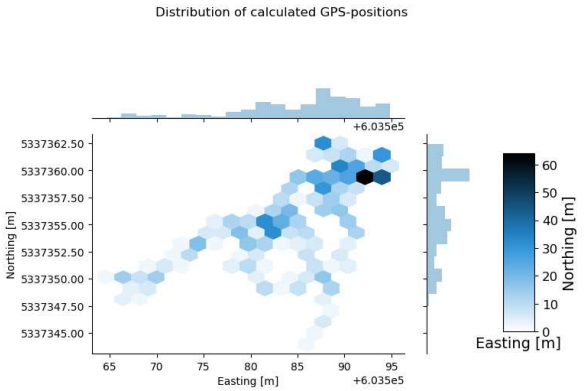

(a) Scatter plot and histogram of RTK system with an AQHA.50.A.301111 antenna.

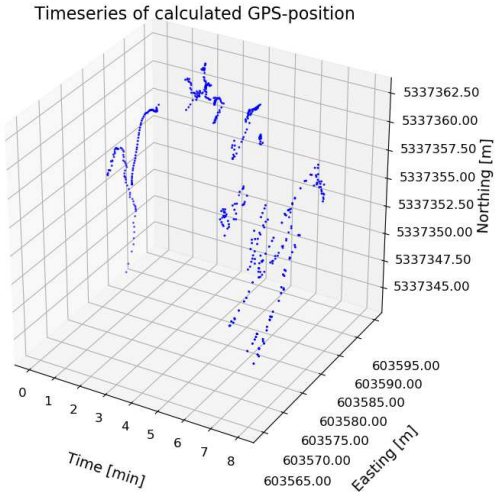

(b) Time series of RTK system with an AQHA.50.A.301111 antenna.

Figure 4.21: Visualization of GPS position data with RS accuracy < 5 m with an AQHA.50.A.301111 antenna.

Table 4.16: Statistical values of RTK system RS accuracy < 5 m with an AQHA.50.A.301111 antenna.

Name	Maximum [m]	Mean [m]	Minimum [m]	σ [m]	Total number of elements	Unique number of elements
UTM-easting	603594.88	603585.38	603564.65	6.63	1007	508
UTM-northing	5337362.46	5337356.16	5337344.00	3.96	1007	508

The RMS value calculated was 7.28 m. Figure 4.21a shows that most position estimations were around 603592 m easting and 5337360 m northing. Most position estimations were calculated 2 times and only 9 estimations once. Figure 4.21b shows that the receiver estimated many different positions and, but stopped being able to estimate a position after minute 8. From minute 8 to minute 45, the receiver was not able to estimate a position and this is the reason why the time line already ends at minute 8.

Results with Taoglas AQHA.50.A.301111 antenna with an RS position estimation accuracy less than 1.5 m.

The mean 3D standard deviation of the RS position was 1.4994 m and the *survey in process* lasted 15 minutes and 8 seconds, respectively. The rover was not able to get a valid GPS-position during the measurement time. The problem could be multipath errors combined with the design of the antenna.

Results with μ-blox ANN-MB antenna with an RS position estimation accuracy less than 0.5 m.

The results of the data analysis are illustrated in Figures 4.22a, 4.22b and Table 4.17. The mean 3D standard deviation of the RS was 0.5 m. The *survey in process* lasted 9 hours 40 minutes and 40 seconds. Although several attempts were made to achieve the same *accuracy* again, it was not reproducible with different antennas or the same antenna setup.

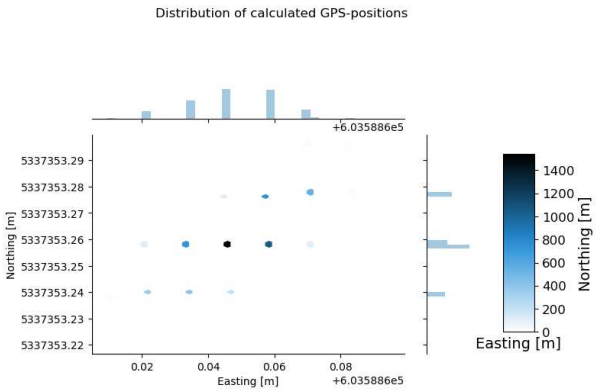

(a) Scatter plot and histogram of RTK system with an ANN-MB antenna.

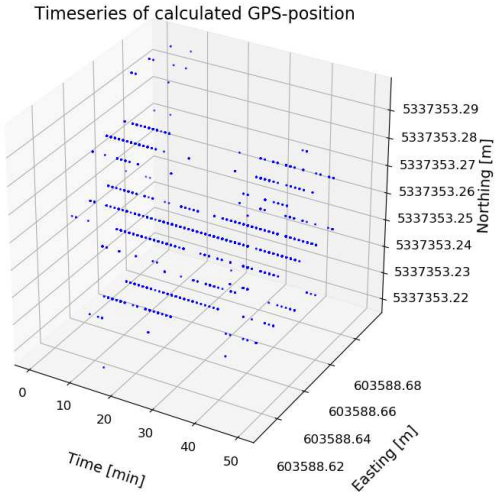

(b) Time series of RTK system with an ANN-MB antenna.

Figure 4.22: Visualization of GPS position data with RS accuracy < 0.5 m with an ANN-MB antenna.

Table 4.17: Statistical values of RTK system RS accuracy < 0.5 m with an ANN-MB antenna.

Name	Maximum [m]	Mean [m]	Minimum [m]	σ [m]	Total number of elements	Unique number of elements
UTM-easting	603588.69	603588.65	603588.61	0.01	6064	19
UTM-northing	5337353.30	5337353.26	5337353.22	0.01	6064	19

The RMS value calculated stood at 0.02 m. Figure 4.22a shows that most position estimations were around 603588 m easting and 533753 m northing. One northing and easting position was estimated 1540 times and other positions were estimated between 1062 and 2 times. Figure 4.22b shows that the receiver estimated one position with deviations of 6 cm in the easting and northing directions.

Comparison of static measurements.

The static measurements in the urban area were the desired stress test for the entire system, which showed that the system could not currently be used in such areas with a guaranteed high accuracy in the cm range. Table 4.18 summarizes the mean value, standard deviation and the RMS of the measurements taken. Table 4.19 summarizes the needed *survey in time* and the accuracy gained of the position of the RS.

Antenna	Measurement	Mean easting [m]	Mean northing [m]	sigma easting [m]	sigma northing [m]	RMS [m]
ANN-MB	Single	603582.52	5337353.81	10.28	4.59	11.26
ANN-MB	RTK 5m	603589.61	5337355.38	1.82	2.29	2.93
ANN-MB	RTK 1.5m	603587.30	5337355.20	1.03	1.90	1.37
ANN-MB	RTK 0.5m	603588.65	5337353.26	0.01	0.01	0.02
HX CHX600A	Single	603566.47	5337353.99	15.30	3.85	15.78
HX CHX600A	RTK 5m	603590.83	5337355.98	1.90	2.07	2.81
HX CHX600A	DGPS 1.5m	603586.12	5337351.95	0.58	1.08	1.22
HX CH6601A	Single	603569.26	5337352.51	12.09	4.33	12.84
HX CH6601A	RTK 5m	603590.48	5337356.89	0.34	0.30	0.45
HX CH6601A	RTK 1.5m	603587.96	5337356.57	0.30	0.32	0.44
CH7603A	Single	-	-	-	-	-
CH7603A	RTK 5m	603586.78	5337353.58	0.47	0.98	1.09
CH7603A	RTK 1.5m	603585.61	5337355.30	7.26	4.74	8.67
A.80	Single	603582.72	5337361.47	6.63	3.8	7.64
A.80	RTK 5m	603589.91	5337357.23	3.19	2.97	4.36
A.80	RTK 1.5m	603592.40	5337357.45	1.12	0.87	1.41
A.50	Single	-	-	-	-	-
A.50	RTK 5m	603585.38	5337356.16	6.63	3.96	7.28
A.50	RTK 1.5m	-	-	-	-	-

Table 4.18: Comparison of results of the static measurements.

The measurements with only one receiver shows that it was not possible to get a valid position estimation with the CH7603A and the A.50 antenna. The mean easting position estimation was between 603566.47 and 603582.72 m, which is a difference of 16.24 m and for the northing position between 5337352.51 to 5337361.47, which is a difference of 8.96 m. The range of the standard deviation σ easting was from 6.63 to 15.30 m and σ northing from 3.8 to 4.59 m. The RMS of one single receiver was between 7.64 and 15.78 m. The highest accuracy was gained with the Taoglas A.80 antenna and the second best was with the μ-blox ANN-MB antenna. The results of the measurements with the RTK system and a minimum position accuracy of the RS of 5 m shows that it was possible to obtain a position estimation with all antennas, but for some of them, only for a matter of minutes. The mean easting position estimation had a range of 603585.38 to 603590.83 m, which is a difference of 5.45 m, and for the northing estimation, between 5337353.58 and 5337357.23 m, which is a difference of 3.65 m. The σ easting featured a range of between 6.63 and 0.34 m and the σ northing, between 3.96 and 0.30 m. The RMS fell between 7.28 and 0.45 m. The highest precision was gained with the Harxon HX CH6601A antenna and the least with the Taoglas A.50 antenna on the rover. It was possible to get a position estimation with 5 of the 6 antennas used for the entire measurement period of 45 minutes; only the Taoglas A.50 antenna experienced difficulties. The results of the measurements with the RTK system and a minimum position accuracy of the RS of 1.5 m show that it was possible to get an estimation for 5 out of 6 antennas; it failed only with the Taoglas A.50 antenna. The mean easting position estimation was between 603585.61 and 603592.40 m, which is a range of 6.41 m and for northing between 5337351.95 and 5337357.45 m, which is a range of 5.5 m. The σ easting ranged between 7.26 and 0.30 m and σ northing between 4.74 and 0.32 m. The RMS had a range of 0.44 to 8.67 m. The antenna with the smallest RMS was the Harxon HX CH6601A and the antennas with the highest RMS was the Taoglas A.80 antenna. It was only possible to obtain once a measurement with the RTK system with the μ-blox ANN-MB antenna used, with an RS accuracy of below 0.5 m and the RMS stood at 0.02 m for this measurement. Table 4.18 shows that RTK improves

the accuracy of the position estimation compared to a single GPS-receiver. An explanation for the bad results of the RTK system with the Taoglas A.50 is that the antenna has the most difficulties with multipath-interference. The average RMS value decreased by using the RTK system. The single receiver system had an average RMS of 11.88 m. If RTK was using a RS with a position accuracy of less than 5 m, the RMS was 3.15 m and with an accuracy of less than 1.5 m of 2.62 m. These values emphasize that the position accuracy of the rover increases if the accuracy of the RS estimation is higher. The accuracy of a single receiver system is less than the results of Svatoň, which confirms my expectations. The results for a RTK measurement with a maximum 5 and 1.5 m RS accuracy are in the range of the results of Svatoň. It is, however, important to note that the test conditions in this thesis are more difficult due to the multipath errors in the GNSS-signals received. The results of only 0.5 m accuracy deviation shows an accuracy which is between 48 to 123 times better than the results by Svatoň.

Antenna	Measurement	Survey in Time [min]	Easting [m]	Northing [m]	Gained Accuracy [m]	RMS [m]
ANN-MB	RTK 5m	307.53	603586.22	5337353.63	5	2.93
ANN-MB	RTK 1.5m	33.72	603586.97	5337353.72	1.499	1.37
ANN-MB	RTK 0.5m	580.67	603586.23	5337353.58	0.5	0.02
HX CHX600A	RTK 5m	1.02	603589.57	5337355.59	1.8118	2.81
HX CHX600A	RTK 1.5m	1	603588.01	5337354.20	1.3763	1.22
HX CH6601A	RTK 5m	1	603590.14	5337355.40	2.1371	0.45
HX CH6601A	RTK 1.5m	2.03	603587.27	5337354.92	1.4998	0.44
CH7603A	RTK 5m	1	603589.12	5337353.42	1.6123	1.09
CH7603A	RTK 1.5m	754.82	603590.41	5337357.24	1.4998	8.67
A.80	RTK 5m	1,1	603592.45	5337357.47	4.9942	4.36
A.80	RTK 1.5m	34.42	603590.41	5337355.58	1.4992	1.41
A.50	RTK 5m	1	603586.49	5337353.11	2.5871	7.28
A.50	RTK 1.5m	15.13	603587.84	5337354.10	1.4994	-

Table 4.19: Survey in time and accuracy of the RS of static measurement obtained.

The results of table 4.19 shows that a long *survey in time* and a high accuracy of the RS do not guarantee 100 percent that a receiver position had few deviations. Although the accuracy of the μ-blox ANN-MB antenna was worse than of the Taoglas A.80 and A.50, the resulting RMS was smaller. The longest survey measured was for the Harxon CH7603A antenna, with an RS accuracy gained of 1.4998 m with an RMS of 8.67 m. The *survey in* lasted only 60 seconds four times, with four different antennas, and the accuracy of the RS fell between 2.5871 and 1.3763 m, with corresponding RMS values between 0.45 and 7.28 m. One reason for these deviations could be better/worse satellite positions and the influence of the multipath error.

The results of the Harxon CH7603A and Taoglas A.50 has to be used with caution since it was impossible to get a position estimation with them throughout all kinds of measurement setting conditions. It is important to note that the most precise measurement did not have the longest *survy in time*. The position estimation during the survey in process depends heavily on the current satellite position and on the multipath errors of the signal. The table also shows that a long *survey in process* does not guarantee high accuracy of the rover position and means that the *survey in process* could use further improvements. Currently, it does not work very reliably in urban environments compared to other techniques like using a fixed position, NTRIP or any other method, such as PPP.

The Harxon CH7603A and A.50 were not able to send valid GNSS-signals to the F9P of the RS during different measurements. Further analysis of the data sheets of the antennas indicate no problems due to the way it was used in

the test [[36], [34], [35]. It seems that these antennas have more difficulties in areas where multipath errors are present. The μ-blox ANN-MB antenna was also immediately used, during the time that the CH7603A and the A.50 were having problems transmitting a valid GNSS-signal, and it was possible to get a position estimation with this antenna immediately. The deviations in the position estimation vary in meter range due to the multipath effect on the GPS-signals [79].

Figures 4.23 and 4.24 show the results only of the RTK measurements with a box plot. The setting of the box plot is that the orange line is the median, the end of the box is the third and first quartile, and the whiskers are placed at a distance which is the difference between the third to the first quartile. If there are any position estimations outside the whiskers, they are drawn as green rectangles. Both figures show that the measurement of the ANN-MB antenna with an RS accuracy below 0.5 m has the highest accuracy. The HX CH6601A antenna has the highest one for the measurements of 1.5 and 5 m, respectively. The results of the A50a antenna is questionable, since the system was only able to get a position estimation for 10 minutes with it. If the RS has an accuracy of only 5 m, the position estimation has much more outliers than the results with 1.5 and 0.5 m. The reason for the big deviation of the measurements with the CH7603A 1.5 m and the A80a 5m could not be clarified. A possible explanation could be problems with transmitting the correction data from the RS to the rover.

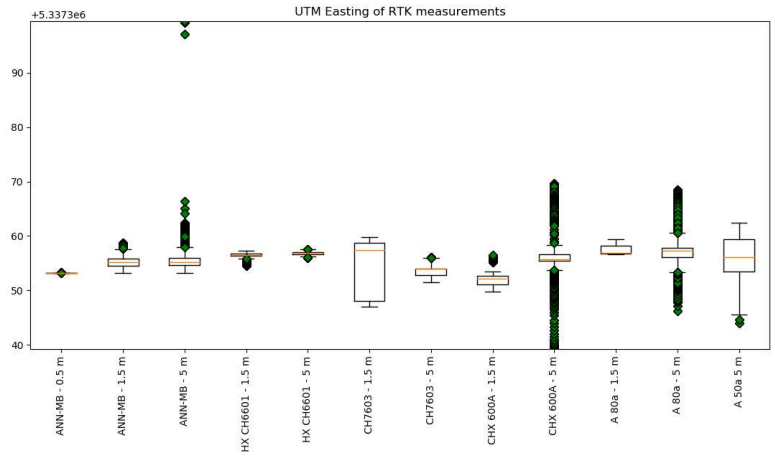

Figure 4.23: RTK UTM easting results for static measurement.

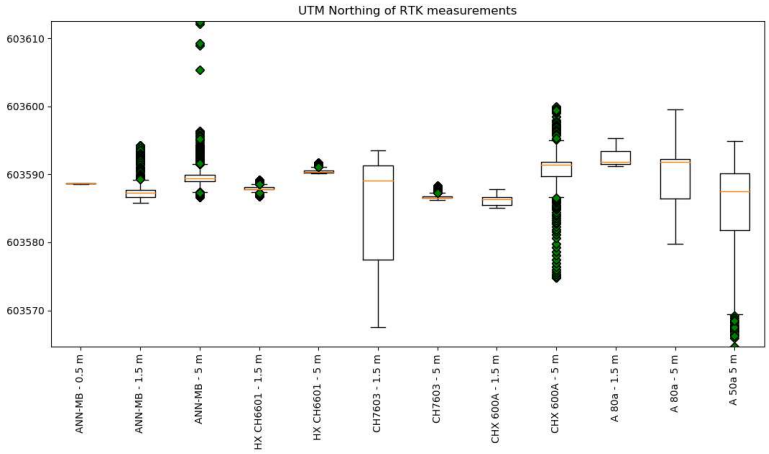

Figure 4.24: RTK UTM northing results for static measurement.

4.2 Dynamic measurements

The dynamic tests consist of walking a predefined pattern. The pattern was similar to the measurements of Svatoň - a rectangle. All dynamic measurements were conducted at the same place, as shown in Figure 4.25, and the system working there is shown in Figure 4.26.

Figure 4.25: Place and track of dynamic measurements. Source: [62]

Figure 4.26: RTK system working at the dynamic measurement place.

4.2.1 Dynamic measurement with the RTK system

This chapter contains the results of the measurements conducted with the RTK system. The antenna on the RS was the μ-blox ANN-MB, and at the rover, all antennas were tested.

Dynamic measurement with ANN-MB with an RS of below 2, 1 and 0.5 m

The results of the RS are shown in Table 4.20 and the position estimation had a DRMS of 0.27 m, with an accuracy, on average, of 0.797 m.

Measurement	RS position easting [m]	RS position northing [m]	RS 3D-accuracy [m]	Survey-In Time [min]
2 m	601433.096	5331152.153	0.8917	1
1 m	601433.064	5331152.279	0.9993	3.28
0.5 m	601432.781	5331151.874	0.5000	21.37

Table 4.20: Glsrs data of DGPS with ANN-MB rover antenna.

The results of the rover are illustrated in Figure 4.27 and show the three measurements conducted with different RS accuracies. The average accuracy stood at 1.85 cm, 1.82 cm and 1.76 cm (2 m, 1 m and 0.5 m measurement). The result of the rover shows that the system is working reliably and is able to reproduce position estimations in the cm range. If in the results of the rover, some markers of the measurement seem to be missing, it is due to the overlay of the visualization markers with the different measurements.

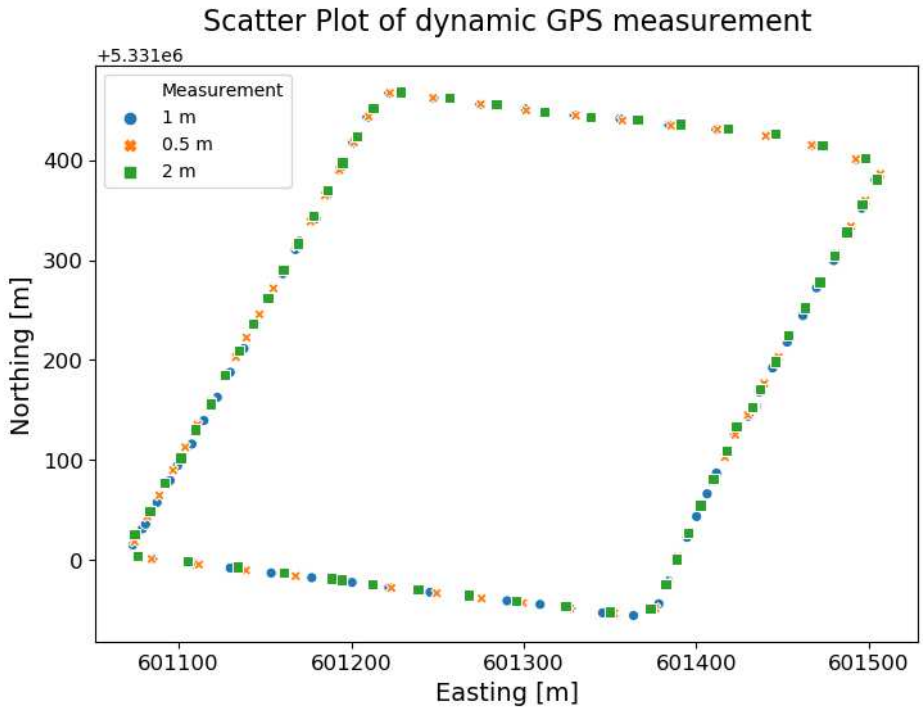

Figure 4.27: Scatter plot of dynamic measurement of RTK with the rover with an ANN-MB antenna.

Dynamic measurement with HX CHX600A with an RS of below 2, 1 and 0.5 m

The results of the RS are shown in Table 4.21 and the position estimation had a DRMS of 0.24 m, with an accuracy, on average, of 0.70 m.

The results of the rover are illustrated in Figure 4.27 and show the three measurements taken with different RS accuracies. The average accuracy stood at 1.89 cm, 1.84 cm and 1.77 cm (2 m, 1 m and 0.5 m measurement).

Measurement	RS position easting [m]	RS position northing [m]	RS 3D-accuracy [m]	Survey-In Time [min]
2 m	601432.309	5331151.614	0.9132	0.17
1 m	601432.593	5331151.971	0.6778	0.17
0.5 m	601432.302	5331151.776	0.4999	19.73

Table 4.21: Data of RS of DGPS with the HX CHX600A rover antenna.

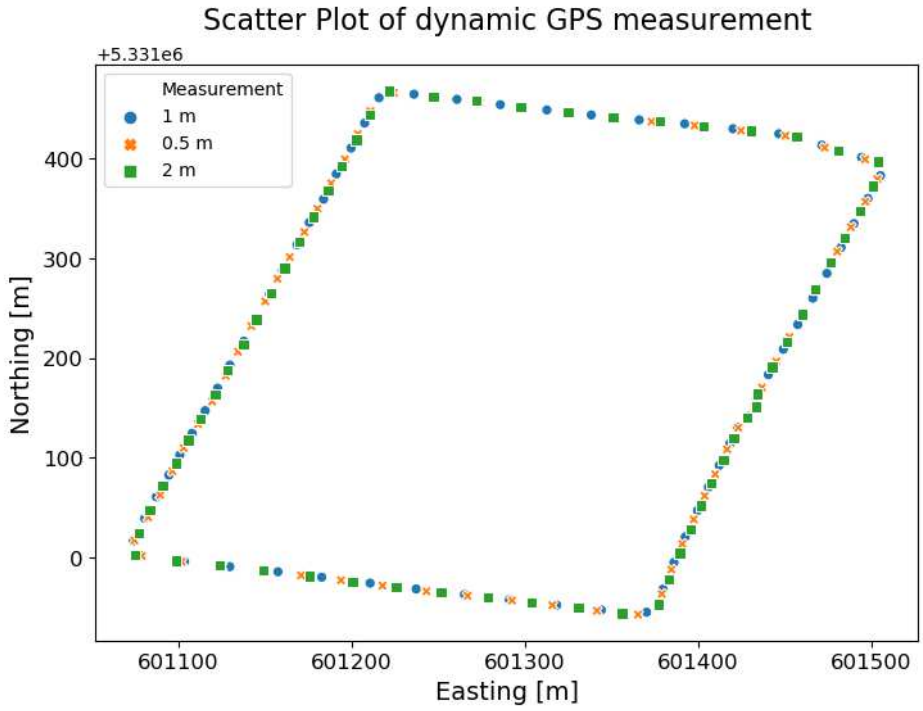

Figure 4.28: Scatter plot of dynamic measurement of the RTK system with the rover with an HX CHX600A antenna.

Dynamic measurement with HX CH6601A with an RS of below 2, 1 and 0.5 m

The results of the RS are shown in Table 4.22, with a position estimation of a DRMS of 0.51 m and an accuracy of, on average, 1.16 m.

Measurement	RS position easting [m]	RS position northing [m]	RS 3D-accuracy [m]	Survey-In Time [min]
2 m	601433.125	5331152.741	1.9780	0.28
1 m	601432.927	5331152.877	0.9980	1.25
0.5 m	601433.005	5331151.948	0.4998	18.92

Table 4.22: RS data of DGPS with the HX CH6601A rover antenna.

The results of the rover are illustrated in Figure 4.29 and show the three measurements taken with different RS accuracies. The average accuracy was 1.83 cm, 1.86 cm and 1.78 cm (2 m, 1 m and 0.5 m measurement).

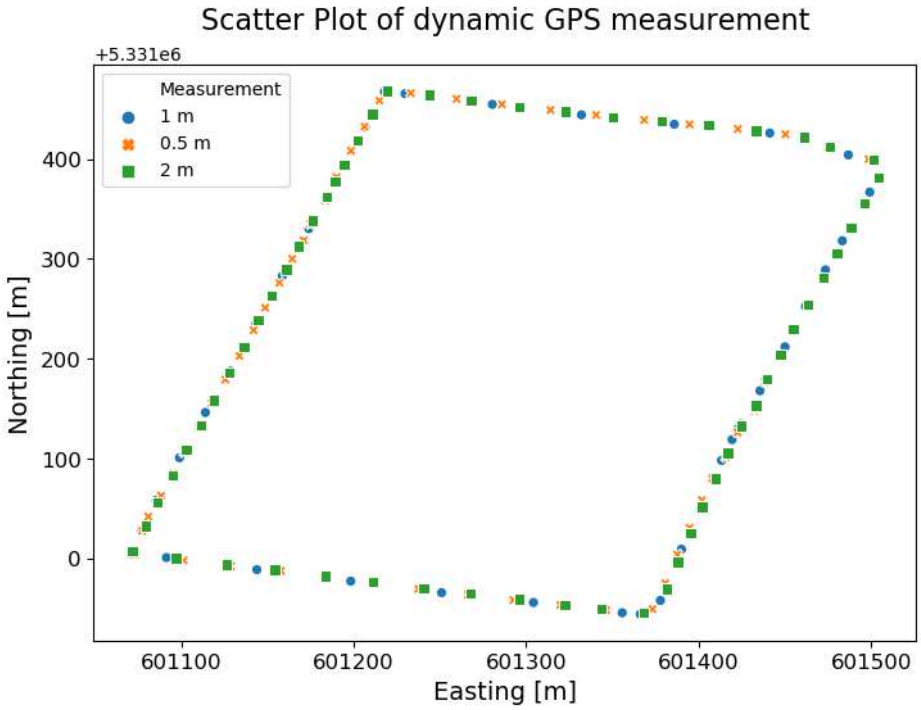

Figure 4.29: Scatter plot of dynamic measurement of the RTK system with the rover with an HX CH6601A antenna.

Dynamic measurement with CH7603A with an RS of below 2, 1 and 0.5 m

The results of the RS are shown in Table 4.23 and the position estimation had a DRMS of 0.40 m, with an accuracy of, on average, 0.67 m.

Measurement	RS position easting [m]	RS position northing [m]	RS 3D-accuracy [m]	Survey-In Time [min]
2 m	601432.857	5331152.707	0.8958	0.17
1 m	601432.526	5331152.558	0.6192	0.17
0.5 m	601432.190	5331152.285	0.4999	12.18

Table 4.23: RS data of DGPS with the CH7603A rover antenna.

The results of the rover are illustrated in Figure 4.30, showing the three measurements with different RS accuracies. The average accuracy was 1.92 cm, 1.83 cm and 1.76 cm (2 m, 1 m and 0.5 m measurement).

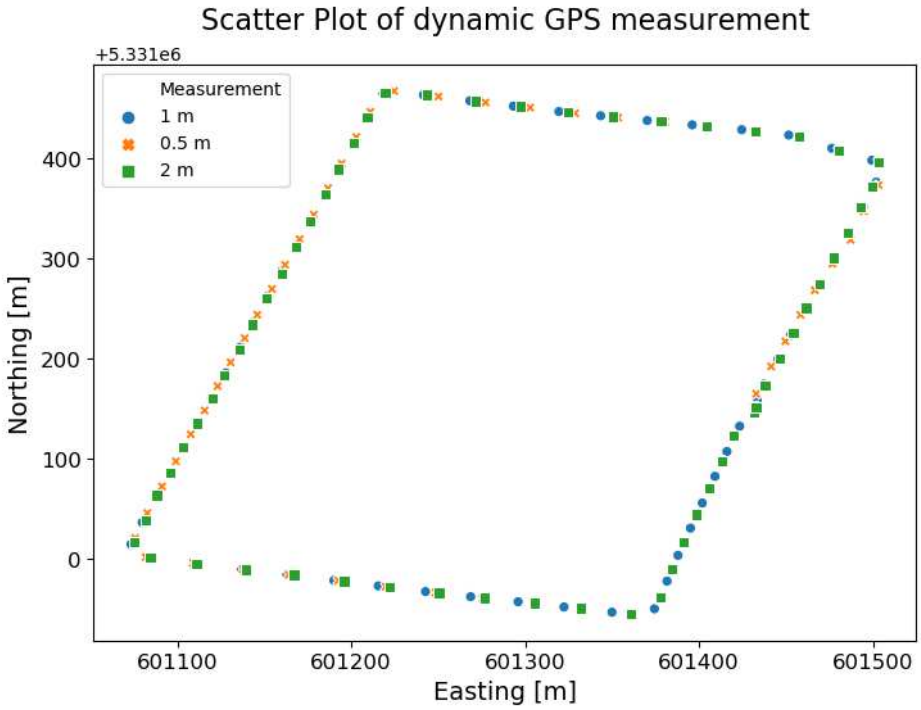

Figure 4.30: Scatter plot of dynamic measurement of the RTK system with the rover with an CH7603A antenna.

Dynamic measurement with A.80 with an RS of below 2, 1 and 0.5 m

The results of the RS are shown in Table 4.24, with a DRMS position estimation of 0.65 m and an accuracy of, on average, 0.81 m.

Measurement	RS position easting [m]	RS position northing [m]	RS 3D-accuracy [m]	Survey-In Time [min]
2 m	601432.611	5331151.415	0.9322	0.17
1 m	601431.959	5331151.226	0.9971	0.87
0.5 m	601432.591	5331152.237	0.4999	11.05

Table 4.24: RS data of DGPS with the A.80 rover antenna.

The results of the rover are illustrated in Figure 4.31 and show the three measurements with different RS accuracies. The average accuracy was 1.86 cm, 1.80 cm and 1.78 cm (2 m, 1 m and 0.5 m measurement).

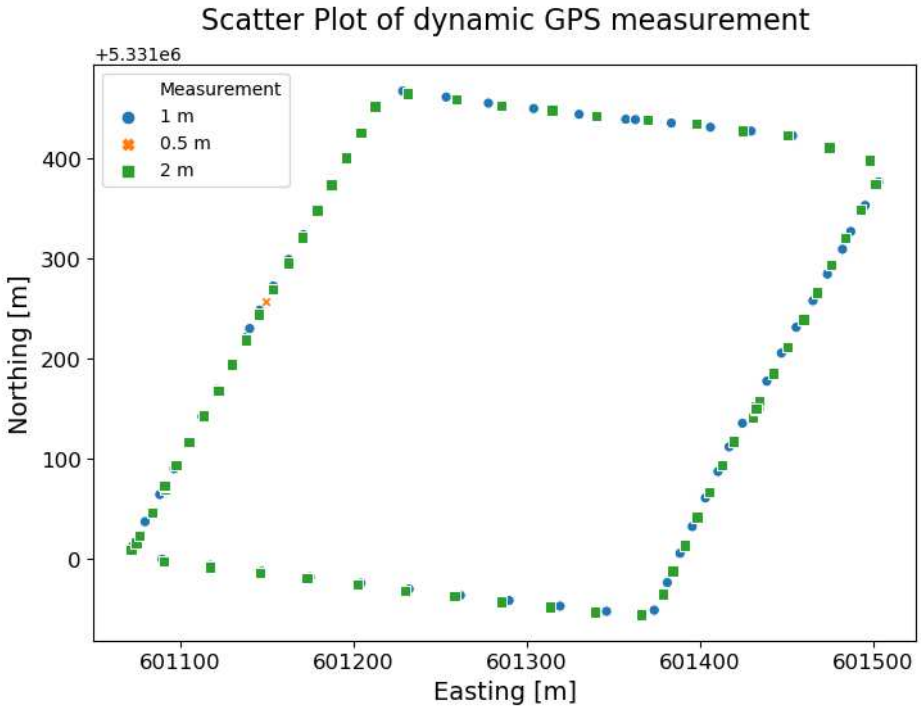

Figure 4.31: Scatter plot of dynamic measurement of the RTK system with the rover with an A.80 antenna.

Dynamic measurement with A.50 with an RS of below 2, 1 and 0.5 m

The results of the RS are shown in Table 4.25 and the DRMS position estimation was 0.63 m, with an accuracy, on average, of 1.16 m.

Measurement	RS position easting [m]	RS position northing [m]	RS 3D-accuracy [m]	Survey-In Time [min]
2 m	601432.995	5331152.434	1.9898	0.95
1 m	601431.865	5331151.928	0.9987	1.33
0.5 m	601432.321	5331152.073	0.4998	13.17

Table 4.25: RS data of DGPS with the A.50 rover antenna.

The results of the rover are illustrated in Figure 4.32 and show the three measurements with different RS accuracies. The average accuracy was 1.92 cm, 1.93 cm and 1.83 cm (2 m, 1 m and 0.5 m measurement).

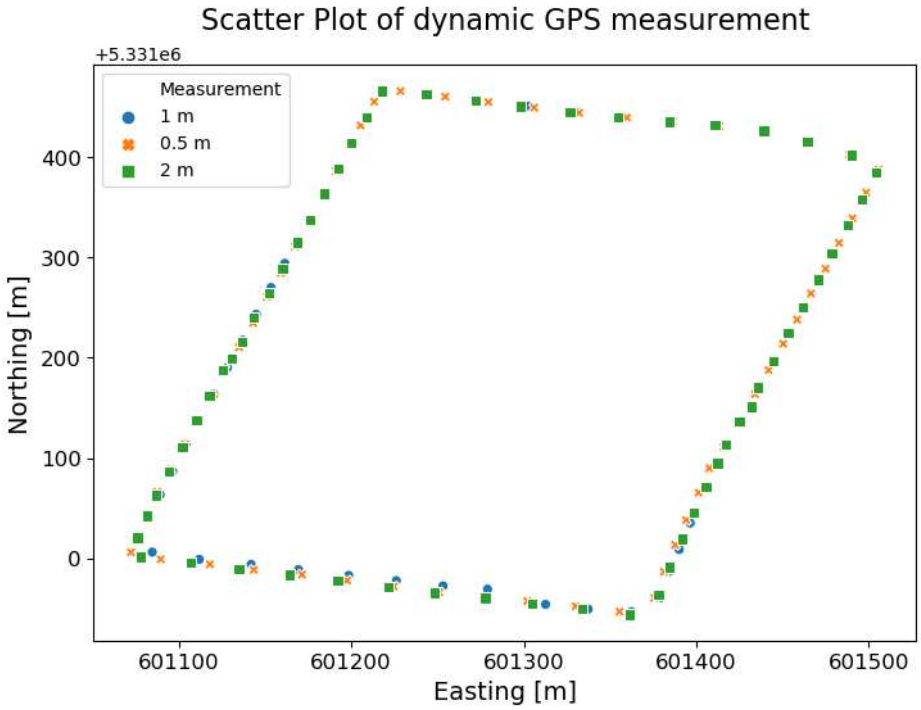

Figure 4.32: Scatter plot of dynamic measurement of the RTK system with the rover with an A.50 antenna.

4.2.2 Comparison of the dynamic measurements

Table 4.26 summarizes the most important results of the dynamic measurements conducted. Compared to the static results, the system was able to calculate valid position estimations with all antennas. This result verifies the assumption that the difficult multipath situation in the urban area was the reason for the problems of some antennas getting a valid GNSS signal. The better surrounding area conditions free of any high obstacles like buildings or trees over one of the receivers, provided a situation likewise free of the difficult multipath errors to resolve. The average accuracy of the rover was of the same magnitude for all measurements. Higher deviations between the measurement could maybe be present if the baseline (the distance between RS and rover) were in the km range. In general, the baseline between the two multi-frequency RTK receivers could be up to 10 km with an accuracy in the cm range [80]. The maximum baseline between the receivers stood at 320 m. The results are much better compared to the results of Svatoň [87]. Without any additional augmentation, in the case of Svatoň's study, the best accuracy was horizontal, at, on average, 1.049 m and, vertically, at 2.37 m and these results are between 109 and 188 time better than that. With SBAS augmentation, the horizontal error was, on average, 0.34 m and the vertical error, 0.96 m, and this means that these results are between 57 and 62 time better. The average survey of 2 m measurements was 0.46 min, for 1 m 1.18 and for 0.5 m 16.07 min. The average 3D position accuracy of the RS was for 2 m, 1.27 m, for 1 m 0.88 m and for 0.5 m 0.5 m. The DRMS of the RS position was for 2 m 0.64 m, for 1 m 0.76 m and for 0.5 m 0.38 m.

The arithmetic mean of the RS of the position estimation is 601432.62 easting and 5331152.12 m northing and the standard deviation for easting is 0.39 m and for northing 0.45 m.

Rover Antenna	Measurement	RS 3D accuracy [m]	Rover average 3D accuracy [cm]	Survey-In Time [min]
ANN-MB	2 m	0.8917	1.85	1
ANN-MB	1 m	0.9993	1.82	3.28
ANN-MB	0,5 m	0.5000	1.76	21.37
HX CHX600A	2 m	0.9132	1.89	0.17
HX CHX600A	1 m	0.6778	1.84	0.17
HX CHX600A	0,5 m	0.4999	1.77	19.73
HX CH6601A	2 m	1.9780	1.83	0.28
HX CH6601A	1 m	0.9980	1.86	1.25
HX CH6601A	0,5 m	0.4998	1.78	18.92
CH7603A	2 m	0.8958	1.92	0.17
CH7603A	1 m	0.6192	1.83	0.17
CH7603A	0,5 m	0.4999	1.76	12.18
A.80	2 m	0.9332	1.86	0.17
A.80	1 m	0.9971	1.80	0.87
A.80	0,5 m	0.4999	1.78	11.05
A.50	2 m	1.9898	1.92	0.95
A.50	1 m	0.9987	1.93	1.33
A.50	0,5 m	0.4998	1.83	13.17

Table 4.26: Overview of dynamic measurements results.

4.3 Range measurements

The range of the system was tested with additional range measurements and these measurements took place northeast of Vienna, as shown in Figure 4.33. The blue circle in Figure 4.33 is the position of the RS and the red line are the positions on which the rover was manually moved. The baseline between RS and rover was up to 2 km. At 2 km, the rover lost the RS signal, which was expected. When the RS is placed in the centre of a field, it is possible to receive the correction signal in an area of 12.57 km or 1256.63 hectares. The average size of cultivated fields depending on the kind of property permit status involved, i.e.,

- professional farming 46.2 hectare,
- sideline farming 18.9 hectare,
- business partnership farming 48.3 hectare, and
- legal entity 346.1 hectare [84].

Under optimal conditions, the current system could cover a field 4 times larger than the biggest average field size in Austria. It is also important to note that if the baseline is larger, it is much more likely that a row of trees or other obstacles will prevent a line of sight connection between the RS and the rover.

Figure 4.33: Overview of place of range measurements. Source: [63]

The RS was placed on a weather station to increase the height of the LoRa antenna. The LoRa antenna was placed at a height of around 5.6 m and the GNSS antenna at around 3.5 m. All components are highlighted in Figure 4.34.

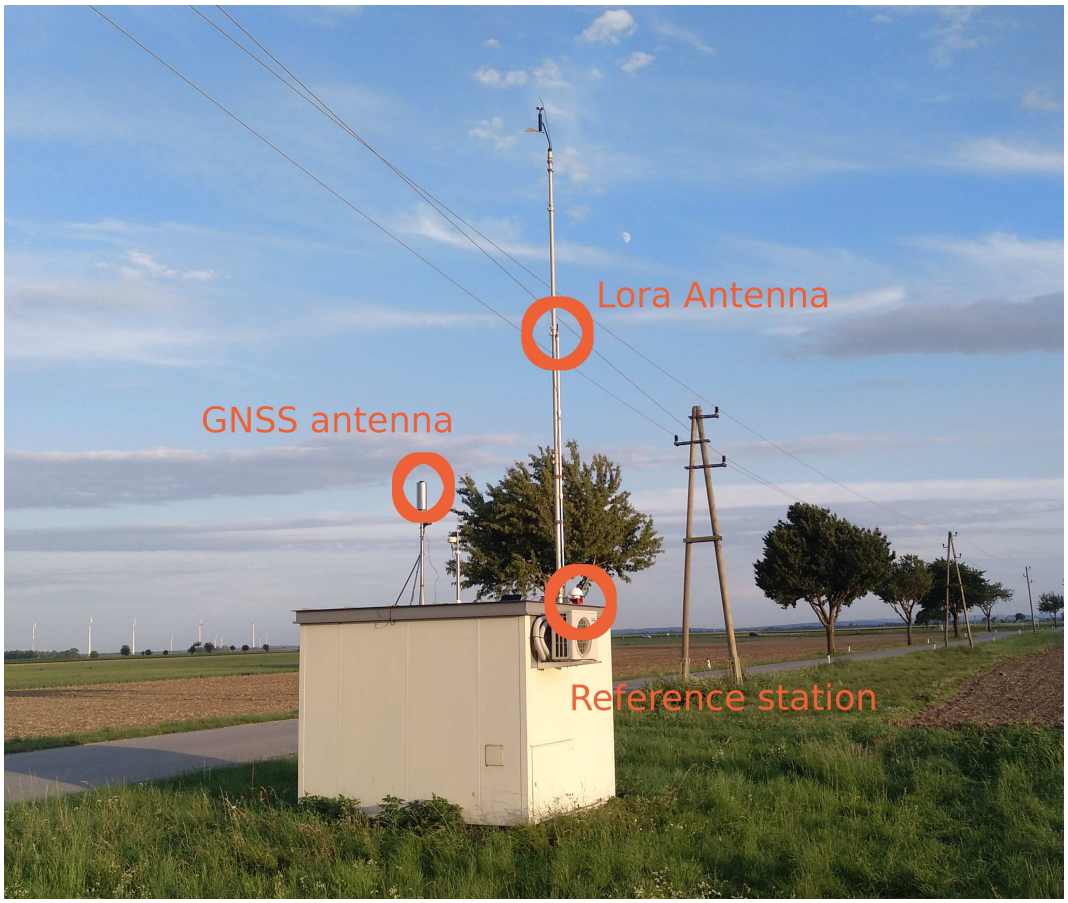

Figure 4.34: RS at the weather station.

The antenna of the rover was mounted at a height of 3.6 m on a rod, as shown in Figure 4.35.

Figure 4.35: Rover with LoRa antenna on a 3.6 m rod.

The results of the range measurement are shown in Figure 4.36. On the x-axis, only the UTM-easting values are displayed, since the measurement had the highest range in the easting direction, while the range in the northing direction featured only a meter range. The measurements were conducted with two different antennas, the μ-blox ANN-MB and the Harxon HX6601a and with both antennas, the same accuracy was indeed achieved. The average accuracy for the measurement was with the ANN-MB antenna 173.96 mm and for the HX6601a, 173.42 mm. During the measurement, the signal between the LoRa antennas was sometimes briefly lost due to misalignment of the LoRa antenna of the rover. However, after a correction of the antenna orientation, the signal was recovered. During that time when no correction signal was received, the accuracy level decreased, but these results were already filtered out. The results show that the system creates a reliable position estimation of up to 2 km if it is not used in a difficult multipath environment.

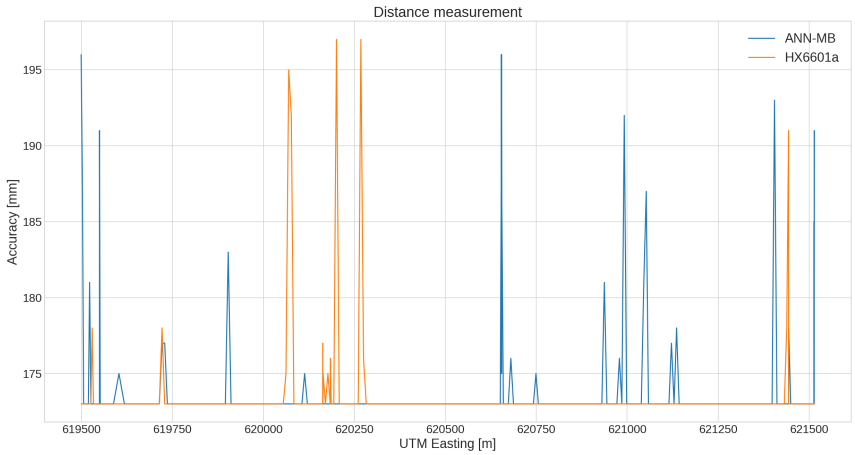

Figure 4.36: Distance measurement accuracy results.

Chapter 5

Summary

The chapter "Introduction" shows the necessity of a well-working RTK system, and the aim of this study and related work. The motivation for this study is to engineer a dual-frequency RTK system which is capable of a position accuracy in cm range under optimal conditions without any difficult multipath conditions with a baseline in the km range. The system should cost less than 1,000 €, which is between 6 and 12 times cheaper then commercial systems (as of the first quarter of 2020). Reasons for purchasing the commercial systems may be, for example, higher reliability since they use different augmentation technologies such as RTK and SBAS together, and also different wireless technologies are combined (radio and telecommunication). This study should have a higher position accuracy and a larger range than the most related study by Svatoň. The best results for static measurements of Svatoň have a DRMS of 1.18 m and for the dynamic measurements, an arithmetic average of 0.34 m. In his work, Svatoň uses only a single frequency system with SBAS to improve his position estimation. The system in this thesis and that of Svatoň are both based on Arduino, but different μ-blox GNSS and radio modules are used. The second chapter "State of the Art" gives a short overview of the development of the GNSSs and introduces the most important theories for the system. It presents the radio-based predecessors like the DASH-DOT and the LORAN system and discusses the development of GPS in more detail with the Transit / NAVSAT systems as the predecessors. The predecessor Transit had the disadvantage that it was not always available for the users and one satellite was only available for 30 minutes and it took between 4 to 8 hours to once again have the possibility of estimating its own position with the next satellite. GPS is one of the current GNSSs and others are GALILEO, GLONASS and BEIDOU. The systems differ slightly in the number of satellites (e.g. 27 by GPS and 35 by BEIDOU) and orbits in which they fly around earth, but all systems consist of a cosmic, control and user segment and the receivers engineered in this thesis fall into the user segment. For the transmission of the GPS signals, BPSK is used to encode the binary states "0" and "1" and different bands are used to transmit these signals. For example, the L1 signal is broadcast on 1575.42 MHz and the L2 on 1227.6 MHz. GPS data is broadcast and distributed with different message formats and the raw navigation message was the first message used by the system, which carries TLM, clock correction and ephemeris data, as well as the almanac and the refraction model. With this information, a GPS receiver is able to estimate its own position and determine the current satellite constellation. It uses this information to calculate its position from the satellites which have the best positions for an accurate estimation, but current systems don't use only this information to do its calculations. Instead, the process is now enhanced by code and phase observations. The GNSS module used in this thesis does not transmit the raw navigation message to the user; the user gets the information of

the current position estimation via NMEA, RTCM or ubx messages. The RTCM messages 105 are transmitted from the RS to the rover with the calculated pseudo-ranges and position for improving the accuracy. For a position estimation, a unique reference system is needed. GPS uses the WGS84, which describes the earth as an ellipsoid. The position quality is described by the terms *accuracy* and *precision* and the formula for calculating the *accuracy* is introduced. The GNSS modules estimate the position not only by using the raw navigation message. It carries out additional measurements based on the pseudo-code and based on the phase of the signals. The pseudo-code and the phase of the signals are also called observables. Both observables are measured because the pseudo-code is first used to calculate a rough position estimation and the result of this step is a float ambiguity number. The phase measurement is then used in a reduced search space in order to obtain an integer ambiguity number (also called fix position estimation). The phase pseudo-range has a higher resolution than the code pseudo-range (1.9 mm to 0.29 m) and if only the code pseudo range is used, the accuracy of the position estimation falls in the meter range. The range measurements are biased by the clock, ionospheric, tropospheric, ephemeris, multipath and DOP errors. Different techniques were developed to mitigate or neutralise them and augmentation methods were engineered to improve the position estimation. Two augmentation methods are discussed in more detail, which are SBAS and DGPS and the second technique is used in this thesis to improve the position estimation of the rover. The proposed system is described in the chapter "RTK System proposal and design" and consists of an RS and a rover. The RS consists of a GNSS and a LoRa antenna; a GNSS module - the μ-blox F9P - is used, and an Arduino Mega as MCU, the LM210 as a LoRa module, along with an LCD screen. In the rover, all components are the same except that the Arduino Mega is replaced by an Arduino Nano. After the *survey in* the RS transmits six RTCM messages to the rover, the rover uses this additional information to improve its position accuracy. The costs of the electronic components of the RS stand at 331.42 € and for the rover, 308.87 € so that one entire system costs 640.28 €. Additional costs have to be added for housing, which are not part of this thesis. Static and dynamic measurements were conducted with six different antennas. The static measurements were carried out in an urban area, including the dynamic measurement on a cultivated field without any higher obstacles. For the static and dynamic DGPS measurements, three different RS position accuracies were used and for the static, it was 5, 1.5 and 0.5 m. For the dynamic one, it was 2, 1 and 0.5 m. The static measurements with 5 and 1.5 m have the same accuracy magnitude as the Svatoň measurements and the accuracy of the 0.5 m measurement is between 48 and 123 better, although the measurements were conducted in a difficult multipath environment. The results of the dynamic measurements were always in cm range and are between 57 and 188 times better than the accuracy gained by Svatoň. Additional range measurements were conducted with two different antennas. The Svatoň system, furthermore, had a maximum tested range of 200 m, and this system has a tested range of up to 2 km, more than 10 times higher. The accuracy of this system is in the cm range within a 2-km baseline and shows no dependency in terms of the distance between the RS and the rover.

Chapter 6

Conclusion

The aim of this thesis was to engineer a multi-frequency DGPS, consisting of two receivers which has the ability to measure the rover position in the cm range with a baseline in the km range but that costs less then 1000 €. All of these aims are accomplished. The DGPS consists of an RS and a rover and the RS uses an Arduino Mega, and the rover, an Arduino Nano as an MCU. The correction data is transmitted via a LoRa antenna to the rover. Both receivers use the μ-blox F9P as a GNSS module. Six RTCM messages are sent from the RS to the rover and the rover uses them to improve its own position estimation. The system was tested with six different antennas and achieved a DRMS between 8.67 and 0.02 m in urban area under static conditions. It is possible to achieve the cm range in urban area if the RS is able to locate its position below 0.5 m of 3D accuracy. The Harxon CH 7603A and the TAOGLAS A.50 antenna system was not, however, able to calculate a position estimation. In an urban area, the system is able to achieve an absolute position quality in the meter range, which is suitable for leisure time use cases. During the dynamic tests and with all the antennas, the system achieved a 3 D accuracy of the rover below 2 cm and these results fall between 57 and 188 times better than the results of the single frequency design by Svatoň. In open terrain, the system could be used for high-precision use cases. The Svatoň system only features a baseline of maximum 200 m, while this study features a 10 times higher baseline of 2000 m, measured on a cultivated field in the outskirts of Vienna. During this range measurement, the accuracy achieved was below 2 cm and shows no dependency on the distance between the RS and the rover. In addition, the system does not use any correction data from additional augmentation services such as SBAS or NTRIP. The cost of the entire system is 640.28 € which is between 9 and 18 times cheaper than the costs of the commercial DGPS systems. The advantage of the system is the compact design and the disadvantage is the requirement of a line of sight between both receivers for transmitting the correction data from the RS to the rover. The system received accuracies in the cm range, reliable in RTK-mode, and with a PDOP below 1.5 with no occurrence of multipath errors.

Chapter 7

Outlook

The aim of this thesis was to engineer a dual-frequency DGPS system based on RTK and it achieves this accuracy in cm range under optimal conditions. Currently, line of sight is necessary for transmitting the correction data from the RS to the rover. For static operations, additional algorithms, such as weighted mean could be used to improve the position accuracy in urban areas. The accuracy could be improved if the system only takes satellites with a higher elevation into account. What's more, the design of the GNSS antennas could be improved to mitigate the multipath effect in urban areas, with a design that features a high gain in higher elevation degrees and no gain or loss in lower elevation degrees. Another possibility for improving the system would be to use the output of the carrier phase distance of both receivers, as, these outputs could be used as inputs of a library for GNSSs like the RTKLIB and the accuracy could be improved by additional software algorithms. It could be possible to calculate the position through software and to compare it to the solution estimated by the F9P; both solutions could be combined in order to arrive at a more accurate position estimation. The position calculation could be additionally improved by integrating an inertial measurement unit (IMU) into the system. The outputs of the IMU could improve the position accuracy by combining the sensor values with the estimated position change and invalid values could be corrected or discarded accordingly. The IMU could be used, furthermore, to calculate new positions at a time when neither a line of sight nor a telecommunication connection is available. Tests were only conducted up to a baseline of maximum 2000 m. Further tests could be conducted to test the accuracy of the system until the maximum distance of the LoRa module is reached (up to 5000 m with a transmission rate of 9.11 Kbps - 2000 m was reached with 18.23 Kbps). With the current baseline measured, it is nevertheless possible to receive the signal in a field which is 4 times higher than the average cultivated field size in Austria. In higher ranges of the km magnitude, however, the LoRa system should be replaced by communication via a mobile telecommunication provider and the system could be further improved by using NTRIP positions to increase the availability and robustness. If the system is enhanced by an additional cellular module, the rover would be able to receive NTRIP correction data via a telecommunication provider. The user could set up their own NTRIP server and transmit the correction data directly to the rover. This approach could be used as a replacement for the RS currently used, as an additional correction data source or as a backup data source if the RS does not have line of sight to the rover. The system showed the advantages of a dual-frequency system compared to a single frequency system and it is expected that in future, only dual-frequency systems will be used for applications, which, however, need a reliable position accuracy in the cm range.

Appendix A

NMEA 0183 message details.

A.1 GGA message

The GGA message contains GPS fix data and the content of the message is illustrated in Table A.1.

Table A.1: Details of GGA message.

Field No.	Name	Unit	Format	Example	Description
0	xxGGA	-	string	$GPGGA	GGA Message ID.
1	time	-	hhmmss.ss	092725.00	universal time coordinated (UTC) Time.
2	lat	-	ddmm.mmmmm	4717.11399	Latitude in degree and minutes.
3	NS	-	character	N	North/south indicator.
4	lon	-	dddmm.mmmmm	00833.91590	Longitude in degree and minutes.
5	EW	-	character	E	East/West indicator.
6	quality	-	digit	1	Quality indicator for position fix.
7	numSV	-	numeric	08	Number of satellites used (0-12).
8	HDOP	-	numeric	1.01	Horizontal Dilution of Precision.
9	alt	m	numeric	499.6	Altitude above mean sea level.
10	altUnit	-	character	M	Altitude units: M.
11	sep	m	numeric	48.0	Geoid separation: Difference between ellipsoid and mean sea level.
12	sepUnit	-	character	M	Geoid separation units: M.
13	diffAge	s	numeric	-	Age of differential correction (null, if DGPS is not used.)
14	diffStation	-	numeric	-	ID of station providing differential corrections (null if DGPS is not used).
15	cs	-	hexadecimal	*5B	checksum
16	<CR><LF>	-	character	-	Carriage return and line feed.

A.2 RMC Message

The RMC message contains the recommended minimum content for GNSS data and is illustrated in Table A.2.

Table A.2: Details of RMC message.

Field No.	Name	Unit	Format	Example	Description
0	xxRMC	-	string	$GPRMC	RMC Message ID.
1	time	-	hhmmss.ss	092725.00	UTC Time.
2	status	-	character	A	Data validity status.
3	lat	-	ddmm.mmmmm	4717.11399	Latitude in degree and minutes.
4	NS	-	character	N	North/south indicator.
5	lon	-	dddmm.mmmmm	00833.91590	Longitude in degree and minutes.
6	EW	-	character	E	East/West indicator.
7	spd	knots	numeric	0.004	Speed over ground.
8	cog	degrees	numeric	77.52	Course over ground.
9	date	-	ddmmyy	091202	Date in day, month and year format.
10	mv	degrees	numeric	-	Magnetic variation value.
11	mvEW	-	character	-	Magnetic variation E/W indicator.
12	posMode	-	character	A	Mode indicator.
13	navStatus	-	character	V	Navigational status indicator.
14	cs	-	hexadecimal	*57	checksum
15	<CR><LF>	-	character	-	Carriage return and line feed.

Bibliography

[1] Airbus. *Eutelsat 172B*. https://www.airbus.com/search.html?q=eutelsat#searchresult-image-all-1. Accessed: 2019-Sep-28. 2017.

[2] AntarktisVerlag. *Weltkarte politisch*. http://www.antarktisverlag.de/epages/63414225.sf/de_DE/?ObjectPath=/Shops/63414225/Products/21-010b/SubProducts/21-010b-0171. Accessed: 2019-Sep-23. 2019.

[3] Arduino. *Arduino Due*. https://www.arduino.cc/en/Guide/ArduinoDue. Accessed: 2019-Jun-09. 2019.

[4] Arduino. *Arduino Mega 2560 Rev3*. https://store.arduino.cc/arduino-mega-2560-rev3. Accessed: 2020-May-21.

[5] Arduino. *Arduino Nano*. https://store.arduino.cc/arduino-nano. Accessed: 2019-Jun-16. 2019.

[6] Arduino. *Arduino Nano (V2.3) User Manual*. https://www.arduino.cc/en/uploads/Main/ArduinoNanoManual23.pdf. Accessed: 2019-Oct-19. 2008.

[7] Arduino. *Delay*. https://www.arduino.cc/reference/en/language/functions/time/delay/. Accessed: 2019-Oct-17. 2019.

[8] Arduino. *Serial.readBytes*. https://www.arduino.cc/reference/en/language/functions/communication/serial/readbytes/. Accessed: 2019-Oct-17. 2019.

[9] AWSM-Tools. *Convert coordinates from Geographic (latitude, longitude) to Universal Transverse Mercator (UTM) coordinate system*. https://awsm-tools.com/geo/geographic-to-utm. Accessed: 2020-May-12.

[10] A. O. Bauer. *Some historical and technical aspects of radio navigation, in Germany, over the period 1907 to 1945*. http://www.cdvandt.org/Navigati.pdf. Accessed: 2019-Jun-22. 2004.

[11] T. Bieniek, B. Van Andel, and T. I. Bø. *Bidirectional UTM-WGS84 converter for python*. https://github.com/Turbo87/utm. Accessed: 2019-Dec-20. 2012.

[12] G. Blewitt. *Basics of the GPS Technique: Observation Equations*. http://www.nbmg.unr.edu/staff/pdfs/Blewitt%20Basics%20of%20gps.pdf. Accessed: 2020-May-03.

[13] K. Bretterbauer and R. Weber. *A primer of geodesy for GIS users*. eng. 2., rev. and extended ed. Geowissenschaftliche Mitteilungen. Vienna: Inst. of Geodesy and Geophysics, Dept. of Advanced Geodesy, 2003.

[14] D. Carnegie, A. Payne, and C. P. "The Design of a Pair of Idnetical Mobile Robots to Investigate Cooperative Behaviours". In: *Cutting Edge Robotics*. Ed. by V. Kordic, A. Lazinica, and M. M. InTech. http://www.intechopen.com/books/cutting_edge_robotics/the_design_of_a_pair_of_identical_mobile_robots_to_investigate_co_-_operative_behaviours Accessed 2019-Oct-02.

[15] K Compton, R. Bennett, and S Hreinsdottir. “Climate-driven vertical acceleration of Icelandic crust measured by continuous GPS geodesy”. English. In: *Geophysical Research Letters* 42.3 (2015), pp. 743–750.

[16] Department of Transportation United States of America. *Global Positioning System Wide Area Augmentation System Performance Standard*. 2008.

[17] K. Deschberger. http://deschberger.landwirt.com/gebrauchte-1391953,Steyr-Trimble-XCN-2050-Spurfuehrsystem.html. Accessed: 2020-Jan-25.

[18] H. Dodel and D. Häupler. “GLONASS”. ger. In: *Satellitennavigation*. Berlin, Heidelberg: Springer Berlin Heidelberg, 2010, pp. 245–255.

[19] H. Dodel and D. Häupler. *Satellitennavigation*. ger. 2., korr. u. erw. Aufl. Berlin [u.a.]: Springer, 2010.

[20] D. Dunning. *What is the difference between RTK FIX & RTK FLOAT?* https://sciencing.com/difference-between-rtk-fix-rtk-float-12245568.html. Accessed: 2019-Oct-25. 2018.

[21] P Enge and P Misra. “Special Issue on Global Positioning System”. eng. In: *Proceedings of the IEEE* 87.1 (1999), pp. 3–15.

[22] Espressif Systems. *ESP8266EX Datasheet*. 6.0. https://www.espressif.com/sites/default/files/documentation/0a-esp8266ex_datasheet_en.pdf Accessed: 2019-Jun-16. Espressif Systems. 2018.

[23] ESRI. *Mean Sea Level, GPS, and the Geoid*. https://www.esri.com/news/arcuser/0703/geoid1of3.html. Accessed: 2019-Sep-23. 2019.

[24] European Global Navigation Satellite Systems Agency. *About EGNOS*. https://egnos-user-support.essp-sas.eu/new_egnos_ops/egnos-system/about-egnos. Accessed: 2019-Oct-12.

[25] H. Flühr. *Avionik und Flugsicherungstechnik : Einführung in Kommunikationstechnik, Navigation, Surveillance*. ger. 2., erweiterte Aufl. Berlin, Heidelberg: Springer Berlin Heidelberg, 2012.

[26] D. Ford. *Satellite positions over Vienna*. https://in-the-sky.org///satmap_radar.php?year=2019&month=11&day=4&skin=1. Accessed: 2019-Nov-11. 2019.

[27] Global Positioning Systems Directorate. *Interface specification IS-GPS-200 Navstar GPS Space Segment/Navigation User Interfaces*. https://www.gps.gov/technical/icwg/IS-GPS-200H.pdf Accessed: 2019-Jun-09. Global Positioning Systems Directorate.

[28] A. Goiser. *Telecommunication*. Technical University Vienna. 2016.

[29] GPS Information. *WAAS and its Relation to Enabled Hand-Held GPS Receivers*. Accessed: 2019-Oct-13. 2012.

[30] M. Grassi. “Autosteer Systems Continue To Evolve”. eng. In: *Croplife* 176.6 (2013), pp. 50–53.

[31] M. S. Grewal, A. P. Andrews, and C. G. Bartone. *Global navigation satellite systems, inertial navigation, and integration*. eng. Third edition. Hoboken: Wiley-Interscience, 2013.

[32] B. Gruber and J. Anderson. “Space Superiority, Down to the Nanosecond: Why the Global Positioning System Remains Essential to Modern Warfare”. eng. In: *Air & Space Power Journal* 27.5 (2013), pp. 98–119.

[33] J. Guo, X. Li, Z. Li, L. Hu, G. Yang, C. Zhao, D. Fairbairn, D. Watson, and M. Ge. “Multi-GNSS precise point positioning for precision agriculture”. eng. In: *Precision Agriculture* 19.5 (2018), pp. 895–911.

[34] HARXON. *D-Helix Antenna HX-CH6001A*. https://en.harxon.com/u_file/product/18_08_08/Harxon%20HX-CH6601A%20Brochure.pdf. Accessed: 2019-Oct-28. 2018.

[35] HARXON. *D-Helix Antenna HX-CH7603A*. https://en.harxon.com/u_file/product/18_08_08/Harxon%20HX-CH7603A%20Brochure.pdf. Accessed: 2019-Oct-28. 2018.

[36] HARXON. *D-Helix Antenna HX-CHX600A*. https://en.harxon.com/u_file/product/18_08_08/Harxon%20D-Helix%20Brochure.pdf. Accessed: 2019-Oct-28. 2018.

[37] B. Hofmann-Wellenhof, H. Lichtenegger, and J. Collins. *Global positioning system : theory and practice*. eng. 5., rev. ed. Wien [u.a.]: Springer, 2001.

[38] B. Hofmann-Wellenhof, H. Lichtenegger, and J. Collins. *Global positioning system : theory and practice*. eng. 5., rev. ed. Wien [u.a.]: Springer, 2001.

[39] J. Hospodka. "Doppler shift satellite navigation - NAVSAT-TRANSIT and adherents". eng. In: *MAD: Magazine of Aviation Development* 1.2 (2013), pp. 11–14.

[40] E. Howell. *NAVSTAR: GPS Satellite Network*. https://www.space.com/19794-navstar.html. Accessed: 2019-Jun-28. 2018.

[41] International GNSS Service (IGS), RINEX Working Group and Radio Techincal Commision for Maritime Servcie Special Committee 104 (RTCM-SC104). *RINEX The Receiver Independent Exchange Format Version 3.04*. 2018.

[42] Joy it. *I2C Serial 20x4 2004 LCD modul*. https://asset.conrad.com/media10/add/160267/c1/-/de/001503752ML01/bedienungsanleitung-1503752-joy-it-sbc-lcd20x4-display-modul-114-cm-45-zoll-20-x-4-pixel-passend-fuer-raspberry-pi-arduino-banana-pi-cubieboa.pdf. Accessed: 2020-May-21.

[43] E. D. Kaplan and C. J. Hegarty. *Understanding GPS/GNSS : principles and applications*. eng. Third edition. GNSS technology and applications series. Boston London: Artech House, 2017.

[44] A. Leick, L. Rapoport, and D. Tatarnikov. *GPS satellite surveying*. eng. 4. ed. Hoboken, NJ: Wiley, 2015.

[45] *LoRa Wireless Communication Module Design Guide*. 1.0. GlobalSat WorldCom Cooperation. 16F. No. 186 Jian 1st Rd Zhonghe Dist. New Taipei City 23553 Taiwan, 2015.

[46] Matplotlib development team. *Matplotlib Version 3.1.3*. https://matplotlib.org/. Accessed: 2019-Dec-20. 2020.

[47] M. Mosavi, R. Zebarjad, and M. Moazedi. "Novel Anti-spoofing Methods Based on Discrete Wavelet Transform in the Acquisition and Tracking Stages of Civil GPS Receiver". eng. In: *International Journal of Wireless Information Networks* 25.4 (2018), pp. 449–460.

[48] G. Möller. *Analyse des GNSS-Referenzstationsnetzes EPOSA : Modellierung systematischer Fehlereinflüsse*. ger. 2010.

[49] National Coordination Office for Space-Based Positioning Navigation and Timing. *GPS Control Segment*. Tech. rep. https://www.gps.gov/systems/gps/control/ Accessed: 2019-Jul-03. U. S. Air Force, 2019.

[50] National Coordination Office for Space-Based Positioning Navigation and Timing. *GPS Space Segment*. Tech. rep. https://www.gps.gov/systems/gps/control/ Accessed: 2019-Jun-10. U. S. Air Force, 2018.

[51] National Coordination Office for Space-Based Positioning Navigation and Timing. *GPS Space Segment*. Tech. rep. https://www.gps.gov/systems/gps/space/ Accessed: 2019-Jun-10. U. S. Air Force, 2019.

[52] National Coordination Office for Space-Based Positioning Navigation and Timing. *Selective Availability*. Tech. rep. https://www.gps.gov/systems/gps/modernization/sa/ Accessed: 2019-Jul-07. U. S. Air Force, 2018.

[53] National Programme on Technology Enhanced Learning. *Carrier Phase based measurements*. Tech. rep. https://nptel.ac.in/courses/Webcourse-contents/IIT-KANPUR/ModernSurveyingTech/lecture4/4_3_Carrier_phase.htm Accessed: 2019-Jun-10. National Programme on Technology Enhanced Learning, 2019.

[54] NAVSTAR. *Global Positioning System Standard Positioning Service Signal Specification*. https://www.gps.gov/technical/ps/1995-SPS-signal-specification.pdf. Accessed: 2019-Jun-06. 1995.

[55] Novatel. *Discussion on RF Signal Propagation and Multipath*. Tech. rep. https://www.novatel.com/assets/Documents/Bulletins/apn008.pdf Accessed: 2019-Jun-09. Novatel, 2000.

[56] Novatel. *GPS Position Accuracy Measures*. https://www.novatel.com/assets/Documents/Bulletins/apn029.pdf. Accessed: 2019-Oct-06. 2003.

[57] Novatel. *RTCMV3 Standard Logs*. https://docs.novatel.com/oem7/Content/Logs/RTCMV3_Standard_Logs.htm. Accessed: 2019-Oct-07. 2019.

[58] Numpy community. *Numpy*. https://numpy.org/. Accessed: 2019-Dec-20. 2020.

[59] J. Nurmi. *GALILEO positioning technology*. eng. Signals and communication technology. Dordrecht [u.a.]: Springer, 2015.

[60] Ocean. *Sea Level Rise*. https://ocean.si.edu/through-time/ancient-seas/sea-level-rise. Accessed: 2020-May-29.

[61] S. O.I., S. A.Y., S. Y.G., and Z. O.I. *Principles of Radio Navigation for Ground and Ship-Based Aircrafts*. eng. Singapore: Springer Singapore, 2019.

[62] OpenStreetMap. *Position of dynamic measurement*. https://www.openstreetmap.org/#map=16/48.1268/16.3648. Accessed: 2020-Jul-02.

[63] OpenStreetMap. *Position of dynamic measurement*. https://www.openstreetmap.org/?mlat=48.23081&mlon=16.63630#map=15/48.2331/16.6236. Accessed: 2020-Jul-30.

[64] OpenStreetMap. *Position of static measurement*. https://www.openstreetmap.org/#map=19/48.18088/16.39442. Accessed: 2020-Jul-02.

[65] L. Pan, C. Cai, R. Santerre, and X. Zhang. "Performance evaluation of single-frequency point positioning with GPS, GLONASS, BeiDou and Galileo". eng. In: *Survey Review* 49.354 (2017), pp. 197–205.

[66] Pandas development team. *pandas 1.0.1*. https://pandas.pydata.org/. Accessed: 2019-Dec-20. 2020.

[67] L. Papula. *Mathematische Formelsammlung : für Ingenieure und Naturwissenschaftler*. ger. 10., überarbeitete und erweiterte Auflage. Wiesbaden: Vieweg+Teubner Verlag / GWV Fachverlage GmbH, Wiesbaden, 2009.

[68] B. Park, J. Lee, Y. Kim, H. Yun, and C. Kee. "DGPS Enhancement to GPS NMEA Output Data: DGPS by Correction Projection to Position-Domain". In: *Journal of Navigation* 66.2 (2013), 249–264.

[69] S. Parker. *Sharper GPS needs even more accurate atomic clocks*. https://theconversation.com/sharper-gps-needs-even-more-accurate-atomic-clocks-38109. Accessed: 2020-May-29.

[70] B. Parkinson and S. Gilbert. "NAVSTAR: Global positioning system-Ten years later". eng. In: *Proceedings of the IEEE* 71.10 (1983), pp. 1177–1186.

[71] PennState College of Earth and Mineral Science. *The Receiver Clock Bias, dT*. https://www.e-education.psu.edu/geog862/node/1716. Accessed: 2020-May-29.

[72] I. G. Petrovski. *GPS, GLONASS, Galileo, and BeiDou for Mobile Devices: From Instant to Precise Positioning*. Cambridge University Press, 2014.

[73] I. G. Petrovski and T. Tsujii. *Digital satellite navigation and geophysics : a practical guide with GNSS signal simulator and receiver laboratory*. eng. Cambridge ; New York: Cambridge University Press, 2012.

[74] Radio technical commission for maritime services. *RTCM STANDARD 10403.2 DIFFERENTIAL GNSS (GLOBAL NAVIGATION SATELLITE SYSTEMS) SERVICES - VERSION 3*. http://read.pudn.com/downloads7

70/doc/comm/3054365/RTCM_&_NMEA_Documents/RTCM32A1.pdf. Accessed: 2020-May-13. 2013.

[75] Radio technical commission for maritime services. *RTCM Standards*. http://www.rtcm.org/about.html#Standards. Accessed: 2019-Jul-21. 2019.

[76] A. J. A. Rodríguez. *GPS Signal Plan*. Tech. rep. https://gssc.esa.int/navipedia/index.php/GPS_Signal_Plan Accessed: 2019-Jul-04. European Space Agency, 2011.

[77] B. Sadasiva Rao, G. Anil Kumar, P. Gopala krishna, P. Srinivasulu, and V. Raghu Venkataraman. "Evaluation of EGM 2008 with EGM96 and its Utilization in Topographical Mapping Projects". eng. In: *Journal of the Indian Society of Remote Sensing* 40.2 (2012), pp. 335–340.

[78] T. Schüttler. *Satellitennavigation: Wie sie funktioniert und wie sie unseren Alltag beeinflusst*. deu. Technik im Fokus. Berlin, Heidelberg: Springer Berlin Heidelberg, 2014.

[79] Septentrio. *APME+ Multipath Mitigation Technology*. https://www.septentrio.com/en/apme-multipath-mitigation-technology. Accessed: 2020-May-09.

[80] Septentrio. *GNSS Corrections Demystified*. https://www.septentrio.com/en/insights/gnss-corrections-demystified. Accessed: 2020-May-10.

[81] SpaceFlightInsider. *GPSIIF*. https://www.spaceflightinsider.com/wp-content/uploads/2014/04/GPSIIF-Boeing.jpg. Accessed: 2019-Sep-23. 2019.

[82] SparkFun. *SparkFun GPS-RTK2 Board - ZED-F9P*. https://www.sparkfun.com/products/15136. Accessed: 2020-May-22.

[83] SparkFun. *SparkFun Ublox Arduino Library*. https://github.com/sparkfun/SparkFun_Ublox_Arduino_Library/blob/master/src/SparkFun_Ublox_Arduino_Library.cpp. Accessed: 2019-Oct-19.

[84] Statistik Austria. *Agrarstrukturerhebung 2016. Betriebsstruktur*. ger. Vienna, 2018.

[85] T. Steinbach. *Ethernet-basierte Fahrzeugnetzwerkarchitekturen für zukünftige Echtzeitsysteme im Automobil*. ger. Wiesbaden: Springer Fachmedien Wiesbaden Imprint: Springer Vieweg, 2018.

[86] J. S. Subirana, J. M. J. Zorzona, and M Hernández-Pajares. *GNSS data processing*. eng. Noordwijk, 2013.

[87] M. Svatoň. "Low-cost implementation of Differntial GPS using Arduino". MA thesis. Linköping University, 2016.

[88] TAOGLAS. *A.80.A.101111*. https://cdn3.taoglas.com/datasheets/A.80.A.101111.pdf. Accessed: 2019-Oct-28.

[89] TAOGLAS. *AQHA.50 Permanent Mount Active Multi-band GNSS*. https://cdn2.taoglas.com/datasheets/AQHA.50.A.301111.pdf. Accessed: 2019-Oct-28. 2018.

[90] TAOGLAS. *GPDF.47.8.A.02*. https://cdn3.taoglas.com/datasheets/GPDF.47.8.A.02.pdf. Accessed: 2019-Oct-28.

[91] TAOGLAS. *GPSF.36.7.A.30*. https://cdn2.taoglas.com/datasheets/GPSF.36.7.A.30.pdf. Accessed: 2019-Oct-28. 2019.

[92] Tec24. https://de.tec24.com/c-129900/m-trimble/t-vario-guide-rtk-spurfuehrungssystem-neu/mid-3427254.html. Accessed: 2020-Jan-25.

[93] Technikbörse. https://www.technikboerse.at/view/gebrauchtmaschine/parallelfahr-system/6527365/case-ih-fm-750-rtk.html?item_position=3&current_page=1. Accessed: 2020-Jan-25.

[94] Technikbörse. https://www.technikboerse.at/view/gebrauchtmaschine/parallelfahr-system/4458977/trimble-fm-750-ez-pilot.html?item_position=1&current_page=1. Accessed: 2020-Jan-25.

[95] Thompson Ramo Wooldridge. *TRW-130 AN/UYK-1 DATA PROCESSING SYSTEM*. Thompson Ramo Wooldridge. 8433 Fallbrook avenue Canoga Park, Califronia, US, 1963.

[96] H. Timmis. *Practical Arduino Engineering*. eng. 1st ed. 2011. Berkeley, CA: Apress : Imprint: Apress, 2011.

[97] u-blox. *ANN-MB series. Multiband, high precision GNSS antennas*. https://www.u-blox.com/en/product/ann-mb-series. Accessed: 2020-Feb-07. 2019.

[98] u-blox. *NEO 6 u-blox GPS Modules Data Sheet*. https://www.u-blox.com/sites/default/files/products/documents/NEO-6_DataSheet_%28GPS.G6-HW-09005%29.pdf Accessed: 2019-Sep-23. u-blox. 2019.

[99] u-blox. *u-blox Neo-6-Series*. https://www.u-blox.com/en/product/neo-6-series. Accessed: 2019-Jun-16. 2019.

[100] u-blox. *u-blox ZED-F9P Interface Description*. Revision 07. 2019.

[101] u-blox. *u-blox ZED-F9P u-blox F9 high precision GNSS module Integration Manual*. Revision 05. 2019.

[102] u-blox. *ZED-F9P u-blox F9 high precision GNSS module Data Sheet*. https://www.u-blox.com/sites/default/files/ZED-F9P_DataSheet_%28UBX-17051259%29.pdf Accessed: 2019-Jun-10. u-blox. 2019.

[103] J. Van Sickle. *GPS for Land Surveyors*. eng. 4. th. Florida: CRC Press, 2015.

[104] M. Waskom. *Seaborn 0.10.0*. https://seaborn.pydata.org/. Accessed: 2019-Dec-20. 2020.

[105] H. Xu, J. Wang, and X. Zhan. “Autonomous broadcast ephemeris improvement for GNSS using inter-satellite ranging measurements”. eng. In: *Advances in Space Research* 49.6 (2012), pp. 1034–1044.

Erklärung

Hiermit erkläre ich, dass die vorliegende Arbeit ohne unzulässige Hilfe Dritter und ohne Benutzung anderer als der angegebenen Hilfsmittel angefertigt wurde. Die aus anderen Quellen oder indirekt übernommenen Daten und Konzepte sind unter Angabe der Quelle gekennzeichnet.

Die Arbeit wurde bisher weder im In- noch im Ausland in gleicher oder in ähnlicher Form in anderen Prüfungsverfahren vorgelegt.

Wien, am 10. September 2020

[Edwin Willegger]